AD-A193 300 ULTRAFAST PHYSICS IN SEMICONDUCTOR MICROSTRUCTURES(U) 1/2
CITY COLL NEW YORK INST FOR ULTRAFAST SPECTROSCOPY AND
LASERS R ALFANO 19 FEB 88 RF-447210 AFOSR-TR-88-0301
UNCLASSIFIED AFOSR-86-0031 F/G 9/1 NL

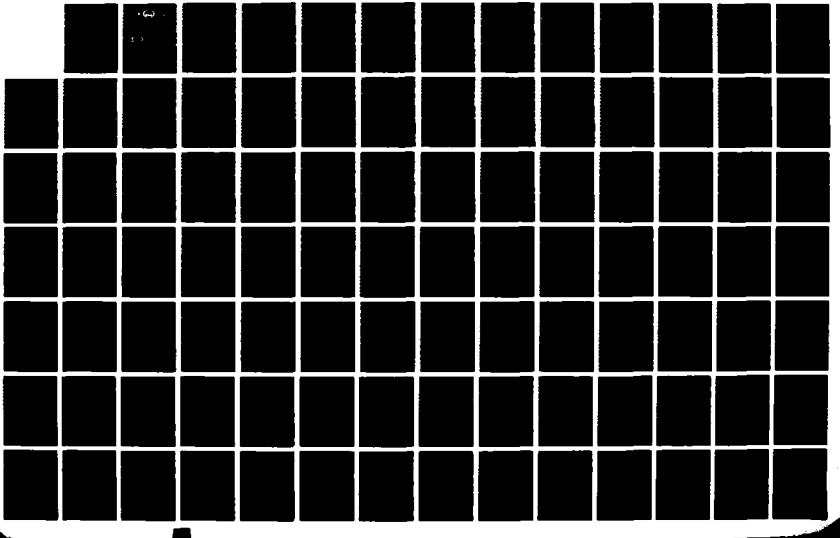

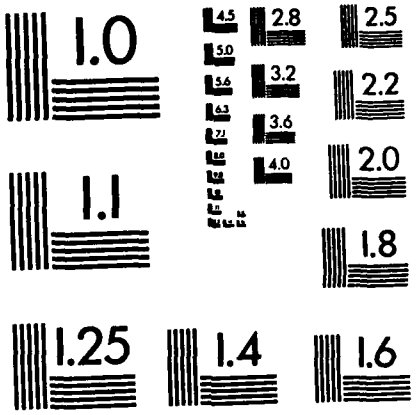
1.0
1.1
1.25
1.4
1.6
1.8
2.0
2.2
2.5
2.8
3.2
3.6
4.0
4.5
5.0
5.6
6.3
7.1

AFOSR-TR- 88-0301

Annual Progress Report on Ultrafast Physics in Semiconductor Microstructures

INSTITUTE
FOR
ULTRAFAST SPECTROSCOPY AND LASERS
AND
PHOTONIC APPLICATION LABORATORY
THE CITY COLLEGE
OF
THE CITY UNIVERSITY OF NEW YORK

PROFESSOR R. R. ALFANO

SECURITY CLASSIFICATION OF THIS PAGE

REPORT DOCUMENTATION PAGE

Form Approved OMB No. 0704-0188

1a. REPORT SECURITY CLASSIFICATION UNCLASSIFIED	1b. RESTRICTIVE MARKINGS
2a. SECURITY CLASSIFICATION AUTHORITY	3. DISTRIBUTION/AVAILABILITY OF REPORT
2b. DECLASSIFICATION/DOWNGRADING SCHEDULE	UNRESTRICTED
4. PERFORMING ORGANIZATION REPORT NUMBER(S) RF-447230	5. MONITORING ORGANIZATION REPORT NUMBER(S) AFOSR-TR- 88-0301
6a. NAME OF PERFORMING ORGANIZATION Department of Physics The City College of N.Y. — 6b. OFFICE SYMBOL (If applicable)	7a. NAME OF MONITORING ORGANIZATION AFOSR/NE
6c. ADDRESS (City, State, and ZIP Code) 138th Street & Convent Ave. New York, NY 10031	7b. ADDRESS (City, State, and ZIP Code) Building 410 Bolling AFB DC 20332-6448
8a. NAME OF FUNDING/SPONSORING ORGANIZATION Dr. G. Witt — 8b. OFFICE SYMBOL (If applicable)	9. PROCUREMENT INSTRUMENT IDENTIFICATION NUMBER AFOSR-86-0031
8c. ADDRESS (City, State, and ZIP Code) Building 410 Bolling AFB DC 20332-6448	10. SOURCE OF FUNDING NUMBERS PROGRAM ELEMENT NO. 61102F — PROJECT NO. 2305 — TASK NO. C1 — WORK UNIT ACCESSION NO.

11. TITLE (Include Security Classification)

Ultrafast Physics in Microstructure and Alloy Systems

12. PERSONAL AUTHOR(S)
Alfano, Robert

13a. TYPE OF REPORT	13b. TIME COVERED	14. DATE OF REPORT (Year, Month, Day)	15. PAGE COUNT
Scientific	FROM 12/1/86 TO 11/30/87	2/19/88	

16. SUPPLEMENTARY NOTATION

17. COSATI CODES			18. SUBJECT TERMS (Continue on reverse if necessary and identify by block number)
FIELD	GROUP	SUB-GROUP	

19. ABSTRACT (Continue on reverse if necessary and identify by block number)

During year two of AFOSR-860031, we have analyzed picosecond photoluminescence data obtained from quasi-two- and quasi-zero-dimensional electron systems in GaAs/AlGaAs multiple quantum wells and CdSSe/glass spherical quantum wells. Important results are: (i) ~~We found~~ nonequilibrium phonons produced in the energy relaxation process of quasi-two-dimensional carriers in a vicinity of phonon wave number q_e could behave like **coherent Bosons** within a short time period. The effects of nonequilibrium phonons for photogenerated carriers in undoped GaAs quantum wells are to slow the energy relaxation and to shorten the recombination lifetime. (ii) Electron-hole recombination dynamics in quasi-OD was interpreted based on the carrier confinement model.

Ultrafast expansion of carriers in asymmetric GaAs quantum wells was observed under picosecond excitation. Dynamical changes in the band structure of GaAs and GaSe were measured under shock waves. Nine papers were published.

20. DISTRIBUTION/AVAILABILITY OF ABSTRACT ☐ UNCLASSIFIED/UNLIMITED ☐ SAME AS RPT. ☐ DTIC USERS	21. ABSTRACT SECURITY CLASSIFICATION Unclass
22a. NAME OF RESPONSIBLE INDIVIDUAL R. R. Alfano Witt	22b. TELEPHONE (Include Area Code) (202) 767-4932 — 22c. OFFICE SYMBOL NE

DD Form 1473, JUN 86 — Previous editions are obsolete. — SECURITY CLASSIFICATION OF THIS PAGE

Table of Contents

Annual Progress Report on Ultrafast Physics in Semiconductor Microstructures

to

AFOSR, Dr. G. Witt, Program Manager

Identification Number: AFOSR-86-0031

from

Robert R. Alfano

The City College of New York

February 19, 1988

Significant progress has been achieved under grant AFOSR-86-0031 in understanding the physics underlying ultrafast transient phenomena that occurs in the semiconductor microstructures. This understanding is essential for making the necessary advances for the future generation of ultrafast microelectronic devices.

Microstructure samples have been obtained primarily from H. Morkoc of University of Illinois and other groups such as M. Niigaki of Hamamatsu Photonic KK, T. Fukunaga of Bertaska of McDonnel Douglas, and Emil Koteles of GTE.

The following summarizes our accomplishments in the major effort on III-V semiconductor microstructures and a minor effort on II-VI compound.

1. Nonequilibrium Phonon Effects on the Energy Relaxation and Lifetime of Photogenerated Carriers in GaAs MQW

We have carried out time-resolved photoluminescence with the finest time-resolution of 2ps performed to date to investigate the ultrafast processes which occurs in undoped GaAs/AlGaAs microstructures.

The existence of a large population of nonequilibrium (hot) phonons after an initial rapid carrier cooling in an undoped multiple GaAs quantum well (55Å) structure excited by 500fs laser pulses is experimentally verified by time-resolved photoluminescence studies using a 2ps-time-resolution streak camera. The hot phonon population is directly monitored by measuring time-resolved phonon replica luminescence below n=1 electron to heavy-hole transition energy. It reaches to a maximum in $\sim$3ps after the end of laser pulse and decays with a 30ps time constant. Its effects on carrier dynamics are the following two aspects. First, the

energy relaxation of carriers after an initial rapid cooling is substantially suppressed due to re-absorption of hot phonons by carriers. Second, the carrier density decay is strongly influenced by the hot phonons in the system which stimulate phonon replica emission. This stimulated phonon replica emission is mainly radiated and highly polarized in the well plane (x-y plane). An effective carrier depletion time [density decreases by a factor of e^{-1} from $n_e(t=0)$] is obtained to be as short as 10ps.

This work is of particular importance to the semiconductor community because it solves the long standing controversial issue regarding the phonon assisted transitions below n=1 electron to hole transition in GaAs quantum wells that was initially suggested by Professor Holonyak's group (see for example, Phys. Today, 40, Oct. 1980). We have explicitly demonstrated that the hot phonons emitted by hot electrons can stimulate phonon-replica-emission.

Part of this work was accepted to be published in Phys. Rev. B.

2. Observation of Ultrafast Lateral Diffusion of Photogenerated Carriers in An Asymmetric GaAs Quantum Well

An experimental investigation of in-plane expansion of photogenerated carriers in a single asymmetric GaAs quantum well is carried out using a streak camera and a subpicosecond laser source at 4.3K. It is found that the carrier expansion process is enhanced in the well plane by restricting carrier expansion in the well direction. The effective diffusivity D^* of photoexcited carrier in the asymmetric well has been directly determined to be $10^6 cm^2/s$ at 4.3K, which is about four orders

magnitude larger than the thermodynamic value in bulk GaAs. The expansion velocity is determined to be $3.2\times10^{8} cm / s$, which is four times larger than the initial Fermi-velocity of the electrons.

The observation of an anomalously fast carrier expansion process in an asymmetric quantum well, but not in the symmetric well is most important. It provides a new insight to the problem of **how to design semiconductor structures in order to obtain the desired carrier transport.**

This work was submitted to Phys. Rev. Lett. for publication.

3. Determination of Band Offsets via Optical transitions in Ultrathin Quantum Wells

This work demonstrates what experimental data from optical transition should be used and how it is sensitive to the Q-value of band offset. We have shown that the precise Q-value can be determined by systematically measuring the n=1 light- and heavy-hole energy spacing (ΔE) in the sensitive zone of well width (15 to 80Å). Furthermore, it is also shown that different connection rules and hole masses yield different Q-value and the appropriate connection rule can be discriminated also by systematically measuring ΔE as well as the energy spacing between ground and first electron eigen state (ΔE_{12}) in the sensitive zone of L_z.

This work was published in Phys. Rev. B, 37, 1048 (1988).

Recently, we are investigating the influence of different connection rules on the exciton binding energy in III-V semiconductor quantum wells, and hence on the

determination of band offset based on the data of ΔE.

4. Physics in semiconductor GaAs and GaSe under laser-driven shock-wave compression

Using a pump-probe technique, the photoluminescence peak of bulk GaAs was observed to blue shift and split into two components under the laser-induced shock wave loading condition. The two components correspond to the transitions from the Γ_6 conduction band to the valence heavy- and light-hole subbands, because of symmetry breaking by the uniaxial shock compression along the [001] direction. From the blue shift, we deduced our picosecond-laser-induced shock pressure of $\sim$ 10kbar.

In GaSe, we observed a broadening of the spontaneous emission which is proportional to the shock pressure and attributed to a shock-wave-induced exciton collision mechanism due to the directional motion of particles in the shocked region.

These works were published in Appl. Phys. Lett. 51, 1789 (1987) and Appl. Phys. Lett. 52, 93 (1987).

5. Optical transition and recombination lifetime in quasi-zero dimensional electron system in CdS_xSe_{1-x}

We report on the observation of optical transitions between quantized levels ($1S$, $1P$) in the conduction and valence bands in quasi-zero dimensional electron systems in CdS_xSe_{1-x} by 4K and 300K photoluminescence measurements. From the relative luminescence intensities arising from the $1S-1S$ and $1P-1P$

transitions, it is shown that the photoexcited electrons (holes) occupied in the different quantized levels in conduction (valence) band are not coupled, or only weakly coupled. Picosecond luminescence studies of the optical transitions using a streak camera reveal a significant influence of three-dimensional confinement on the recombination probabilities of photogenerated electrons and holes. The recombination life time of electrons and holes in quasi-zero dimensional system decrease with the diameter (d) of system from 210ps for d=10.2nm to 70ps for d=7.4nm at 4K. The ratio of recombination life time for $1S-1S$ transition and $1P-1P$ transition seems to be independent of the diameter of system, and is measured to be about 3.5. This ratio can be interpreted by the calculated squared transition matrix elements and the nonradiative processes.

This work was published in Appl. Phys. Lett. 51, 1839 (1987).

List of Participating Scientific Personnel

1. R. R. Alfano ---- Distinguished Professor
2. Kai Shum ---- Assistant Professor
3. K. Wong ---- Research Associate
4. M. Junnarkar ---- Research Associate (left on 1/28/88)
5. H. Chao ---- Graduate Student
6. A. Katz ---- Graduate Student
7. S. Lee ---- Graduate Student
8. W. B. Wang ---- Graduate Student
9. Mi Yan ---- Graduate Student
10. Sheryl Zhao ---- Graduate Student
11. Toni Seas ---- Graduate Student

List of Publications

(1) "Effects of nonequilibrium phonons on the energy relaxation and recombination lifetime of photogenerated carriers in undoped GaAs quantum wells", Kai Shum, M. R. Junnarkar, H. S. Chao, R. R. Alfano, and H. Morkoc, accepted to be published in Phys. Rev. B, 1988.

(2) "Observation of ultrafast lateral expansion of energetic carriers in an asymmetric GaAs quantum well", Kai Shum, H. S. Chao, M. R. Junnarkar, R. R. Alfano, T. Hederson, and H. Morkoc, submitted to Phys. Rev. Lett.

(3) "Electron-hole recombination lifetimes in a quasi-two-dimensional electron system in CdS_xSe_{1-x}", Kai Shum, G. C. Tang, M. R. Junnarkar, and R. R. Alfano, Appl. Phys. Lett. 51, 1839 (1987).

(4) "Reply to [Comment on 'Determination of valence band discontinuity via optical transitions in ultrathin quantum wells']", Kai Shum, C. Zhang, P. P. Ho, and R. R. Alfano, Phys. Rev. B 37, 1408 (1988).

(5) "Energy relaxation and ballistic diffusion of photoexcited carriers in symmetric and asymmetric quantum wells", Kai Shum, M. R. Junnarkar, H. S. Chao, R. R. Alfano, and H. Morkoc, SPIE Vol.793, 6 (1987).

(6) "Confinement effects on the scattering of electrons by polar optical phonons in semiconductor quantum wells", Kai Shum and R. R. Alfano, SPIE Vol.793, 70 (1987).

(7) "Optical transitions and recombination lifetimes in quasi-zero dimensional electron system in CdS_xSe_{1-x}", Kai Shum, G. C. Tang, M. R. Junnarkar, and R. R. Alfano, SPIE Vol. 793, 150 (1987).

(8) "Shock-wave-induced collision broadening of the photoluminescence spectra in GaSe", X. Z. Lu, S. Lee, R. Garuthara, and R. R. Alfano, Appl. Phys. Lett. 51, 1789 (1987).

(9) "GaAs photoluminescence under picosecond-laser-driven shock compression", X. Z. Lu, R. Garthara, S. Lee, and R. R. Alfano, Appl. Phys. Lett. 52, 93 (1987).

Appendix

Effects of nonequilibrium phonons on the energy relaxation and recombination lifetime of photogenerated carriers in undoped GaAs quantum wells

Kai Shum, M. R. Junnarkar, H. S. Chao, and R. R. Alfano

Institute for Ultrafast Spectroscopy and Lasers

Departments of Electrical Engineering and Physics

The City College of New York, New York, New York, 10031

and

H. Morkoc

Coordinated Science Laboratory, University of Illinois at

Urbana-Champaign, Urbana, Illinois 61801

ABSTRACT

Time-resolved and time-integrated photoluminescence studies of an undoped multiple GaAs quantum well structure excited by 0.5ps laser pulses have revealed several important experimental observations on the behavior of photoexcited carriers. A large population of nonequilibrium longitudinal optical phonons produced in the energy relaxation process of hot carriers manifests itself by the nonequilibrium phonon stimulated phonon-replica which located at $\sim$ 30meV below n=1 electron-hole transition. The energy relaxation is substantially suppressed due to the existence of nonequilibrium phonons after an initial rapid cooling (0-5ps). The number of photoexcited carriers

decreases anomalously fast within the first 30ps after the excitation by laser pulse. An effective carrier depletion time is determined to be as short as 10ps. A mechanism which leads to such a short carrier depletion time is associated with the nonequilibrium phonon stimulated phonon-replica.

PACS numbers: 63.20.Kr, 72.20.Jv, 73.40.Lq.

I Introduction

Recently, there have been growing interest in studying the dynamics of photogenerated carriers in semiconductor quantum well structures since it reflects the fundamental interactions among electrons, holes and phonons. These interactions determine the performance of ultrahigh speed electronic and optoelectronic devices. In the case of bulk semiconductors, the slowing of hot carrier relaxation is attributed to either screening[1] of electron-phonon interaction or re-heating of carriers by nonequilibrium (NE) phonons produced in the relaxation process of hot carriers.[2,3] A comparative study[4] of the hot electron cooling rates in undoped multiple quantum well (MQW) structures and in bulk GaAs by time-resolved measurements of optical absorption and gain concluded that the rates were approximately same at a photogenerated carrier density of 2.5×10^{17} cm^{-3}. This is expected from a simple theory[5] in which lattice is treated as a heat bath for quasi-equilibrium carriers. In the case of modulation doped MQW structures, quasi-steady-state experiments have been carried out from two groups[6,7] to investigate the interaction of electrons and holes with phonons. These experiments have generated conflicting results regarding the presence[6] or absence[7] of NE phonons. Time-resolved PL measurements with ~20ps time resolution were reported by Ryan *et al.*[8] who found that the cooling of hot carriers was anomalously slow after 40ps.

Reviewing the aforementioned previous works two important points were noticed. First, one can not extract information on the initial carrier relaxation process either from quasi-steady-state experiments or from time-resolved measurements with time resolution greater than 10ps. To assess the importance of NE phonon effect on the energy relaxation of hot carriers one uses a corresponding theory to match the experimental carrier temperature cooling curve or the logarithm of power loss as function of the inverse of the carrier temperature. There has been no report on the direct evidence for existence of NE phonons in quantum well structures under high photoexci-

tation. It is necessary to study the initial carrier relaxation process to substantiate the existence of NE phonons and its importance on the hot-carrier relaxation since the phonon lifetime is about 7ps. Second, one can not easily obtain information on photo-generated carrier lifetime in modulation doped MQW structures because the large doped-in carrier density is comparable to the photoexcited carrier density. Furthermore, carrier lifetime can influence the cooling of hot carriers.[9] Therefore, it is necessary to study photogenerated carrier dynamics in undoped MQW structures in order to obtain information both on the energy loss rates and on the carrier lifetime.

In this paper, experimental observations are reported from the measurements of time-resolved photoluminescence (PL) with a 2ps time resolution and time-integrated luminescence spectra from an undoped GaAs MQW structure with dependences on lattice temperature, excitation intensity, and polarization. The NE phonons emitted by hot electrons are directly observed by measuring the time-integrated as well as time-resolved phonon replica luminescence lying below the n=1 electron to heavy-hole transition energy. The energy relaxation of hot electrons is found to be substantially suppressed when a large population of NE phonons is present after an initial rapid cooling. The photoexcited carrier density extracted from a fitting of time-resolved PL profiles at different emitted photon energies decreases non-exponentially and very rapidly within the first 30ps. An effective carrier depletion time is determined to be as short as 10ps. The mechanism leading to such short carrier depletion time is associated with NE phonon stimulated phonon-replica.

II Sample

The undoped GaAs/$Al_xGa_{1-x}As$ MQW structure investigated was grown by molecular-beam epitaxy on a (001)-oriented undoped GaAs substrate. The MQW consists of 50 periods of 55Å thick GaAs and 100Å thick $Al_{0.3}Ga_{0.7}As$ layers, and followed by a 1.2*um* GaAs buffer layer. The lateral size of the structure is about 2×4*mm*. The good quality of sample is confirmed by well resolved heavy-hole and

light-hole excitonic structures of room temperature PL spectra. The FWHM for the heavy-hole excitons is about 13meV. The sample was mounted on the cold finger in an optical helium cryostat.

III Experiment

An ultrashort laser pulse of 0.5ps duration at 620nm was used to excite the electron-hole pairs in the sample. Most of light is absorbed in both the GaAs wells and the AlGaAs barriers. Photogenerated carriers in the barriers will either diffuse to the GaAs buffer layer or be captured into the wells. The latter will result in uncertainty about carrier density in the wells by a fact of ~ 3. Residual transmitted light is absorbed in the GaAs buffer layer. The diameter of excitation area is about $160um$. To avoid damaging of the sample surface, the maximum excitation power is adjusted such that photogenerated carrier density is on order of $10^{19}cm^{-3}$. The 0.5ps laser pulse was generated from a colliding-pulse passive mode-locked dye laser and amplified by a four-stage dye amplifier pumped with a frequency doubled Nd: YAG laser operated at 20Hz. In order to keep the time resolution of Hamamatsu streak camera system within 2ps, PL was spectrally resolved using different narrow band filters. The luminescence intensities were corrected for the nonlinearity of streak rate, the spectral response, and the transmission of each narrow band. For the time-integrated PL measurements, a Stanford boxcar and a GaAs photomultiplier were used.

IV Results and Discussion

1. Steady-state

Time-integrated luminescence spectra from the MQW structure excited by the 0.5ps laser pulse at various lattice temperatures (T_L) are shown in Fig.1. These spectra were taken in a conventional backward Raman configuration $z(y,y)\bar{z}$, where z is the growth direction. In order to eliminate radiation from the edges of the sample,

the luminescence spot was first imaged on an aperture with aid of a streak camera and then re-focused onto a vertical slit of a grating spectrometer. Several features are displayed in the data shown in Fig.1. (1) The emission band A on high energy side of the spectra arises from the recombination of photogenerated n=1 electron-hole. The peak of A shifts towards the low energy side as the T_L increases. An high energy tail on the peak A develops with increasing T_L.

(2) A broad emission band C at low energy side of the spectra arises from the GaAs buffer layer. The total emission intensity of C decreases as T_L increases.

(3) The most interesting feature of the spectral data is the appearance of an emission band B, located about 30meV below the n=1 electron-heavy-hole transition. This B emission band is attributed to the NE phonon stimulated phonon-replica. The following four reasons support this assignment to the B band:

(i) This B emission band does not appear in the PL spectra taken at low power excitation about $1W/cm^2$ at 4.3K using a cw 488nm line of an argon-ion laser. However, the PL spectra using a very weak train of laser pulses (120fs) directly from the colliding-pulse passive mode-locked dye laser as the excitation source, with an excitation power density in range of 10^{-5}–$10^{-3}W/cm^2$, shows a weak electron to acceptor emission band separated by 17meV from the n=1 electron-heavy-hole transition accompanied by its phonon-replica[10] at low temperatures. This extrinsic emission band disappeared completely when the sample temperature was raised to $\sim$ 80K, whereas the B band displayed in Fig.1 exists up to room temperature. Moreover, the relative time-integrated PL intensity of the B to A band under 0.5ps light pulse excitation shown in the Fig.1 decreases as the excitation power density decreases. The B band in Fig.1 is hardly visible when the excitation power density is lower than $10^{-3}P_m$, where $P_m \sim 10^{12}W/cm^2$ is the maximum value of the excitation power density. This contradicts what is generally expected for impurity emission. Since the concentration of acceptors is low in our sample as confirmed by the luminescence stu-

dies using the weak train of 120fs light pulses, an impurity emission band should be more readily apparent and pronounced at lower excitation. Therefore, the B emission band shown in Fig.1 can not be attributed to electron to acceptor luminescence under high excitation.

(ii) The intensity ratio between the B and A emission bands as indicated by triangle in Fig.2 increases as lattice temperature increases. To convince the emission band B arises from NE phonon stimulated recombination process, we calculate the sum of occupation numbers both for the equilibrium phonons (lattice temperature T_L) and for the NE phonons (carrier temperature T_c) by assuming the carrier temperature is same as the effective temperature for the NE phonons after 30ps. This will be discussed later with the carrier temperature. The calculated result is shown by the solid line in Fig.2. The fitting of the total phonon occupation number to the obtained intensity ratio from the spectra is impressively good. This implies that the intensity of band B is well correlated with the LO-phonon population. Because of the participation of NE phonon the intensity of B band (see also time-resolved luminescence at 780nm in Fig.4) is strongly enhanced especially at low temperatures. This further supports our assignment of the B band to the NE phonon stimulated phonon replica.

(iii) It is also not possible to attribute the emission band B to the emission from renormalized band-band transition because the peak position of the A band (766.7nm) and the B band at 4.3K do not change with variation of excitation intensity by a factor of $\sim 10^3$. A further support to above statement is the fact that the spectral position of peak A exactly coincides with each other for the two different luminescence studies using different light excitation sources: one is the weak 120fs-pulse train with a repetition rate of 125MHz, and the other is the amplified 0.5ps-pulse with a 20Hz repetition rate.

(iv) We have also studied the polarization of the emission bands A, B, and C by

measuring "right-angle"[11,12] $z(y,x)y$ and $z(y,z)y$ integrated luminescence spectra. It was found that the B band emitted at the sample edge along the y-direction (see inset of Fig.3) was highly polarized in the x-direction. The A and C emission bands were depolarized, independent of excitation power density and lattice temperature. The intensity ratio between the x- and z-direction for the B band is about 20 in the lattice temperature range from 4.3 to 300K at full excitation power density P_m. But, the ratio is strongly dependent on the excitation power density at a given lattice temperature. For example, at $T_L = 20K$, the ratio decreases from 20 to ~6 as the excitation power density decreases from P_m to $0.017P_m$. Fig.3 shows the spectra for $T_L = 100K$ at two different excitation intensities. The lower solid trace was taken in $z(y,x)y$ configuration (TE polarization) at the excitation density of $0.017P_m$. It is identical to the spectrum taken in $z(y,z)y$ configuration (TM polarization) which is not shown. The B band disappears due to the absence of large population of NE phonons at the low excitation and high lattice temperature. The upper solid and broken traces are the TM and TE spectra at the full excitation P_m, respectively. The intensity ratio of TE and TM remains 20. excitation P_m. It should be pointed out that the energy position of A band in Fig.3 is lower than that in Fig.1 by ~4meV while the position of B band remains unchanged. This low energy shift of A band is due to the self-absorption effect. The polarization behavior of B band is consistent with the results from Raman scattering experiments reported by Zucker *et al.*[12] where the pump photons are provided by the external laser source. In our case the pump photons arise from the recombination of n=1 electron and n=1 heavy-hole at the subband edges. This process is strongly enhanced by the presence of a large number of NE phonons emitted by hot-electrons at high excitation. The depolarized feature of the band C is expected since the emission is from the GaAs buffer layer. However, the polarization behavior of the emission band A is not understood. In terms of the selection rule of dipole recombination described by Iwamnra *et al.*[13], the emission intensity

of n=1 electron-light-hole for the TE polarization should be four times larger than that for the TM polarization. There should be no TM emission arising from n=1 electron-heavy-hole recombination. It should be mentioned here that the B band in the Fig.1 which was detected along the z-direction is depolarized and much weaker, at least a fact of 20, than detected along the y-direction. The former is expected due to the symmetry and the latter provides an important rule for understanding a fast carrier density decreasing process which will be discussed in the *time-resolved* section.

In order to further substantiate our assignment of the B band, two additional questions must be addressed:

(1) Why no phonon replica appears on the high energy side of the A band, if a large NE phonon population really arises? A high energy replica would arise from a recombination of an energetically elevated electron (hole) by absorbing a phonon and hole (electron). However, the elevated electron (hole) will be very quickly scattered by the other hot electrons (holes) through a strong electron-electron, electron-hole, and hole-hole interaction before it recombines with a hole (an electron). Therefore, the high energy replica can not be observed in PL spectra. But, this re-heating process should result in a retardation of hot carrier cooling which is indeed consistent with the time-resolved PL data described in the next section.

(2) Why is the energy separation between the peaks of A and B bands (E_{AB}), on order of $\sim$ 30meV which is smaller than expected (36meV)? The 30meV energy separation in fact gives a further strong support of our assignment of the B band. In an equilibrium state, the interaction strength of electron and LO phonon in a bulk GaAs is proportional to $\frac{1}{\vec{Q}^2}$, where $\vec{Q}$ is the phonon wave vector. Therefore, the phonons in vicinity of $\vec{Q} = 0$ would be expected to more strongly couple with electrons giving rise to a phonon replica at just 36meV below its primary emission band. In our highly photoexcited MQW sample, LO phonons are driven to a NE state by a rapid initial energy relaxation process of photoexcited hot electrons. The develop of these

NE both in time domain and in two-dimensional wave vector space ($\vec{q}$, parallel to the well plane) has been recently studied by several groups.[14,15] Two important results on the number of NE LO phonon population are : (i) At given q, it can reach to a maximum in about 0.5 - 3ps and then decrease. (ii) At a given time, it increases steeply from a minimum of q_{min}, reaches to a maximum at q_c, and then decreases. **What is essential concerning the question is that there is a maximum NE LO phonon population which is located both in a narrow wave vector space of the vicinity of q_c and in the well plane and lasts in a short time period.** This portion of NE phonons behaves like **coherent Bosons.** The existence of the "coherent Bosons" will tend to increase the number of the Bosons (near q_c) in the system with a rate proportional to the present number of Bosons resulting in a stimulated phonon emission process. This process can give rise to a phonon replica emissions, when an electron in the conduction subband recombines with a hole in the valence subband, not only a photon but also a phonon or more phonons will be emitted to join the Boson system. In order to conserve the momentum of electron-phonon system in this recombination, the electron must possess a momentum of q_c (neglecting the momentum of the emitted photon) which is associated with a kinetic energy of $E_{q_c} = \frac{\hbar^2 q_c^2}{2m_c}$. Therefore, the energy E_{AB} should be equal to LO phonon energy minus E_{q_c} which is about 6meV corresponding to the values of $1.03\times10^6 cm^{-1}$ and $0.067m_0$ for q_c and electron effective mass m_c. Thus, this gives 30meV for E_{AB}.

Over years, there has been much debate[13,16-18] over the interpretation of the spectral features locate below the n=1 electron to heavy-hole transition energy, mainly because many species exist in this energy region: LO-phonon replica, impurity states, and many body band gap renormalization. Holonyak and co-workers[17] have demonstrated the LO-phonon participation in GaAs-AlGaAs based QW laser emission by observing more than one LO-phonon sidebands in the laser operation below the n=1 confined-particle transition. Recently, Skolnick *et al.*[18] confirmed that a peak

below the n=1 electron-heavy-hole transition is phonon replica by observing the coupling at both the GaAs- and InAs-like bulk LO-phonon energies of InGaAs QW. Our measurements support these arguments.

2. Time-resolved

Time-resolved PL intensities of the MQW structure at 4.3K were measured over the spectral range from 720 to 780nm. Four representative streaks at given selected wavelengths are shown in Fig.4. The emission centered at 770nm arises from the recombination of band edge electron and heavy-hole. The radiation with wavelengths less than 770nm are from the recombination of hot carriers. The time-resolved luminescence intensity of the phonon replica is centered at 780nm. Each luminescence profile is an average from 10 individual shots using a prepulse[19] for averaging. The left peak of the dotted curve is the prepulse which reflects the 2ps temporal resolution. The right peak on the same curve is the Rayleigh scattering light from the sample surface which defines the "zero" time for our analysis. Several features appear in the data displayed in the Fig.4. (i) The rise time for all the luminescence profiles are instrumental; a 2ps up-limit reflects the rapid thermalization, capturing, and initial cooling. (ii) The shape of rise-part of luminescence profile at 780nm is similar to that at 770nm, but delayed by $\sim$ 3ps. This implies that the emission at 780nm does not originate from the same band as the emission at 770nm; otherwise, the rise-part of the luminescence at 780 should start at the same zero point as that at 770nm. The delay of $\sim$ 3ps is consistent with our assignment of the emission band center at 780nm to the stimulated phonon-replica. This 3ps is the time required to establish a large population of NE phonons at q_r. (iii) The luminescence decay time[20] of 30ps (broken curve) for the phonon replica emission at 780nm is shorter than the luminescence decay time of 60ps at 770nm. This supports that the emission at 780nm can not be due to impurity emission at high excitation.

To study the NE phonon effect on energy relaxation process quantitatively, carrier temperature and density as function of time should be determined simultaneously. An expression in the time domain is introduced to fit the time-resolved PL data by using two adjustable parameters, namely, the carrier density[21] (n_c) and the electron temperature (T_c). For the direct optical transition in MQW, the luminescence intensity is given by:

$$I(E_i, t) = C_i(1-e^{-t/\tau_r})[\,|M_{e-hh}|^2\rho_e f_e \rho_{hh} f_h + |M_{e-lh}|^2\rho_e f_e \rho_{lh} f_h\,], \quad (1)$$

where the $\rho_{e,hh,lh} \sim m_{e,hh,lh}$ are the density of state for electron, heavy-hole, and light-hole; the $M_{e-hh(lh)}$ is the matrix element[22] for electron to hh(lh) transition; C_i absorbed all the constant factors including the corrections for detector response and the transmission of each narrow band filters used; τ_r is the rise time of luminescence and is set to be $\sim$ 1ps which is an up-limit of thermalization time of electron-hole system;

$$f_{e,h} = \frac{1}{e^{(\epsilon_i - u_{e,h})/KT_c} + 1} \quad (2)$$

is the Fermi-Dirac distributions for the electrons in conduction band (with subscript e) and for the holes in valence band (with subscript h).

An **unique** set parameters of $T_c(t)$ and $u_e(t)$ was determined by consistently fitting **all** the luminescence profiles detected at different photon energies E_i. Three calculated luminescence profiles corresponding the experimental data are shown in Fig.4 by the thick solid curves.

The determined T_c as function of time is plotted as the solid curve in Fig.5. The shaded area reflects the extent of the uncertainty in deducing the carrier temperature within the first 4ps due to our limited time resolution. The plotted data in Fig.5 is interpreted as follows. Carrier-carrier collisions quickly leads to a thermalized distribution at very high T_c within 1ps due to a large number of hot carriers excited.[23] Although an initial thermalization process of carriers can only be probed by fem-

tosecond spectroscopy. An initial cooling of the thermalized distribution is studied with our present time resolution of 2ps, providing information about the energy relaxation and the density decay of photogenerated carriers. The initial cooling within first 5ps is very fast (250K/ps) reflecting both the screening[1] and NE phonon effects are small. After the initial cooling, a large number of longitudinal optical phonons in a finite wavevector space accumulates due to the finite phonon lifetime.[24] The phonons emitted by the hot electrons are reabsorbed by the electrons as a reverse process of the emission giving rise to a slower cooling for the hot carriers.[3] It should be emphasized here that the rapid initial cooling rules out the importance of significant screening of electron-phonon interaction in the present study. If the initial screening was important,[1] the initial rapid cooling would be slowed and a NE phonon population would not be built up.

Another important observation displayed in the Fig.5 is that the time constant for the slow decay component of carrier temperature cooling curve is ~30ps which is same as the decay time of the NE phonon stimulated phonon replica emission at 780nm (see Fig.4). This suggests that ~5ps is required for the electron system and the NE phonon system to be essentially equilibrated with each other. The coupled electron-phonon system decays with a common decay constant of about 30ps. It should be emphasized that this time constant (30ps) is the lifetime of NE phonons which differ from the equilibrium phonon lifetime of ~7ps. The longer lifetime for the NE phonons than equilibrium phonon is due to the coupling between the hot electrons and NE phonons.

The determined quasi-Fermi-energies for electrons and holes are plotted in Fig.6. The changes of u_e and u_h are very rapid with the first 10ps reflecting a rapid decrease of the carrier density. The behavior of the degeneracy for electrons and holes with function of time is reversed due the difference in effective masses for the electrons and holes.

The quasi-equilibrium distribution functions for the electrons and the holes can be experimentally determined from $T_c(t)$ and $u_{e,h}(t)$. Using these distributions the energy loss rates for the electrons and holes can be obtained. The energy loss rate ($P_{e,hh}$) is defined as follows:

$$P_{e,hh} \equiv \frac{d\ <E>_{e,hh}}{dt} = \frac{d}{dt}\ [\ \frac{\int_0^\infty \epsilon\, f\ (T_e, u_{e,hh}, \epsilon) d\,\epsilon}{\int_0^\infty f\ (T_e, u_{e,hh}, \epsilon) d\,\epsilon}\ ]. \qquad (3)$$

When the electron-hole system is treated as the Maxwell-Boltzmann gas, the energy loss rate for the carriers (c=e,hh) is given by:

$$P_c = K \frac{dT_c(t)}{dt}. \qquad (4)$$

It should be pointed that the energy loss rates for the electrons and heavy-hole obtained by Eq.(3) are the *net* loss rates. These include the energy loss due to electron(hole)-phonon interactions and the energy exchange between electrons and holes by carrier-carrier scattering. The hole-phonon scattering rate was calculated[25] and measured[6] to be 2.5 to 3 times larger than the rate for the electrons due to the additional coupling through the deformation-potential. The energy transfer from electrons to holes should be expected in our photogenerated carrier system as long as the characteristic time for the electron-hole scattering is shorter than the electron-phonon scattering time.

The determined energy loss rates using Eqs. 3 or 4 are shown in Fig.7. The solid and dotted curves were obtained from Eq.3 for the electrons and heavy-holes, respectively. The dot-dashed curve was obtained from Eq.(4). It should be pointed out that the curves obtained from either Eqs.3 or 4 are the experimental data because the distribution function $f\ (T_c, u_{e,h})$ was experimentally determined. The broken line in the Fig.7 is calculated based on the simple theory[5] where the lattice is treated as a heat bath for the quasi-equilibrium carriers.

The salient features of the data displayed in the Fig.7 are:

(i) The energy loss rate for the electrons is more than two orders smaller than predicted by the simple theory[5] (broken line). The reason for the difference arises from the re-heating of electrons by the NE phonons. The energy loss rate determined for the electrons by scattering with LO-phonons via the wave-vector dependent Frohlich interaction may be even smaller than what we have determined because the net energy loss rate determined from Eq.3 is sum of rates due to electron-phonon interactions and electron-hole interactions. The smaller P_{hh} than P_e is because of the presence of light-hole population and the different masses for the electron and hh which leads to different behavior of quasi-Fermi energies for the electron and hh as function of time.

(ii) The *net* energy loss rates for the electrons and heavy-holes almost follow the rate determined from Eq.(4). The reasons for this are the rapid decrease of u_e as shown in the Fig.6 as well as the slow cooling of the carrier temperature which result in $u_e / KT_e < 0.5$, making the electron-hole system behave more like a Boltzmann gas.

(iii) The energy loss rates increase as T_e increases. The curves in the Fig.7 even bends over and approaches the maximum value of $5.3\times10^{-8}W$ for bulk GaAs. This "bending" behavior reflects the initial rapid cooling of hot carriers and was also observed by Shah *et al*.[6] This may be the indication for the presence of NE phonons in the system.

The average phonon emission time[7,8] for hot carrier to emit a LO phonon is defined by:

$$\tau_{avg} = \frac{E_{LO}}{P_e} e^{-E_{LO}/KT_e} . \qquad (5)$$

The value of τ_{avg} as function of the carrier temperature is plotted in Fig.8. This is just another way to describe the energy relaxation process. As can be seen the τ_{avg} **is not a constant but carrier temperature dependent and hence time dependent.** For $T_e > 1200K$ or $t < 5$ps the τ_{avg} remains at a value of about 1ps. At the initial

stage of carrier cooling only an up-limit of 0.9ps was determined from the data shown in the Fig.4. The theoretical predicted value should be $\sim 0.16ps$ [7] which is consistent with our value within the limited time resolution. As time t > 5ps (or $T_c < 1200K$) the τ_{avg} increases quickly with decrease of the carrier temperature reflecting that a large NE phonon population is built up and the carrier cooling is suppressed. At $T_c = 480K$, τ_{avg} is 10ps. Ryan *et al.*[8] obtained a constant value of 7ps for τ_{avg} by studies of time-resolved PL of modulation doped-MQW. The reason for this is simply because their time resolution of $\sim$20ps did not allow them to monitor the entire carrier cooling process.

Information about the time dependence of initial carrier population can be obtained using the experimentally determined distribution function $f_{e,h}$. The densities are obtained by the following expressions:

$$n_e(t) = \int_0^\infty \rho_e \, f_e \, d\epsilon ; \tag{6}$$

$$n_{hh}(t) = \int_0^\infty \rho_{hh} \, f_h \, d\epsilon ; \tag{7}$$

$$n_{lh}(t) = \int_{\Delta E}^\infty \rho_{lh} \, f_h \, d\epsilon , \tag{8}$$

where ΔE is the energy separation between the hh- and lh-subbands at the zone center. The carrier densities for the electrons, heavy-holes, and light-holes as function of time are plotted in Fig.9. The quantity of $ln\,[n_e(t)]$ is also plotted in this figure as a broken curve.

The salient feature of the data in the Fig.9 is that the carrier density decreases non-exponentially and varies (by a factor of 10) rapidly within the first 30ps after the excitation by laser pulse. One can not define a single carrier lifetime due to the non-exponential nature of the density curves. However, an effective carrier depletion time [density decreases by a factor of e^{-1} from $n_e(t=0)$] is deduced to be as short as 10ps. The slow component of density decay curve reflects part of bimolecular recombination process. The fast decrease of carrier density occurring in such a short time period cannot be accounted for by the usual bimolecular recombination, which is a

much slower process, on a nanosecond time scale in a bulk GaAs and about 350ps in quantum well structure with well thickness of $\sim$5nm.[26] Several other possibilities should be pointed out and discussed:

(i) Rapid carrier diffusion process may be utilized[27] to shorten the lifetime of the carriers within an excited spot. Assuming the velocity of photoexcited carriers moving in the directions perpendicular to the z-axis is on an order of $10^7 cm/s$, an extremely small radius of about $1um$ for the excitation spot would be required to decrease carrier density by a factor 10 in the excited region. Since the radius of the excitation spot was abcut $160um$ in our experiment, the carrier diffusion out of the excited region can not result in the ultrafast depletion time of 10ps.

(ii) Auger recombination resulting from strong electron-electron Coulomb interaction may be very efficient and causes a substantial shortening of carrier lifetime at high carrier density in a quasi-two-dimensional carrier system. But from a comparative study,[28] Auger recombination in semiconductor MQW structure and bulk were found to be close to each other. Using a value of $1.5\times10^{-29} cm^6 s^{-1}$ for the nonradiative Auger rate in bulk GaAs at room temperature,[29] Auger recombination lifetime at carrier density of $10^{19} cm^{-3}$ should be 670ps which is about 100 times larger than the carrier depletion time. However, a detailed study of Auger recombination in semiconductor MWQ structures under the condition of high carrier density, high carrier temperature, low lattice temperature, and presence of a large population of NE LO phonons does not exist in the literature.

(iii) Finally, let us consider what role the NE phonons can play in reducing the initial carrier depletion time to 10ps. As discussed in the *steady-state* section, there is a stimulated phonon emission process accompanied by an intense stimulated phonon replica which is mainly radiated at the sample edge and propagates parallel to the well plane. We found that the stimulated phonon replica detected along the y-direction also had a decay time constant about 30ps which is same as that detected

along the z-direction. Therefore, it is most likely that the initial rapid carrier depletion is due to the participation of the NE LO phonons which stimulates the emission of phonon replica. It should be noted that this stimulated process is remarkablely different from the regular stimulated emission process in which phonons do not participate. As in semiconductor lasers, the stimulated emission is less effective at room temperature. Moreover, a longitudinal optical phonon (LO)-phonon replica plays no significant role in the laser operation of bulk GaAs, which is expected because of the weak electron-phonon coupling. Therefore, the prominence of phonon-assistant recombination in our quantum well structure is due to the presence of a large number of NE LO-phonons produced in the relaxation process of hot carriers. *By employing the NE-phonon model we able to explain not only the slow carrier cooling but also the ultrashort carrier depletion time in highly photoexcited undoped quantum well structures.*

V Conclusion

With 2ps time resolution we are able to study the initial energy relaxation of the hot carriers and the decrease of carrier density simultaneously. The existence of a large population of NE phonons in highly excited semiconductor quantum well structures is experimentally verified. Its effect on the energy relaxation is to slow down the cooling rate after an initial rapid cooling (0-5ps). A new mechanism used to explain the ultrashort carrier depletion time $\sim 10ps$ deduced from the fitting of time-resolved PL profiles at different emitted photon energies is proposed to be associated with NE phonon stimulated phonon replica emission rather than other nonradiative processes.

VI Acknowledgments

The research was funded by the U.S. Air Force Office of Scientific Research under Grant No. AFOSR-86-0031. We thank Jimmy Zheng for the technical help and K. Bajaj for helpful discussions.

Reference

(1) R. J. Seymour, M. R. Junnarkar, and R. R. Alfano, Solid State Commun. 41, 657(1982).

(2) J. Shah, Solid-State Electronics, 21, 43(1978).

(3) H. M. van Driel, Phys. Rev. B, 19, 5928(1979).

(4) C. V. Shank, R. L. Fork, R. Yen, J. Shah, B. I. Greene, A. C. Gossard and C. Weisbuch, Solid State Commun. 47, 981(1983).

(5) E. M. Conwell, "High Field Transport in Semiconductor" (Academic, New York, 1967).

(6) J. Shah, A. Pinczuk, A. C. Gossard, and W. Wiegmann, Phys. Rev. Lett., 54, 2045(1985).

(7) C. H. Yang, Jean M. Carlson-Swindle, A. Lyon, and J. M. Worlock, Phys. Rev. Lett., 55, 2359(1985).

(8) J. F. Ryan, R. A. Taylor, A. J. Turberfield, A. Maciel, J. M. Worlock A. C. Gossard, and W. Wiegmann, Phys. Rev. Lett. 53, 1841(1984)

(9) K. Leo, and W. W. Ruhle, Solid State Commun., 62, 659(1987).

(10) Kai Shum, M. R. Junnarkar, H. S. Chao, R. R. Alfano, (unpulished).

(11) R. Sooryakumar, D. S. Chemla, A. Pinczuk, A. C. Gossard, W. Wiegmann, and L. J. Sham, Solid State Comm., 54, 859(1985).

(12) J. E. Zucker, A. Pinczuk, D. S. Chemla, A. C. Gossard, and W. Wiegmann, Phys. Rev. Lett., 53, 1280(1984).

(13) H. Iwamnra, T. Saku, H. Kobayashi, and Y. Horikoshi, J. Appl. Phys., 54, 2692(1983).

(14) W. Cai, M. C. Marchetti, and M. Lax, Phys. Rev. B, 35, 1369(1987).

(15) P. Lugli, and S. M. Goodnick, Phys. Rev. Lett. 59, 716(1987).

(16) N. Holonyak, Jr., R. M. Kolbas, W. D. Laidig, B. A. Vojak, H. Hess, R. D. Dupuis, and P. D. Dapkus, J. Appl. Phys., 51, 1328(1980).

(17) P. Blood, E. D. Fletcher, P. J. Hulyer, and P. M. Smowton, Appl. Phys. Lett., 17, 1111(1986).

(18) M. S. Skolnick, K. J. Nash, P. R. Tapster, D. J. Mowbray, S. J. Bass, and A. D. Pitt, Phys. Rev. B, 35, 5925(1987).

(19) The absolute intensity at different transition energies was obtained with same excitation condition. To do this, we fixed the channel plate gain, temporal analyzer gain, prepulse intensity as well as time scale for the weakest signal (at high energy tail) to be detected. The intensity of pre-pulse was then treated as the standard of excitation level.

(20) The decay times were obtained by fitting the data in Fig.4 to the expression of $I(E,t) = I_0[1-e^{-t/\tau_r}]e^{-t/\tau_d}$, where the parameters I_0, τ_r, and τ_d are the proportional constant, the rise time, and the decay time, respectively.

(21) The quasi-Fermi energy of holes (u_h) is related to the quasi-Fermi energy for electrons (u_e) and the carrier temperature by the relation of $n_e = n_{hh} + n_{lh}$, and is given by $u_h = KT_c \ln[e^{a\ln(1+e^{u_e/KT_c})} - 1]$, where $a = \frac{m_e}{m_{hh} + m_{lh}}$.

(22) The ratio of squared matrix elements between $e-hh$ and $e-lh$ was estimated from a calculation by Y. C. Chang and G. Sanders, Phys. Rev. B, 32, 5521(1985).

(23) For a recent review, see J. Shah and R. F. Lehery in "Semiconductors Probed by Ultrafast Laser Spectroscopy" edited by R. R. Alfano, Academic Press, New York,1984; pg.45.

(24) R. K. Chang, J. M. Ralston, and D. E. Keating, in "proceeding of the International Conference of Light Scattering Spectra of Solid", edited by G. B. Wright (Springer-Verlag, New York, 1969), pg.369.

(25) M. Costato, and L. Reggiani, Phys. Status Solidi (b) 58, 47(1973).

(26) E. O. Gobel, H. Jung, J. Kuhl, and K. Ploog, Phys. Rev. Lett., 51, 1588(1983).

(27) Y. Silberger, P. W. Smith, D. J. Eilenberger, D. A. B. Miller, A. C. Gossard, and W. Wiegmann, Opt. Lett. 9, 507(1984).

(28) B. Sermage, D. S. Chemla, D. Sivco, and A. Y. Cho, IEEE J. Quantum Electron., vol. QE-22, 774(1986).

(29) A. Haug, J. Phys. C 16, 4159(1983).

Figure Caption

Fig.1 Time-integrated luminescence spectra at various lattice temperatures. The peaks A, B, and C are explained in the text.

Fig.2 Triangles are the ratios of the peak intensity of B and A indicated in the Fig.1. The solid curve is explained in the text.

Fig.3 Time-integrated PL spectra taken in the geometry as shown in the inset at 100K.

Fig.4 Time-resolved PL profiles (thin solid curves) from the symmetric MQW at 4K at various wavelengths. The narrow peaks within 0-10ps are the pre-pulses used for averaging. The next peak of dotted curve is the Rayleigh scattering light from the sample surface. The thick broken curve is generated by an expression of $I(E,t)=I_0[1-e^{-t/\tau_r}]e^{-t/\tau_d}$ and the thick solid curves are generated by Eq.(1).

Fig.5 Experimentally determined carrier temperature as function of time. The shaded area indicates the extent of uncertainty in deducing carrier temperature within first 4ps.

Fig.6 Experimental determined quasi-Fermi energies for electrons (up solid curve) and for holes (down solid curve).

Fig.7 Experimentally determined *net* energy loss rates for electrons (e) and heavy-holes (hh) obtained from two quasi-equilibrium Fermi-Dirac distribution functions. The dot-dashed curve is obtained from Maxwell-Boltzmann distribution function. The broken line is theoretical result for bulk GaAs without the effects of screening and nonequilibrium phonons. The power unit is 10^{-10} watts.

Fig.8 Experimentally determined average phonon emission time as function of carrier temperature.

Fig.9 Experimentally determined carrier densities as function of time. e for electron, hh for heavy-hole, and lh for light-hole. The broken curve is the nature loga-

rithm plot of electron density.

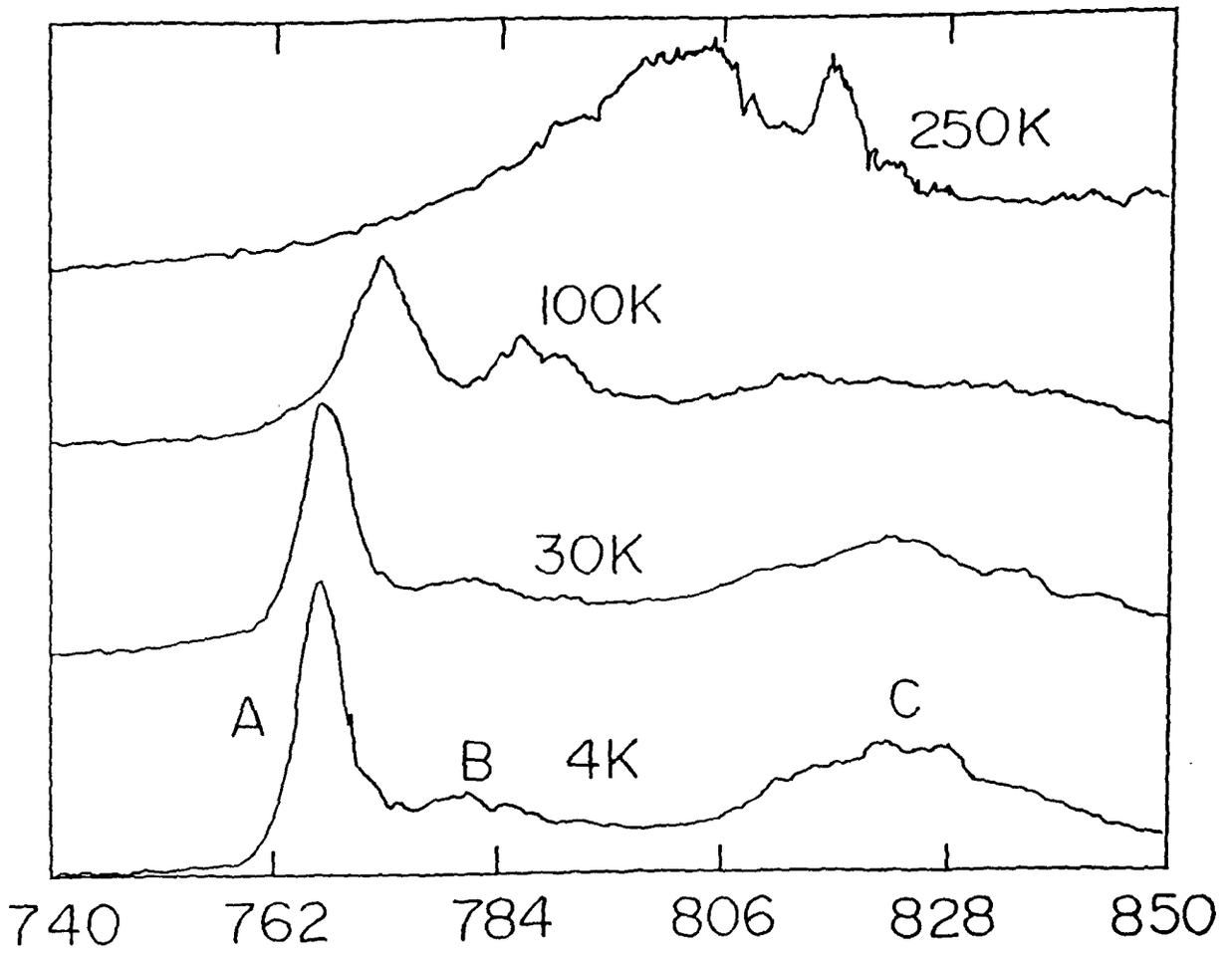

Fig.1

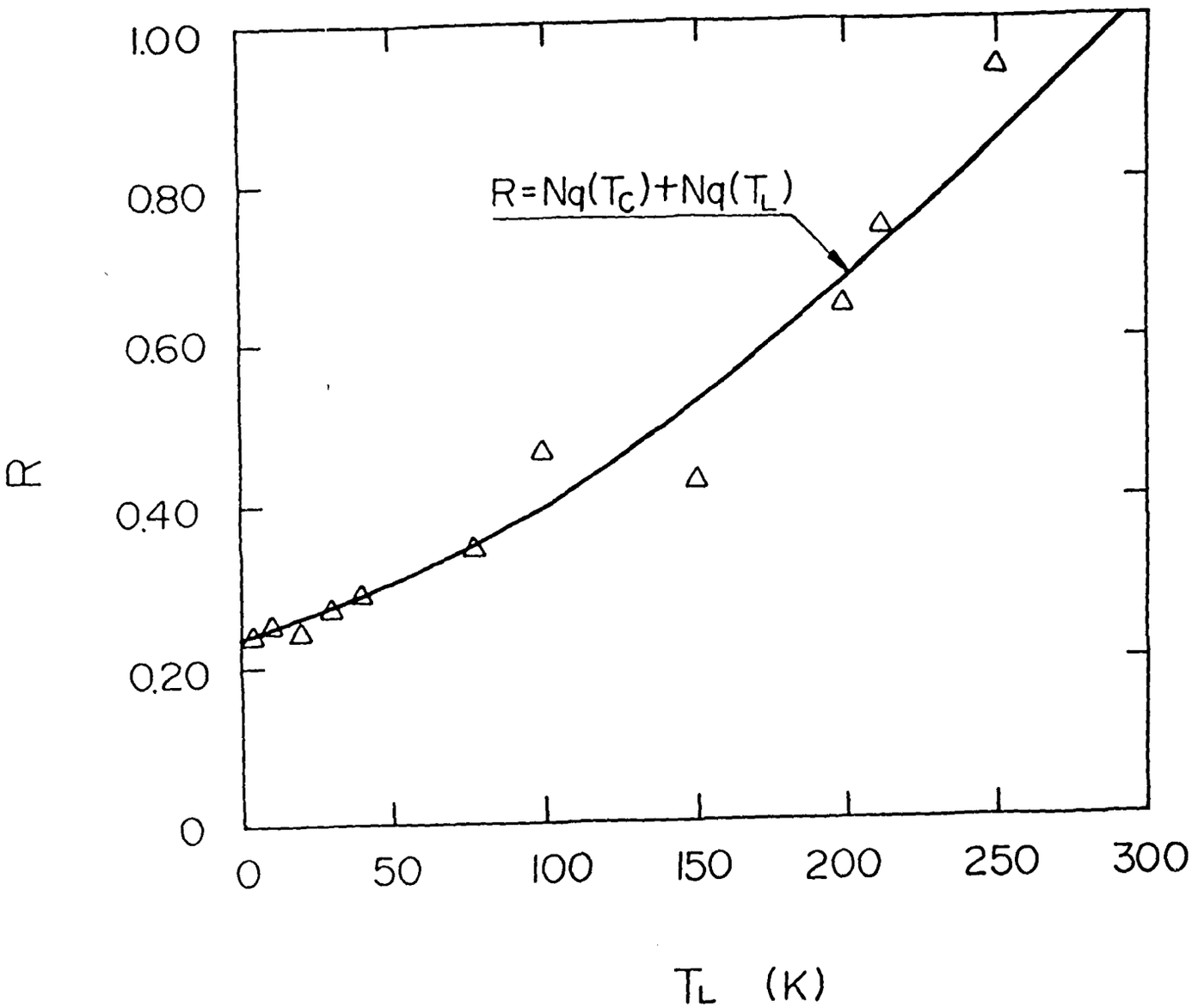

Fig.2

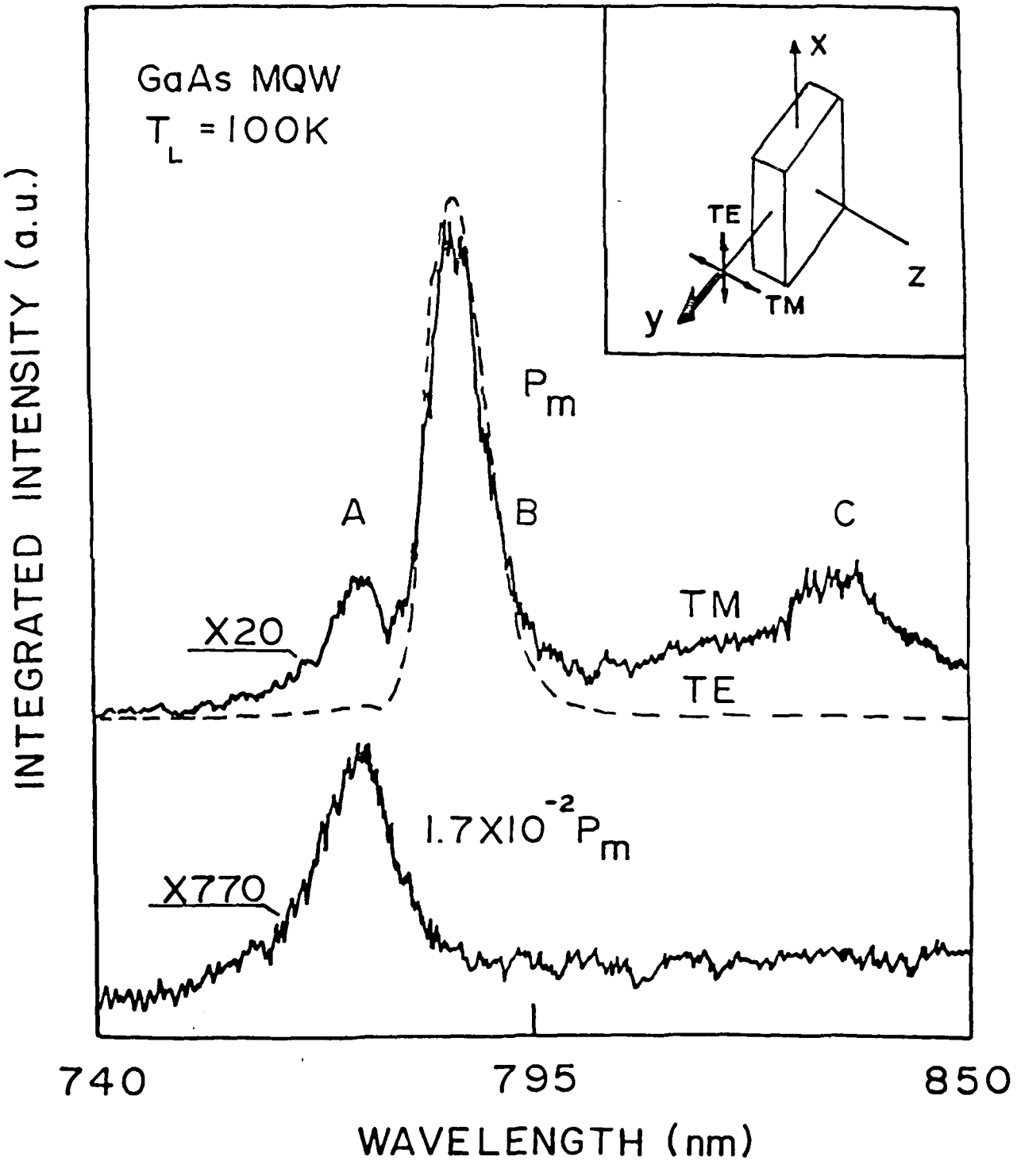
GaAs MQW
T_L = 100K
X
TE
TM
Z
y
P_m
A
B
C
TM
TE
X20
$1.7X10^{-2}P_m$
X770
INTEGRATED INTENSITY (a.u.)
740
795
850
WAVELENGTH (nm)

Fig.3

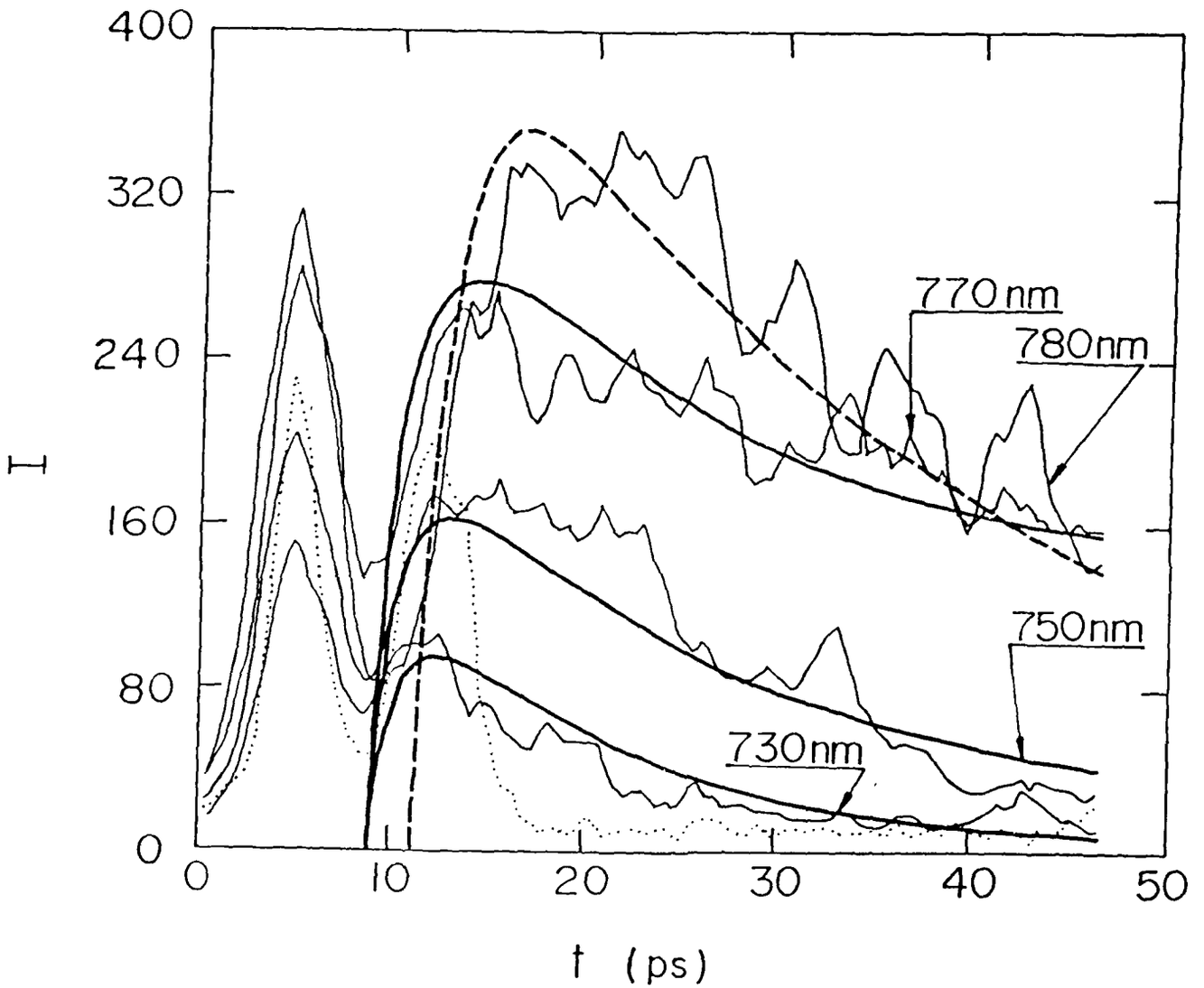
400
320
240
160
80
0
I
0
10
20
30
40
50
t (ps)
770nm
780nm
750nm
730nm

Fig.4

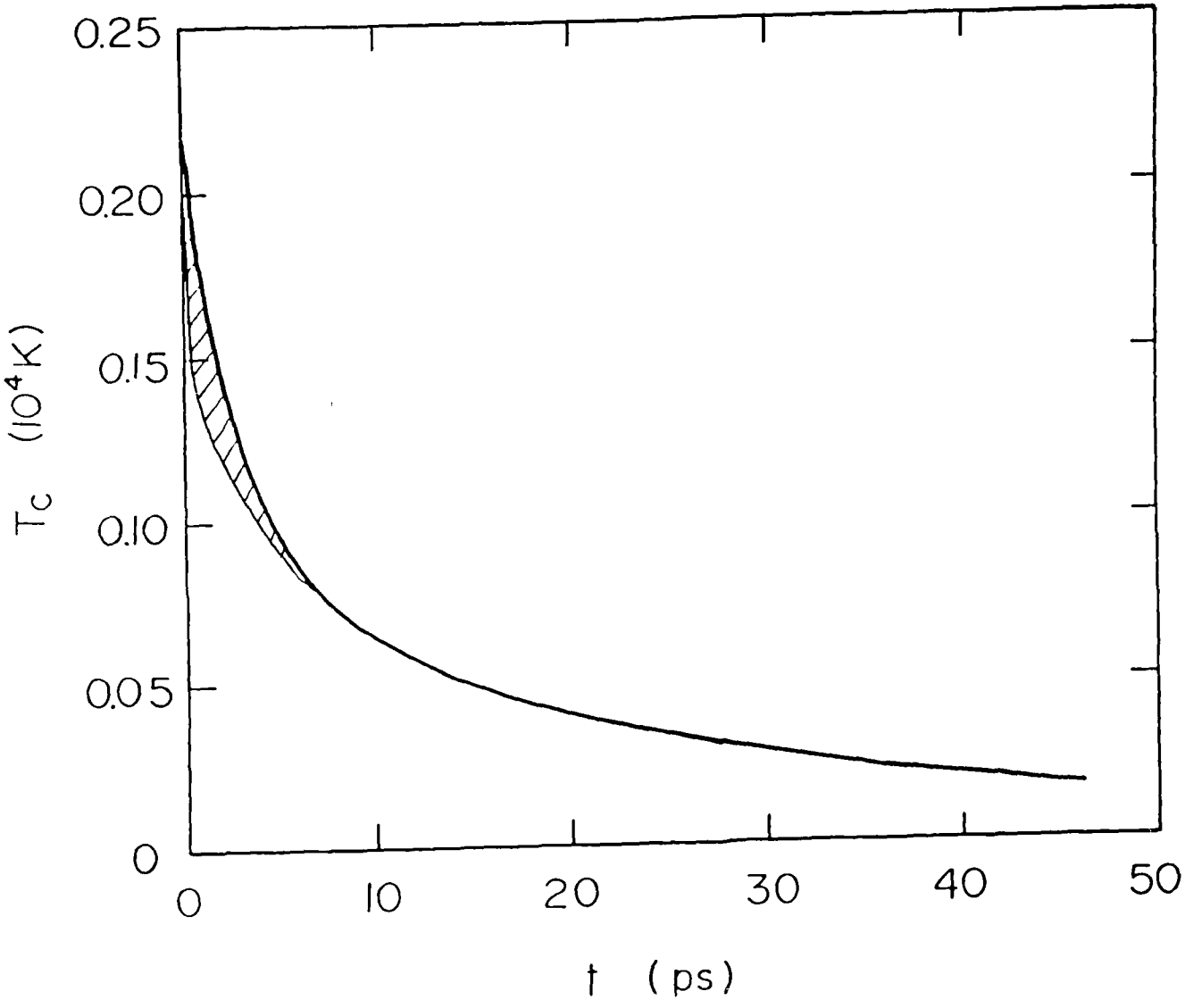

Fig.5

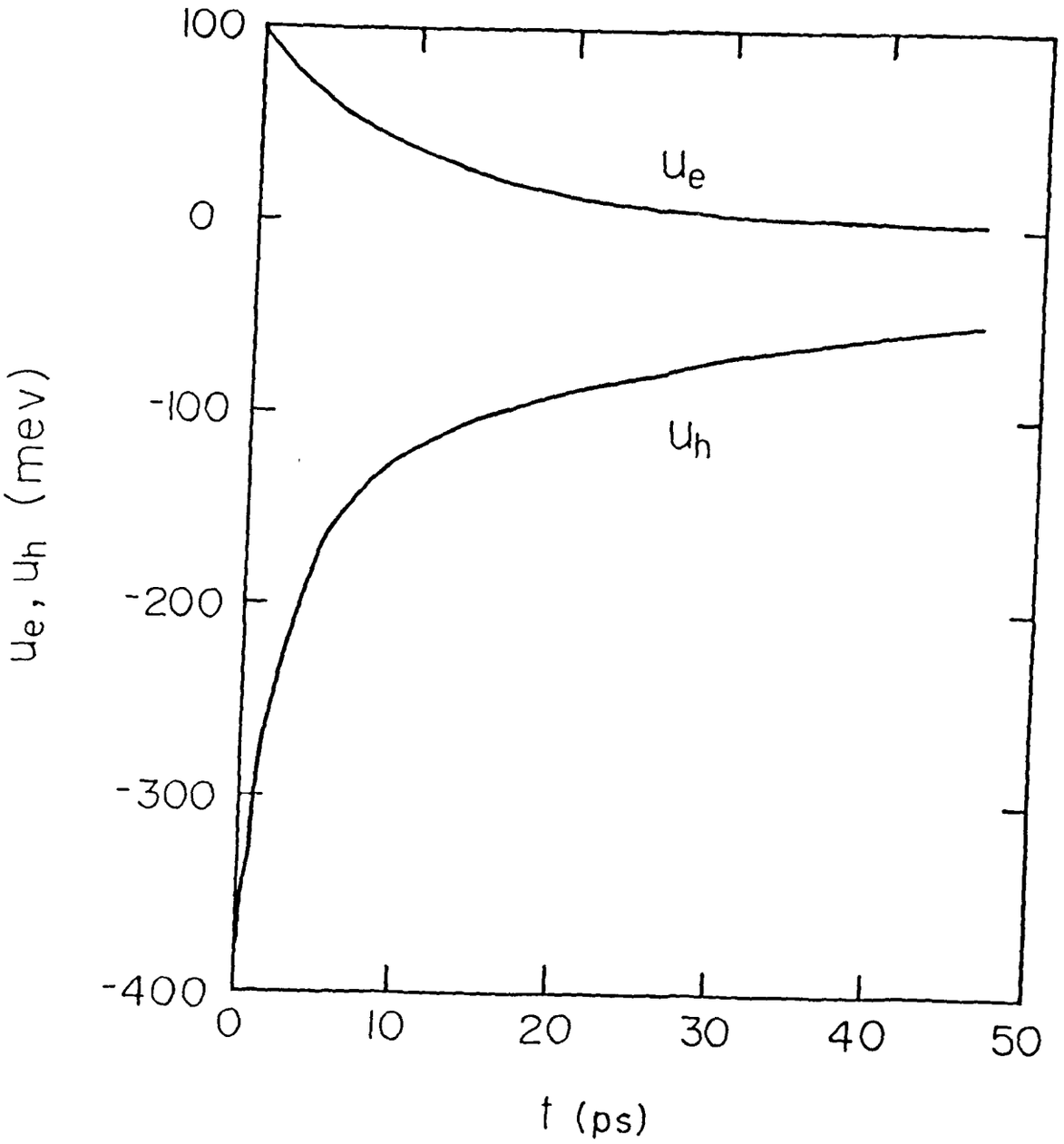

Fig.6

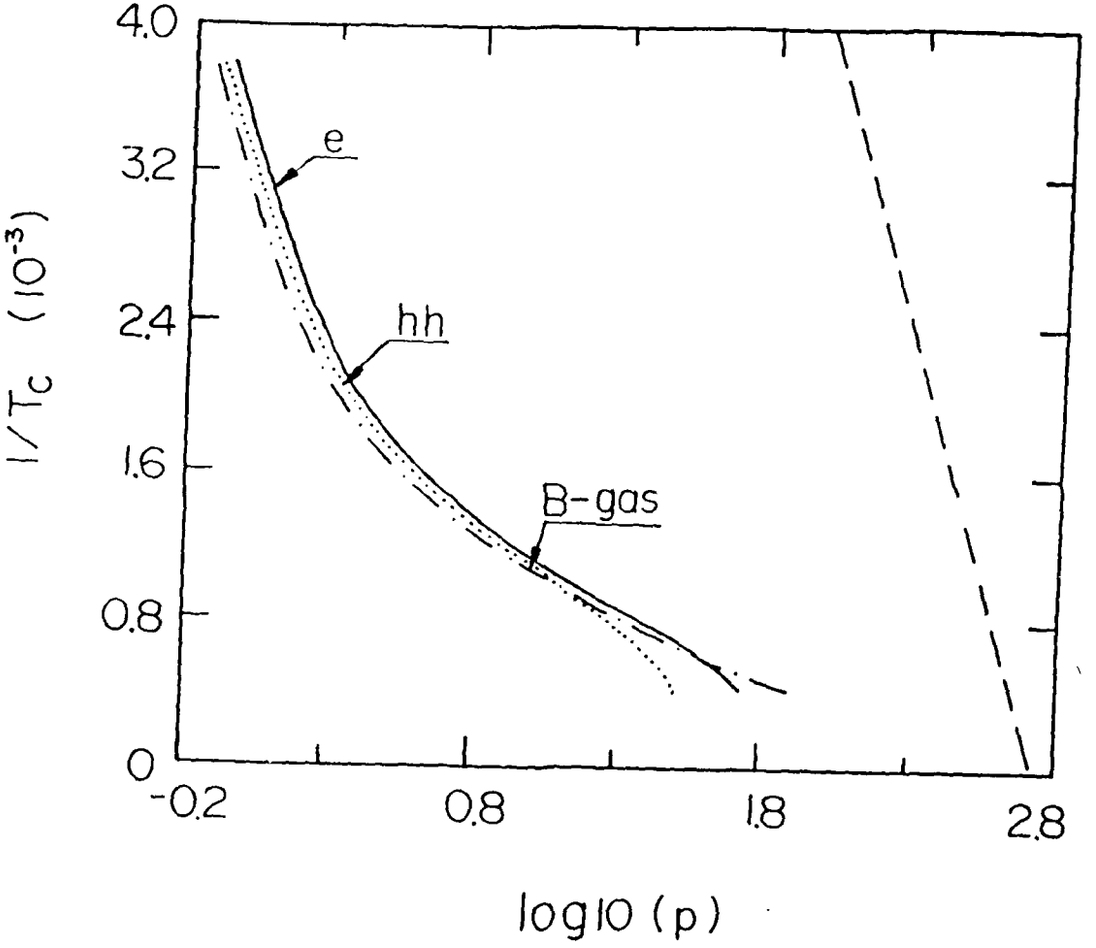

Fig.7

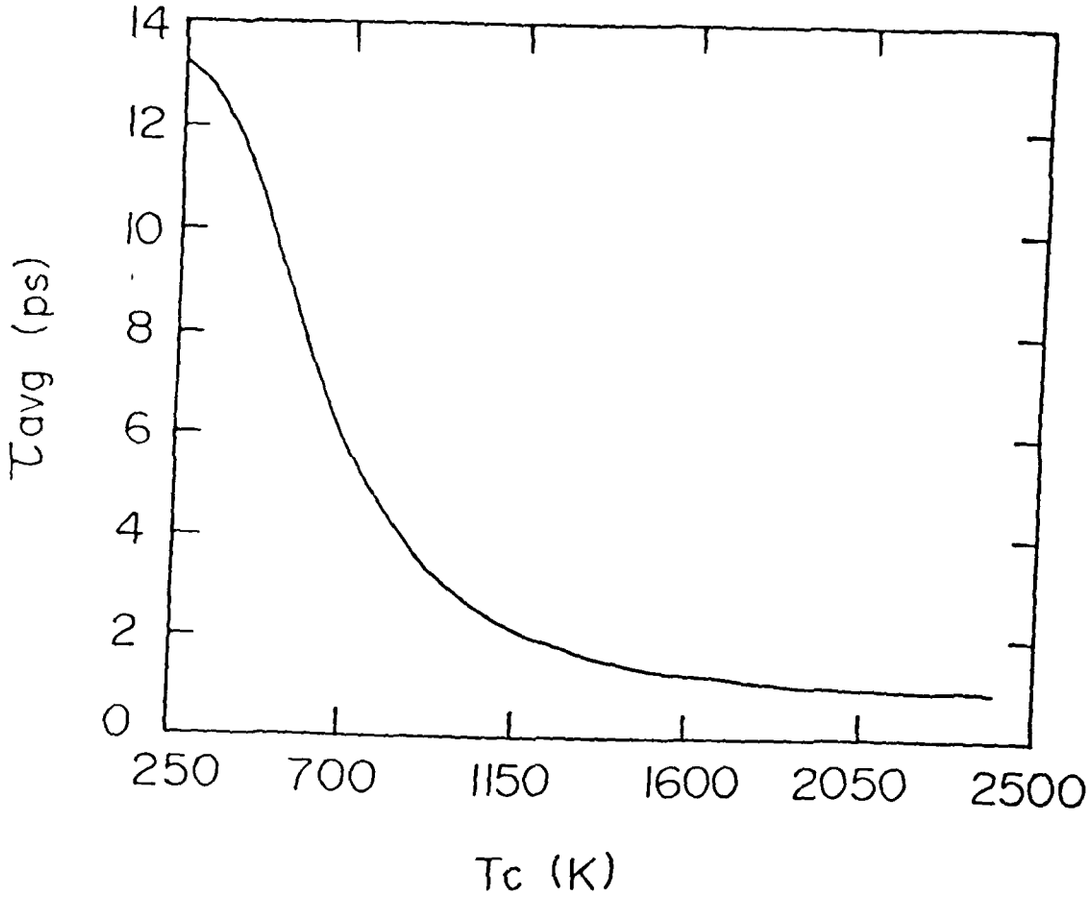

Fig.8

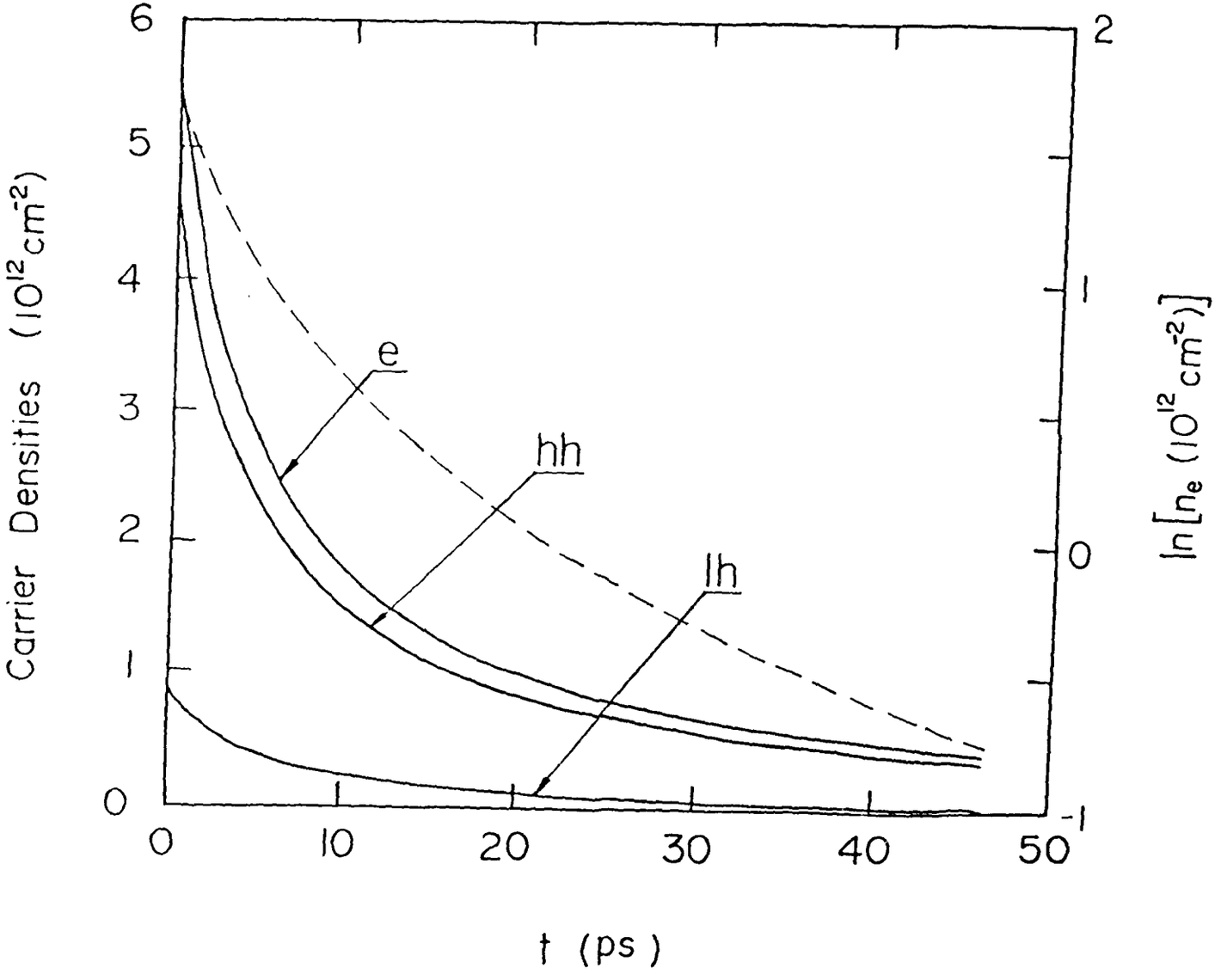
Carrier Densities ($10^{12}cm^{-2}$)
$\ln[n_e\ (10^{12}cm^{-2})]$
e
hh
lh
t (ps)
0
10
20
30
40
50
0
1
2
3
4
5
6
-1
0
1
2

Fig.9

Observation of Ultrafast Lateral Expansion of Energetic Carriers in An Asymmetric GaAs Quantum Well

Kai Shum, H. S. Chao, M. S. Junnarkar, and R. R. Alfano

Institute for Ultrafast Spectroscopy and Lasers

Departments of Electrical Engineering and Physics

The City College of New York, New York, New York, 10031

T. Hederson, and H. Morkoc

Coordinated Science Laboratory, University of Illionis at

Urbana-Champaign, Urbana, Illinois 61801

ABSTRACT

Lateral expansion of energetic carriers excited by an intense 0.5-ps laser pulse in a single asymmetric GaAs quantum well is investigated at 4.3K using a streak camera. On a picosecond time scale, it is observed that the carriers expand from the excitation spot at an ultrafast speed of $\sim 10^8 cm/s$. A comparison, under identical conditions, of the asymmetric and symmetric quantum well results sheds light on the mechanism that leads to such an extraordinary large carrier expansion velocity.

PACS numbers: 66.30.Dn, 72.20. Jv., 73.40. Lq.

Over several years, spatial expansion of photoexcited carriers in semiconductor bulk and microstructures has been a subject of great interest. Based on the photoluminescence (PL) data, Forchel *et al.*[1] have suggested that the fast **ambipolar diffusion** of optically excited carriers in a wide varity of semiconductors (e.g., Si, Ge, GaAs, CdS, and ZeSe) at a speed comparable to Fermi velocity is essential for the understanding the broad line shape of the luminescence spectra. Later, Steranka and Wolfe[2] pointed out that the fast-diffusing model[1] overestimated carrier expansion velocity by an order of magnitude on nanosecond time scale in indirect-gap Si due to neglecting the local lattice heating effect. Subsequently, Tsen[3] confirmed the results of Steranka and Wolfe[2] on a picosecond time scale by time-resolved Raman scattering. Using excite-probe technique, Majumder *et al.*[4] found the carrier expansion velocity was smaller than Fermi velocity in the direct-gap CdS and CdSe. In contrast, many groups deduce from their experiments carrier expansion velocity $v_e \geq 10^7 cm/s$ in GaAs[5,6] and CdSe.[7,8] This value is roughly equal to the Fermi velocity of carriers and exceeds group velocities of longitudinal and transverse acoustic phonons by about 2 orders of magnitude, thus, supporting the fast-diffusing model of Forchel *et al.*[1] in these direct-gap polar materials. Theoretically, Wautelet and Van Vechten[9] have inferred that hot carriers generated by nanosecond laser pulses will be confined near the excitation spot; while a spatial expansion of photoexcited carriers is expected from both hydrodynamic[5,10] and thermodiffusive[11] points of view. Recently, Steranka and Wolfe[2] have suggested that nonequilibrium (NE) phonon effects[12] (**phonon wind**) must be taken into account in a more realistic description of the dynamic carrier expansion process. The NE phonons created in hot-carrier relaxation process provide a large driving force for carrier expansion.

In GaAs/AlGaAs system, the band-discontinuities at the interfaces of GaAs and AlGaAs leads to the formation of two-dimensional electronic energy subbands in the

GaAs region. Recent Raman-scattering studies by Sood *et al.*[13] provided evidence for the presence of interface phonon modes and confined longitudinal optical (LO) and transverse optical (TO) phonons in GaAs well layer. One would like to kown how carrier confinement, modified phonon modes, and well shape influence the dynamic process expansion of photoexcited carriers in a quantum well structure. Most recently, Tsen and Morkoc[14] have shown no influence of the effects of reduced dimensionality for carriers and phonons on photogenerated carrier expansion in GaAs/AlGaAs symmetric MQW structures using picosecond time-resolved Raman scattering at a low carrier density of $\sim 10^{16} cm^{-3}$. Their measured expansion velocity of $8.6\times10^{6} cm / s$ is consistent with the fast-diffusing model of Forchel *et al.*[1]

In this letter, we report on the first **real time** investigation of ultrafast hot carrier **expansion process** associated with an ultrashort carrier depletion time of $\sim$ 10ps in an asymmetric GaAs quantum well at 4.3K using a 2-ps-resolution streak camera system. By studies of time-resolved PL arising from the recombination of energetic electron and hole detected from a lateral displaced region $\sim 300um$ away from the center of the excitation spot which is $\sim 160um$ in diameter, it is observed that the hot carriers expand from the excitation spot at an ultrafast speed of $\sim 10^{8} cm / s$. Through a **comparison** of the **symmetric** and **asymmetric** quantum well results under identical conditions, it is concluded that the observation of such a fast **hot carrier expansion process** is made possible **only** in the **asymmetric** well with the higher energy barrier such as to prevent from carrier expansion in the well direction. Density and cooling of photogenerated carriers are independently determined by analysis of time-resolved PL from the excitation spot. We have demonstrated that cooling of hot carriers is severely slowed by the NE phonon heating effect and the carrier density decays very rapidly within the first 30ps after the excitation by 0.5ps laser pulse due to the NE phonon stimulated phonon replica.

In our experiments, an intense laser pulse of 0.5ps at 620nm was used to excite

the electron-hole pair density of $\sim 10^{19} cm^{-3}$. The excitation source is from a colliding-pulse passive-mode-locked dye laser amplified by a four-stage dye amplifier pumped with a frequency doubled Nd: YAG laser operated at 20Hz. The undoped GaAs/$Al_xGa_{1-x}As$ asymmetric and symmetric quantum wells investigated in this work were grown by molecular-beam epitaxy on a (001)-oriented undoped GaAs substrate. The asymmetric quantum well consists of layers from the front surface to substrate 150Å $Al_{0.3}Ga_{0.7}As$, 50Å GaAs well, 200Å AlAs (asymmetric barrier), and followed by $1um$ $Al_{0.3}Ga_{0.7}As$, and $0.2um$ GaAs buffer. The symmetric well structure used for the comparative studies consists of 50 periods of 55Å GaAs and 100Å $Al_{0.3}Ga_{0.7}As$ layers followed by a $1.2um$ GaAs buffer layer. The excellent quality of the samples are confirmed by well resolved heavy-hole and light-hole excitonic structures in room temperature PL spectra.

First, we discuss the measurements of the differences in the spatial widths of time-integrated laser and PL intensity profiles on the sample surface. The hot PL profiles (solid curves) detected within a spectral window of 35nm (90meV) centered at 700nm (1.771eV) for the asymmetric and symmetric wells along with the profiles (broken) of corresponding exciting laser at a fixed intensity are plotted in Fig.1a and Fig.1b, respectively. The gain of detecting system was adjusted such that the maximum intensities recorded for the PL and laser were roughly same. The insets show the potential profiles of the asymmetric and symmetric wells. It is clear that the half-width of PL profile for the asymmetric well is much broader than for the symmetric wells. This implies that the energetic carriers (about 3 LO-phonon energies above the subband edge) in the asymmetric well is much more mobile than in the symmetric well.

By making use of the two electronic windows of the streak camera, time-resolved PL intensities of the asymmetric well, $I_{w1}(t)$ and $I_{w2}(t)$, from the excited and unexcited regions, respectively, were measured. The subscripts w1 and w2

($r_1 \rightarrow r_2$) stand for the two windows as being positioned in the Fig.1. The $I_{w1}(t)$ and $I_{w2}(t)$ (thin solid curves) measured at 4.3K with $\sim$2ps time resolution are displayed in Fig.2. The peak of the broken curve is the Rayleigh scattering light (620nm) from the sample surface which defines the "zero" time for our analysis. The thick solid curves are the theoretical fits which will be discussed below. As can be seen the rise of the I_{w1} is time-resolution limited, while the rise of I_{w2} is much slower than that of the I_{w1}. The slow rise time[15] of I_{w2} ($\tau_r^{w2} \geq 100$ps) is essential to suppoort that the luminescence detected from the laterally displaced w2 indeed arises from the recombination of electron and hole which come from the w1. It eliminates one possible artifact that may lead to anomalously strong luminescence detected from the w2. Such a possibility arises from the 1*um* layer of $Al_{0.3}Ga_{0.7}As$ which is next to the AlAs barrier. This layer is also highly excited by the 620nm laser pulse. Possible recombination radiation (although we did not detect for the asymmetric well, neither for the symmetric well) from $Al_{0.3}Ga_{0.7}As$ layer will excite carriers within the well. This secondary excitation would not be limited to the originally excited region giving rise secondary luminescence. Since the speed of light in GaAs is about 100*um* /ps, the luminescence intensity I_{w2} would rise quite similarly with the I_{w1}. This is contrary to our experimental observation.

Having known the expansion distance (294*um*) from the center of the w1 to the inner edge of the w2 and assuming the time it takes for carriers to expand from the w1 to w2 where they recombine is equal to the rise time of I_{w2}, an up-limit of the expansion velocity v_e is estimated to be about $2.94\times10^8 cm/s$ (294*um* / 100ps).

The decay of the I_{w1} is dependent upon a transient carrier distribution in the w1 which determines the number of carriers in the given energy space as function of time. In order to obtain the carrier distribution (assumed to be Fermi-Dirac distribution), the time-resolved PL profiles detected in narrow (20meV) spectral regions which cover the whole emission band were measured from the region w1 at 4.3K.

We have introduced an expression[16] using the carrier temperature [$T_c(t)$] and the quasi-Fermi-energy for electrons [$u_c(t)$] as a set of parameters to consistently fit these measured profiles. Three typical measured profiles as well as theoretically fitted curves (thick solid) are plotted in Fig.3a. The subband edge luminescence is centered $\sim$760nm. The cooling of hot carriers is substantially slowed down after $\sim$5ps due to reabsorption of NE phonons by the carriers.[16-18] The electron density $n_c(t)$ and ln [$n_c(t)$] are plotted in Fig.3b. The salient feature of the plotted data is that the carrier density decreases nonexponentially and very rapidly form 0 to 30ps. One can not define a single lifetime to describe the carrier density decay. However, an effective carrier depletion time [the time for n_c to decrease by a factor of e^{-1} from $n_c(t=0)$] can be deduced to be as short as 10ps. Such an extremely rapid carrier density decrease can not be accounted for by an usual bimolecular recombination which is in nanosecond time scale for a bulk GaAs and about 350ps for a quantum well structure with well thickness of $\sim$50Å.[19] But it can be explained consistently by the participation of NE phonons in the highly excited system. Since NE phonons are localized both in a wavevector space and in a real physical space (in the well plane) they will behave like **coherent Bosons.** The existence of the coherent Bosons will tend to increase the number of the Bosons in the system with a rate proportional to the present number of Bosons. This is a stimulated phonon emission process and can be accomplished by a phonon replica, when an electron recombines with a hole, not only a photon but also a phonon or more phonons will be emitted to join Boson system. Such a NE phonon stimulated phonon replica has been reported previously by Holoayak *et al.*[20] We have recently confirmed[16] this novel process in the symmetric wells by monitoring the phonon replica which is mainly radiated in the lateral x-y plane in time domain as well as detailed polarization studies of integrated luminescence spectra.

Using the determined carrier distribution, the solid curve as shown in Fig.2a is

theoretically generated to fit the measured I_{w1}. Good fitting indicates that the photogenerated carrier system is not a purely diffusive system.

We now discuss possible origins for the observed anomalously large expansion velocity of the energetic carriers in the asymmetric quantum well but not in the symmetric quantum well.

According to the thermodiffusive model,[1,11] a classical diffusion equation[7] can be employed to fit $I_{w2}(t)$. Assuming the initial photogenerated carrier profile is a symmetric bell-shaped function[7] the carrier density as function of time t and distance r can be written as

$$n(r,t) = n_0 e^{-t/\tau_d^{*2}} \left(1 + \frac{16 \log 2\, D^* t}{a^2}\right)^{-1/2} e^{-\frac{r^2}{a^2/4\log 2 + 4D^* t}}, \qquad (1)$$

where D^* is an *effective* diffusion constant for the energetic carriers in the given spectral region and time scale of ~20ps, n_0 is the carrier density at the center of laser spot, and a is a width-parameter for the initial carrier profile which is determined to be $120um$. When electrons and holes move together in the lateral x-y plane of the asymmetric quantum well, i.e. ambipolar diffusion applies to the present case, the luminescence detected from the w2 should be given by:

$$I_{w2}(t) \sim \int_{r_1}^{r_2} n^2(r,t)\, dr \quad . \qquad (2)$$

Using the above expression to fit the measured I_{w2}, two parameters of D^* and τ_d^{*2} have been precisely determined to be $0.7\times10^6 cm^2/s$ and 13ps, respectively.

It should be investigated whether the determined values for D^* and τ_d^{*2} can be interpreted from the thermodiffusive model.[1,11] Several aspects are discussed below:

(1) The value of D^* is four orders magnitude greater than the regular impurity scattering limited diffusivity. The enhancement of D^* may arise from high carrier temperature and the screening effects[8] at high carrier density. However, the screening effects do not seem to be effective since the initial carrier cooling is very rapid.[16]

(2) The decay rates of carriers which are located in the same energy space but in the different spatial regions of the w1 and w2 are comparable reflecting the dominant process for carrier density decay is not due to the carrier expansion out from the w1 but due to the NE phonon stimulated phonon replica. It is further inferred that a large number of the NE phonons emitted by hot electrons may exist in an area of at least $\sim 300um$ in diameter. These phonons which have momenta parallel to the x-y plane relax to acoustic phonons of large momentum and then these acoustic phonons may drive[2] the carriers outside the excited region. A rough estimation seems support this argument. Let us take a value of 10^{-8} dynes per pair[2] for acoustic phonon-wind force, an excess energy of 140meV per electron-hole pair, and an acceleration time of 1.3ps. Then, a value of $2.8\times10^{8}cm/s$ for carrier expansion velocity is predicted by phonon-wind model.[2,12]

(3) From the determined D^* and τ_d^{*2}, the expansion velocity is calculated by $v_e = \sqrt{\frac{D^*}{\tau_d^{*2}}} = 2.3\times10^{8}cm/s$ which is consistent to the thermodiffusive model[1,11] and the estimated up-limit. In a two-dimensional electron system quasi-Fermi-energy is proportional to carrier density. Therefore, the Fermi-velocity v_F and hence v_e is proportional to the square root of the carrier density. Then, our observed $v_e = 2\sim3\times10^{8}cm/s$ at the high carrier density of $\sim 10^{19}cm^{-3}$ is consistent with the measured $v_e = 8.6\times10^{6}cm/s$ by Tsen and Morkoc[14] at the low carrier density of $\sim 10^{16}cm^{-3}$.

(4) Using the determined D^* and τ_d^{*2}, an *effective* "diffusion length" is calculated to be $30um$. According to this value, there would be no significant carriers in the region of w2 which is $\sim 300um$ away from the excitation center. But the total detected photons from the w1 and w2 within the first 20ps after the excitation by the laser pulse is comparable. This might be again interpreted by the phonon-wind model[2] in which the concept of conventional diffusion length may not apply since the collisions between carriers and phonons no longer limit how far carriers can be

drifted.

(5) Finally, it must be noted that the anomalously fast expansion is only observed in the asymmetric well. This is very interesting because such a simple modification of quantum well shape in comparison with the symmetric well makes a big difference on the dynamic carrier expansion process. Due to the asymmetric well shape there are no transmission states (virtual states or unconfined states) above the lower energy barrier unlike the symmetric well case. This is an intrinsic property of the asymmetric quantum well. The photogenerated carriers may be immediately scattered by the higher energy barrier and obtain momenta from the interface which assists carriers to expand rapidly in x-y plane.

In summary, we have observed for the first time the ultrafast expansion of the energetic carriers in the asymmetric quantum well. It is found that the unique well shape of the asymmetric quantum well is responsible for the observation of the extraordinary large expansion velocity of the energetic carriers. However, no distinction has been made among various models to explain the observed ultrafast carrier expansion process. Both the rapid carrier density decay and the slow cooling of hot carriers in the asymmetric and symmetric wells are attributed to the presence of the nonequilibrium phonons generated by the energy relaxation of photoexcited carriers.

The research was supported by the U.S. Air Force Office of Scientific Research under Grant No. AFOSR-86-0031. We thank K. Bajaj for helpful discussions.

Reference

(1) A. Forchel, H. Schweizer, and G. Mahler, Phys. Rev. Lett. 51, 501 (1983).

(2) F. M. Steranka and J. P. Wolfe, Phys. Rev. Lett. 22, 2181 (1984), and Phys. Rev. B 34, 1014 (1986).

(3) K. T. Tsen, Phys. Rev. B 35, 4134 (1987).

(4) F. A. Majumder, H. E. Swoboda, K. kempf, and C. Klingshirn, Phys. Rev. B 32, 2407 (1985).

(5) K. M. Romanek, H. Nather, J. Fisher, and E. O. Gobel, J. Lumi., 24/25, 585(1981).

(6) Charles L. Collins, and Peter Y. Yu, Solid State Commun., 51, 123(1984).

(7) A. Cornet, M. Pugnet, J. Collet, T. Amand, and M. Brousseau, J. Phys. (Paris) Collq. c7, 42, 471(1981).

(8) Mahesh R. Junnarkar, and R. R. Alfano, Phys. Rev. B, 34, 7045(1986).

(9) M. Wautelet and J. A. Van Vecten, Phys. Rev. B 23, 5551 (1981).

(10) M. Combescot, Solid State Commun. 30, 81 (1979).

(11) G. Mahler, G. Maier, A. Forchel, B. Laurich, H. Sanwald, and W. Schmid, Phys. Rev. Lett. 47, 1855 (1981).

(12) L. V. Keldysh, JETP Lett. 23, 87 (1976).

(13) A. K. Sood, J. Menendez, M. Cardona, and K. Ploog, Phys. Rev. Lett. 54., 2111, 2115, (1985).

(14) K. T. Tsen, and H. Morkoc, Phys. Rev. B, 34, 6018 (1986).

(15) Apparently, the value of τ_r^{*2} seems to be ~20ps. However, in order to precisely determine the value of τ_r^{*2} using a expression of $I_{w\text{-}2}(t) \sim (1 - e^{-t/\tau_r^{*2}}) e^{-t/\tau_d^{*2}}$, one has to kown the decay time of τ_d^{*2}. The value of τ_d^{*2} is determined to be 13ps by fitting the $I_{w\text{-}2}(t)$ employing an ambipolar diffusion model as discussed below. Since the decay of $I_{w\text{-}2}$ is so fast, we cannot confidently determine the

true rise time of the I_{w2}. However, a low-limit of τ_r^{w2} is obtained to be ~ 100ps.

(16) Kai Shum, M. R. Junnarkar, H. S. Chao, R. R. Alfano, and H. Morkoc, Solid State Electronics (in press), and Phys. Rev. B (to be published).

(17) J. Shah, IEEE J. Quantum Electron., vol. QE-22, 1728(1986).

(18) P. Lugli, and S. M. Goodnick, Phys. Rev. Lett. 59, 716 (1987).

(19) E. O. Gobel, H. Jung, J. Kuhl, and K. Ploog, Phys. Rev. Lett., 51, 1588(1983).

(20) N. Holonyak, Jr. R. M. Kolbas, W. D. Laidig, B. B. Vajak, H. Hess, R. D. Dupuis, and P. D. Dapkus, J. Appl. Phys. 51, 1328 (1980).

Figure Caption

Fig.1 Time-integrated spatial profiles of laser and the luminescence in a spectral window of 35nm centered at 700nm at 4.3K from the asymmetric well (a) and symmetric wells (b). The w1 ad w2 are regions where the time-resolved luminescence profiles are obtained. The insets show the potential profiles of the asymmetric and symmetric wells.

Fig.2 Time-resolved photoluminescence of the asymmetric well at 4.3K from the spatial region of the w1 (a) and w2 (b). The solid curves are the theoretical fits as discussed in the text.

Fig.3(a) Time-resolved photoluminescence from the asymmetric quantum well at 4.3K at various wavelengths. (b) The electron density decay curves.

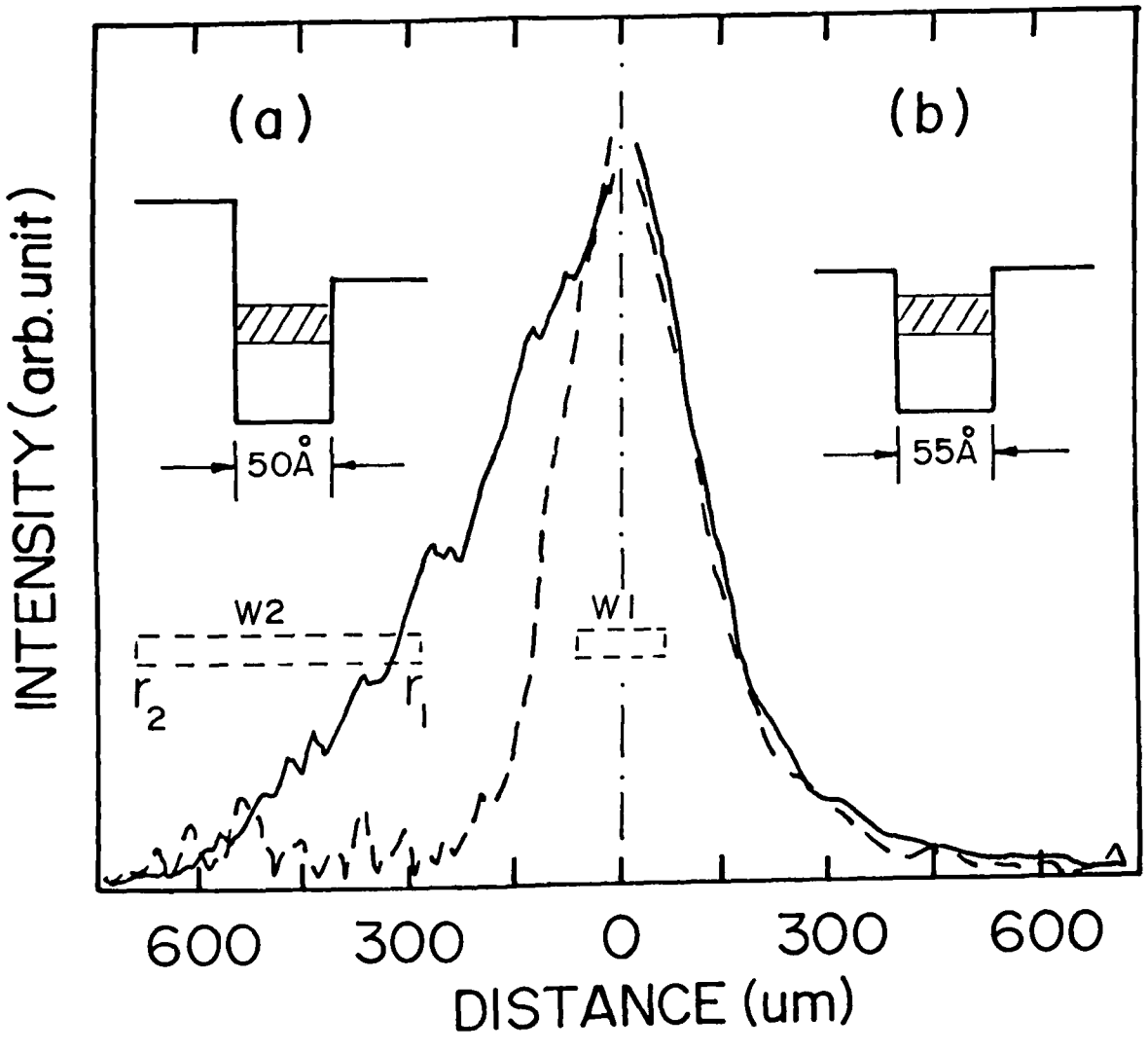
(a)
(b)
50Å
55Å
W2
W1
r_2
r_1
INTENSITY (arb.unit)
600
300
0
300
600
DISTANCE (um)

Fig.1

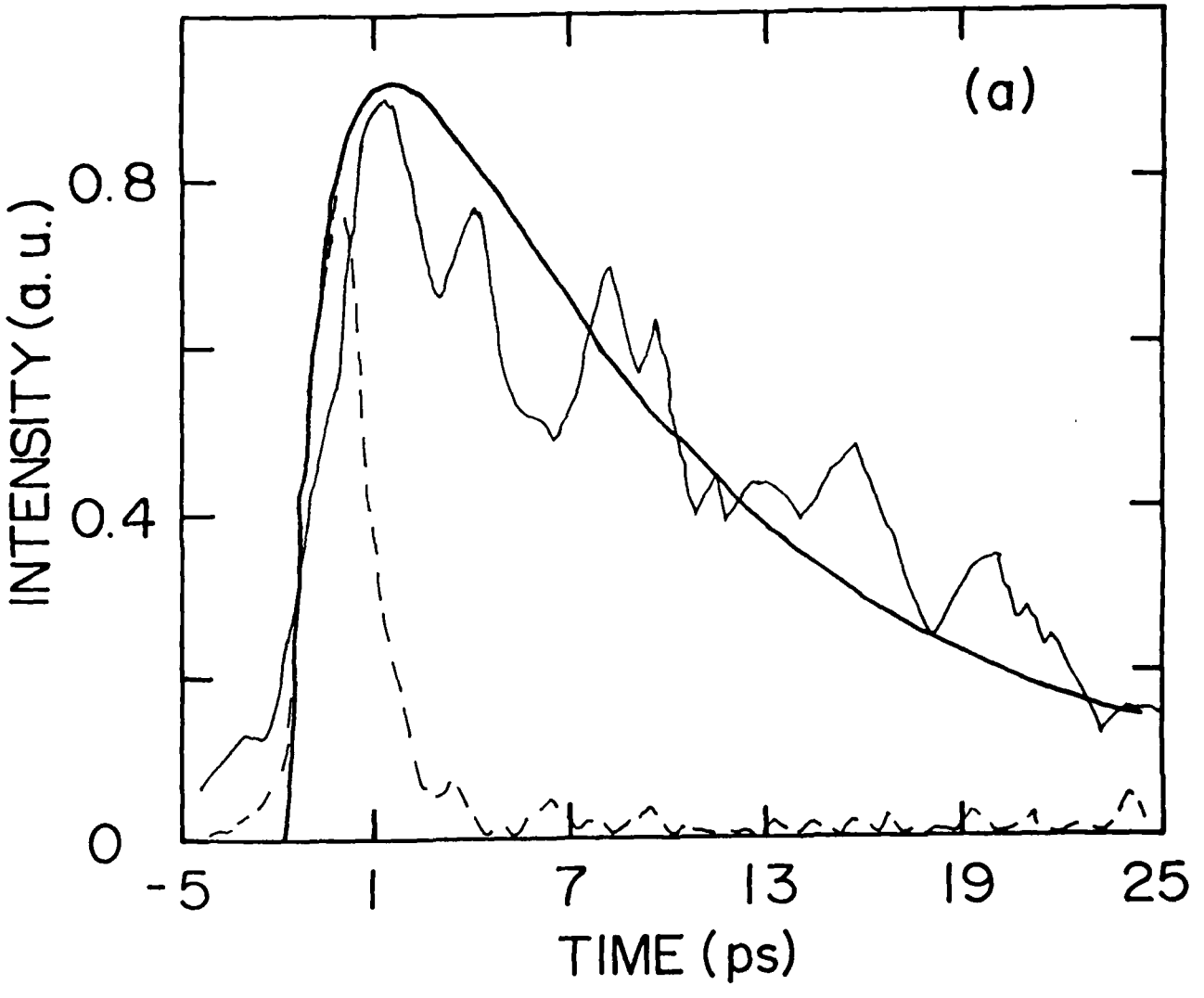

Fig.2a

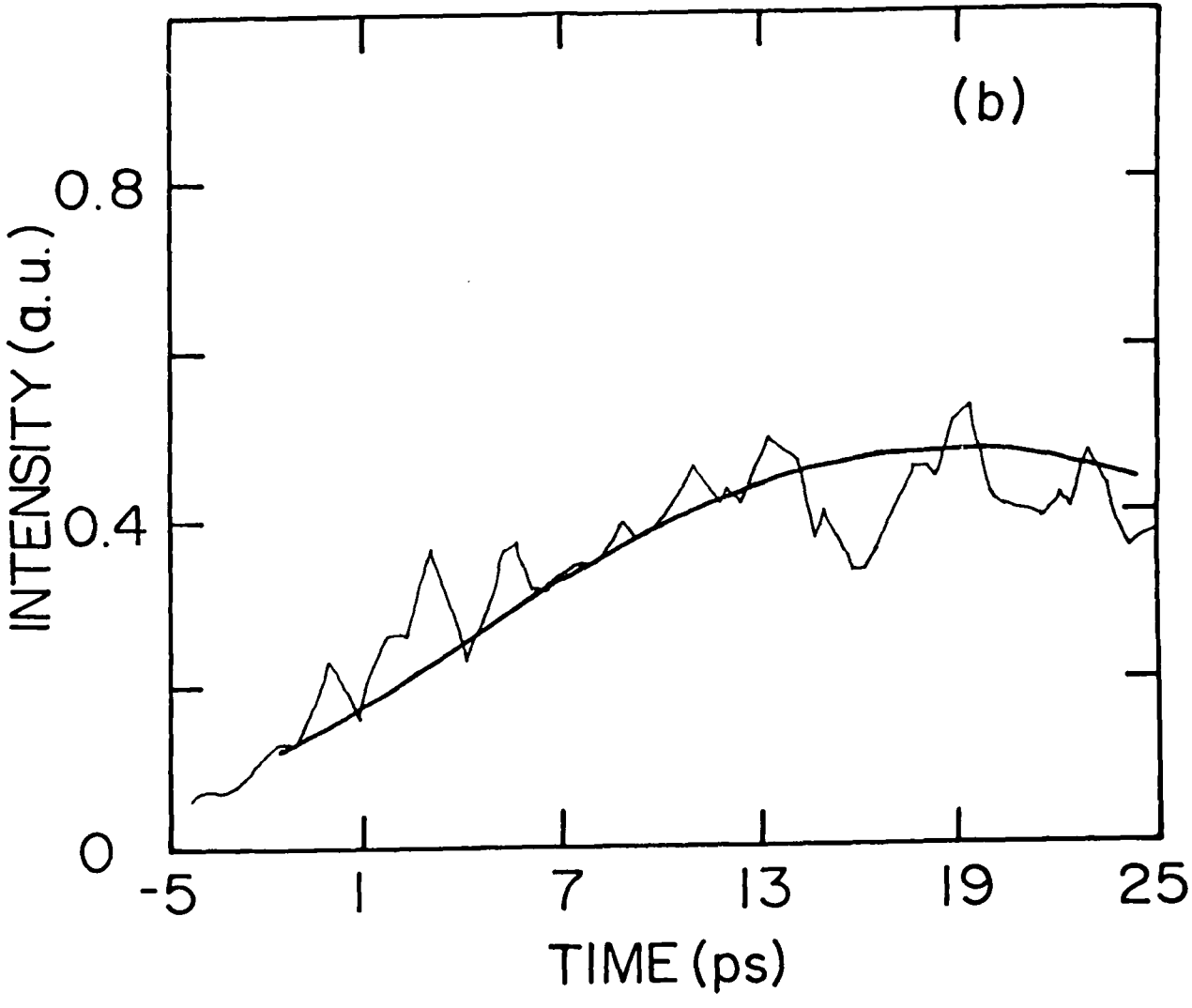

Fig.2b

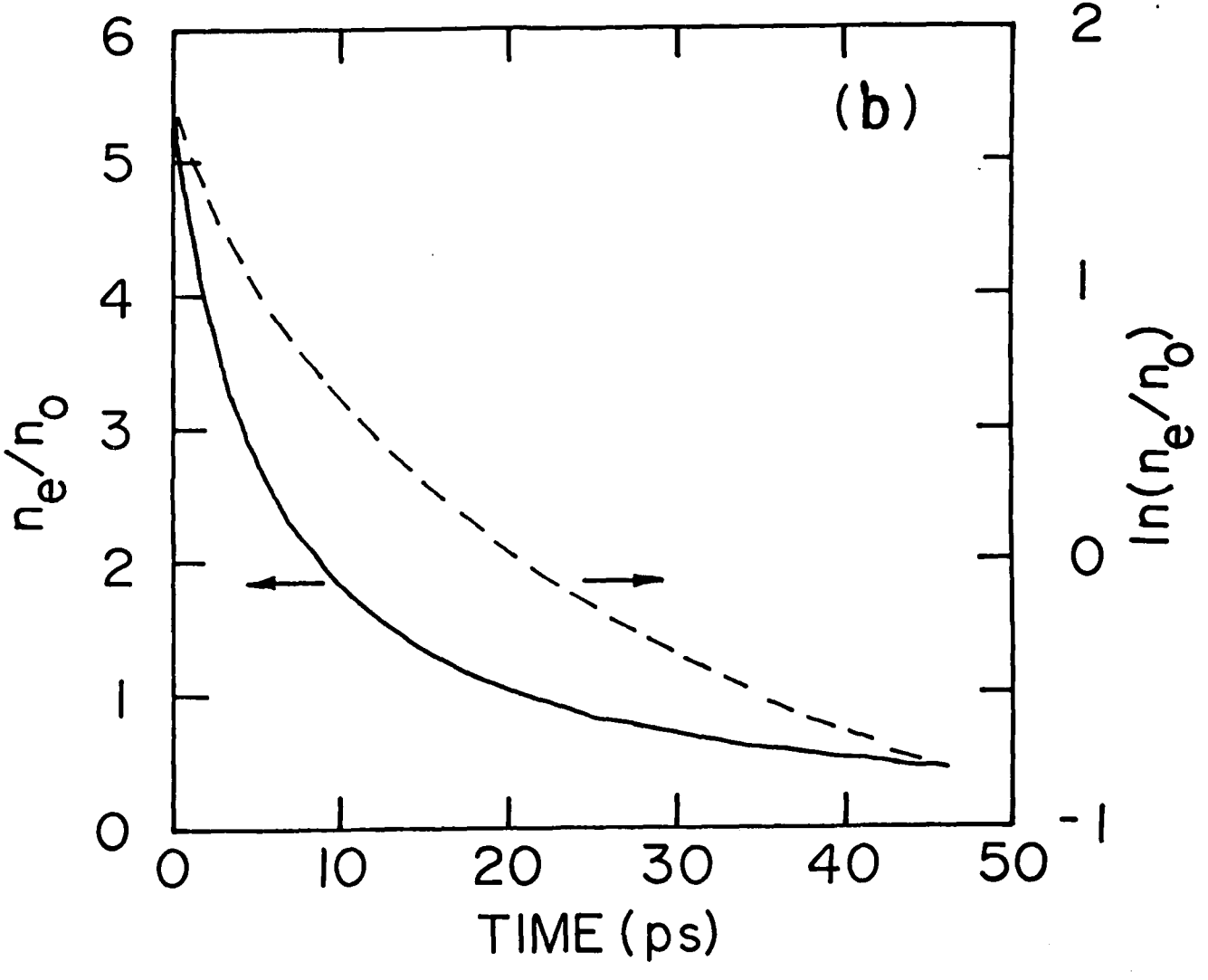

Fig.3b

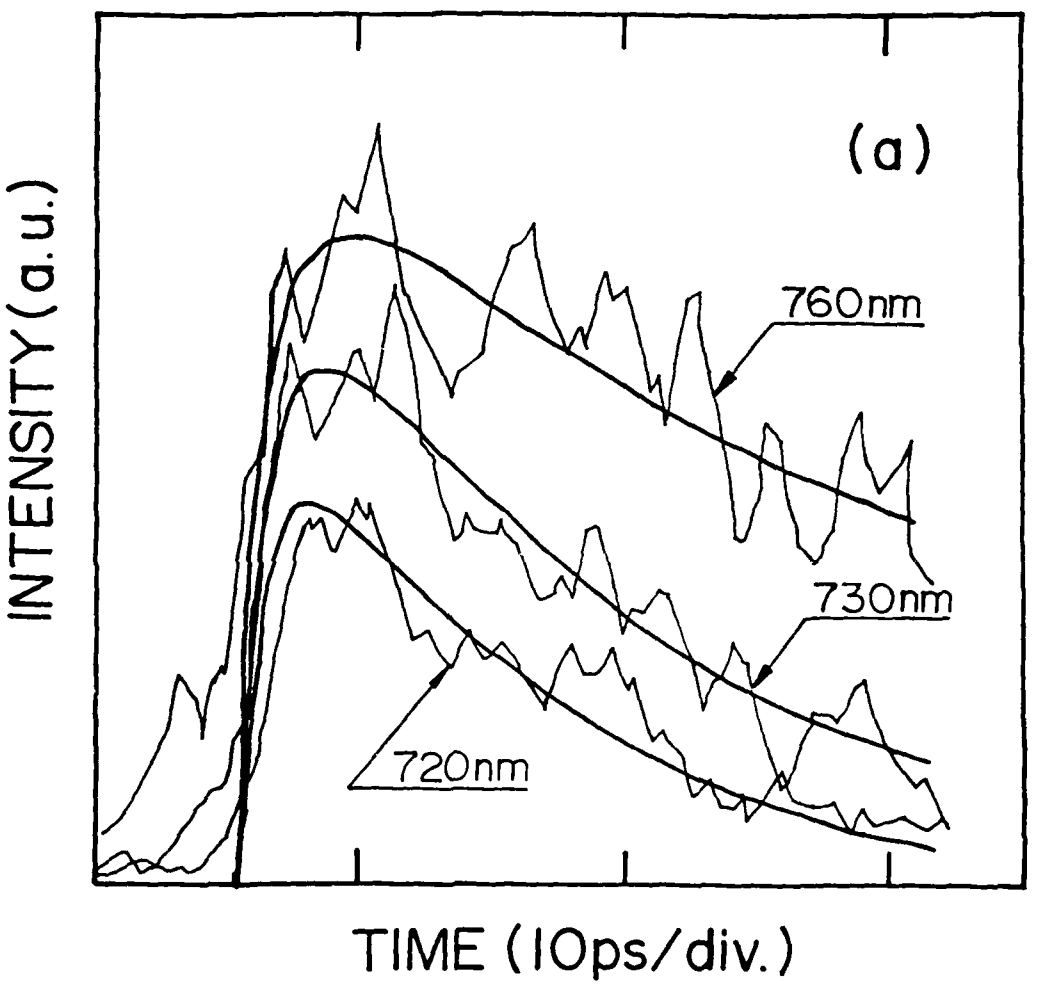

Fig.3a

Electron-hole recombination lifetimes in a quasi-zero-dimensional electron system in CdS_xSe_{1-x}

Kai Shum, G. C. Tang, Mahesh R. Junnarkar, and R. R. Alfano
Institute for Ultrafast Spectroscopy and Lasers, Departments of Electrical Engineering and Physics, The City College of New York, New York, New York 10031

(Received 1 December 1986; accepted for publication 25 September 1987)

The recombination lifetimes for the radial and angular quantum number conserved $1S$–$1S$ and $1P$–$1P$ transitions from three-dimensionally confined electrons in CdS_xSe_{1-x} were measured by time-resolved photoluminescence (PL). The assignment of the observed transitions was supported by calculations of eigen energy levels and squared matrix element ratio for these transitions as well as well-resolved PL peaks arising from $1S$–$1S$ and $1P$–$1P$ transitions.

Recently, carriers localized in semiconductor microstructures have attracted much attention because of their novel optical properties for potential device applications. Electrons localized in semiconductor crystallites of diameters ranging from 30 to 800 Å embedded in a transparent insulating matrix are confined in three dimensions.[1-3] Such quasi-zero-dimensional (quasi-0D) electron systems also exist in bulk alloy semiconductors due to compositional fluctuations.[4] Electronic motion in these systems no longer follows a well-defined energy momentum relation because the Hamiltonian of the system does not commute with the momentum operator due to potential discontinuity at the crystallite surface. The envelope wave functions in spherical coordinates $[r,\theta,\phi]$ and eigen energies of conduction electrons and valence holes localized in an infinite spherical well within the effective mass approximation are given by

$$|nLm\rangle = C_{nL} j_L(\chi_{nL} r) Y_{Lm}(\theta,\phi) \tag{1}$$

and

$$E_{nL} = \hbar^2 \chi_{nL}^2 / 2m_{e,h} a^2, \tag{2}$$

respectively, where the subscripts n, L, and m are effective radial, angular, and magnetic quantum numbers, respectively; the j and Y are the spherical Bessel and spherical Harmonic functions, respectively; a is the radius of crystallite; and $m_{e,h}$ is the effective mass of electron or the isotropic hole mass.[5] The values of χ_{nL} for the lowest two states of either conduction electron or valence hole $1S$ and $1P$ are π and 4.49, respectively. S stands for $L=0$ and P for $L=1$. The allowed transitions which conserve angular and radial quantum numbers are $1S$–$1S$, $1P$–$1P$, and higher transitions. The physical picture of quasi-0D electron system described above has been experimentally verified by several groups.[1-3] Large and fast optical nonlinearities arising from photogenerated electron hole pairs have been reported in quasi-0D electron systems.[6,7]

In this letter, we report on measurements of ultrashort recombination lifetimes of the radial and angular quantum number conserved $1S$–$1S$ and $1P$–$1P$ transitions in quasi-0D electron systems in CdS_xSe_{1-x} at 4.3 K using a streak camera detection system. The time-resolved photoluminescence (PL) detected at various emission energies allows us to unambiguously identify the $1S$–$1S$ and ^1P–$1P$ transitions. The recombination lifetime of $1P$–$1P$ transition was measured to be 3.5 times shorter than the $1S$–$1S$ transition. The ultrafast decay of the $1P$ excitation may have practical importance for the construction of ultrafast reversible optical switches. The assignment of the observed S and P transitions was supported by calculations of eigen energy levels and squared matrix element ratio for these transitions, as well as the observation of optical transitions in steady-state PL.

The samples investigated were four optical glass filters Corning 2-61, 2-59, 2-58, and 2-64. The value of x for each sample was accurately obtained from chemical analysis.[8] A second harmonic (530 nm) of a Nd-glass laser pulse of 8 ps duration was used to excite the samples on the front surface. The maximum optical energy incident onto the front surface was about 40 μJ. The spot size was about 8×10^{-3} cm^2. For steady-state PL experiments, an argon-ion laser, a Spex double grating spectrometer, an S-20 photomultiplier, and a lock-in amplifier were used.

The time-resolved PL profiles obtained at various emission energies at 4.2 K for sample 2-58 are shown in Figs. 1(a)–1(e). The left curve in Fig. 1(a) shows the temporal profile of the exciting laser pulse which reflects the time resolution of the detection system (10 ps). The dotted curves in Fig. 1 are the double-exponential fits to the data with a value of 12 ps for the rise time τ_r. The decay times of these time-resolved luminescence profiles show only two distinct values. For emission energies ranging from 2.213 to 2.175 eV and from 2.1 to 1.967 eV the decay times are 29 and 100 ps, respectively.

The decay time as function of emitted photon energy E for four quasi-0D electron systems at 4.2 K is summarized in Fig. 2. For a comparison, the exciton lifetime versus exciton energy in a quasi-0D system in a bulk $CdS_{0.53}Se_{0.47}$ alloy compound studied by Kash *et al.*[9] is also included in this figure. The most remarkable feature of interest in the data is the appearance of two distinct energy regions in which the decay time is different by a factor of about 3.5 for the samples 2-64, 2-58 and the bulk $CdS_{0.53}Se_{0.47}$ while the other two samples do not show this feature because either $1P$ electron and hole were not excited or the luminescence from the $1P$–$1P$ electron-hole recombination was not detected. It is expected that the decay time should be nearly invariable over the energy range of emission if only the lowest confined state $1S$ for electrons and holes is occupied. The wide spectral range most likely reflects the crystallite size distribution and the fluctuations in the value of x from crystallite to crystallite. When the two lowest states $1S$ and $1P$ are substantially occupied and the recombination lifetimes associated with these two states are considerably different, a steplike change of decay time will be observed in two distinct energy regions.

 0003-6951/87/481839-03$01.00

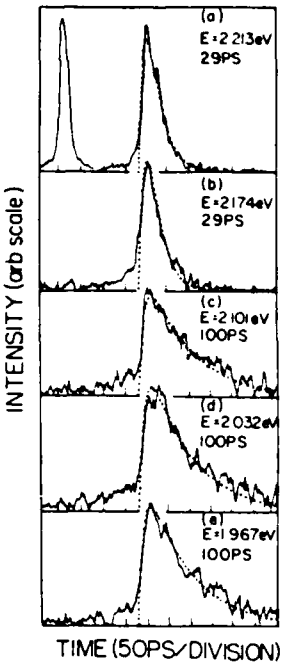

FIG. 1. Time-resolved PL profiles detected at different energies (a)–(e) for the sample 2-58 at 4.2 K. The dotted curves are the theoretical fit with 12 ps for rise time and decay times are indicated on the corresponding profiles. The left curve of (a) is the temporal response profile to the laser pulse used to excite the samples.

The exact lifetime ratio in the two energy regions depends on the transition matrix elements. The above argument should in principle explain what we observed. However, the energy dependence of localized exciton lifetime in the bulk compound $CdS_{0.53}Se_{0.47}$ as displayed in Fig. 2(e) also exhibits a steplike feature. The explanation given by Kash *et al.*[9] was based on the model suggested by Cohen and Sturge[4] where the exciton migration goes from a site with higher energy into another site with lower energy. This raises a question whether the exciton migration mechanism can apply to the present case. Since exciton migration must involve a transport over a relatively large distance due to the nature of the exciton-phonon interaction,[4] such migration may occur in relatively large crystallites. This apparently may explain the results observed in samples 2-58 and 2-64. In smaller crystallites the migration does not occur in correspondence with the samples 2-61. However, the exciton migration picture

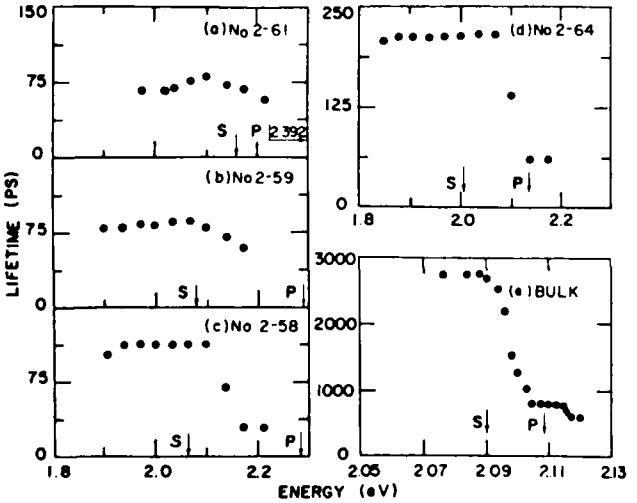

FIG. 2. Lifetimes are plotted as function of emitted photon energy. The sample temperature for (a), (b), (c), (d) is 4.2 K and for (e) is 2 K. The arrows indicate the energy positions for the $1S$–$1S$ transition (S) and the $1P$–$1P$ transition (P).

cannot explain the steplike energy dependence of lifetime as well as the ratio with the value of about 3.5 because the depth of a potential well caused by compositional fluctuations is entirely random in nature. Furthermore, the exciton lifetime would increase monotonically with a decrease of exciton energy.

A two-state ($1S$,$1P$) model is introduced here which consistently interprets all the results shown in Fig. 2 as well as other results observed by Cohen and Sturge[4] and reported by Kash *et al.*[9] It is possible that the excitons are confined by the potential wells in the bulk alloy compound which have two lowest states designated by $1S$ and $1P$. The exciton in higher lying state $1P$ can be scattered to the lower lying state $1S$ by emission of phonons instead of migrating from site to site.

In order to verify the two-state model, we have calculated the eigen energy levels of the quasi-0D electron systems and the recombination lifetime ratio for $1S$–$1S$ and $1P$–$1P$ transitions. The confinement energy for the ground states (E_{1S}) is equal to $E^e_{1S} + E^h_{1S}$ for the quasi-0D electron systems, where E^e_{1S} and E^h_{1S} are the lowest confinement energies for electrons and holes, respectively. These energies were calculated from the bulk band gaps[10] at 300 K and the measured peak energies of the first derivative of room-temperature reflectance ($dR/d\lambda$) by subtraction. Using the electron effective mass, the isotropic hole effective mass given in Ref. 4, and the measured E_{1S}, the effective diameter of crystallite for each sample and eigen energies were calculated based on Eq. (2) and listed in Table I. The emitted photon energies at 4.2 K for $1S$–$1S$ and $1P$–$1P$ transitions in Table I were obtained by adding corresponding confinement energies to the values of bulk gap[10] at 4.2 K. These calculated energy positions are located in Fig. 2 as arrows labeled by S and P for clarity and are in reasonable good agreement with the two-state model.

The radiative lifetime ratio for $1S$–$1S$ and $1P$–$1P$ can be predicted following the approach given by Casey and Panish.[11] The matrix element for a transition from localized state in conduction band to the localized state in valence band is $M = M_b M_{\rm env}$, where M_b is the average matrix element for the Bloch states for bands in absence of new eigen states due to the confinement and $M_{\rm env}$ is the envelope part of the matrix element which is $M_{\rm env} = \langle 1L \,|\, 1L \rangle$. Since the $1P$ state is a threefold degeneracy state with magnetic quantum number of -1, 0, and 1, the envelope matrix element ratio of $|M_{\rm env}|^2_{1P-1P}$ to $|M_{\rm env}|^2_{1S-1S}$ can be readily calculated to be 5. When the 4 K recombination lifetimes are purely radiative, then the ratio for τ_{1S}/τ_{1P} should be equal to 5. The discrepancy between the predicted value of 5 and the experimentally measured value of 3.5 for τ_{1S}/τ_{1P} arises from the existence of nonradiative transitions. A simple rate equation analysis helps to substantiate this statement. Suppose $1/\tau_{1i} = 1/\tau_{ri} + 1/\tau_{ni}$, where $i = S,P$; $\tau_{ri(p)}$ and $\tau_{ni(p)}$ are the radiative and nonradiative recombination lifetimes for the $1S(P)$–$1S(P)$ transition, respectively. The ratio is $\tau_{1S}/\tau_{1P} = (\tau_{rs}/\tau_{rp})[(\tau_{rp} + \tau_{np})/(\tau_{rs} + \tau_{ns})]$. When $\tau_{ns} \sim \tau_{np}$ and $\ll \tau_{rs}, \tau_{rp}$, then $\tau_{1S}/\tau_{1P} \sim 1$; hence, there should be only one lifetime. This is opposite to the experimental results. On the other hand, the ratio τ_{1S}/τ_{1P} is about 3.5 when

TABLE I. Measured energy peak of first derivative of reflection at 300 K, bulk energy gaps at 4.2 and 300 K, the calculated confinement energies, emission energies for $1S$–$1S$ and $1P$–$1P$ transitions and effective diameters (d), the measured lifetimes for $1S$–$1S$ and $1P$–$1P$ transitions as well as their ratio are displayed.

No.	Sample CdS_xSe_{1-x} x	d (Å)	(300 K) Energy peak for $dR/d\lambda$ (eV)	(300 K) Bulk gap[a] (eV)	Confined energy (meV) $E^e_{1s}+E^h_{1s}$	E^e_{1s}	E^h_{1s}	E^e_{1p}	E^h_{1p}	4 K emission energy[a] (eV) $1S$–$1S$	$1P$–$1P$	ΔE[b]	4 K lifetime (ps) $1S$	$1P$	τ_{1s}/τ_{1p}
2-61	0.27	74	2.0120	1.7857	226	187	39	382	80	2.156	2.392	220	70	20[d]	3.5
2-59	0.121	80	1.9366	1.7333	203	168	35	344	72	2.078	2.291	224	85	24[d]	3.5
2-58	0.081	80	1.9245	1.7143	210	174	36	356	74	2.065	2.284	c	100	29	3.5
2-64	0.168	102	1.8666	1.7429	124	103	21	211	43	2.004	2.134	c	210	60	3.5
Bulk	0.530	250		1.9368	17	14	3	29	6	2.090	2.108		2750	790	3.5

[a] From Ref. 10.
[b] Measured energy separation (meV) between S and P peaks at 300 K from Fig. 3(a).
[c] Peaks are broad and unresolved.
[d] The anticipated values assuming a same ratio τ_{1s}/τ_{1p} for the samples 2-58 and 2-64.

nonradiative recombination lifetimes ($\tau_{ns}=\tau_{np}$) are about 5 times larger than the radiative lifetime τ_{rp} of the excited state $1P$ for the assumption of $\tau_{1P}\sim\tau_{rp}$ and $\tau_{1S}\sim\tau_{rs}$.

Steady-state PL studies at 4 and 300 K were performed to substantiate our findings from the picosecond studies. In Fig. 3(a), 300 K PL spectra of sample 2-61 at various excitation levels (see figure caption) are plotted. The broken vertical line indicates the peak position of $dR/d\lambda$. As expected the salient feature in the luminescence spectra is the appearance of a two-peak structure separated by 220 meV on the high-energy side of the broken vertical line. Based on the two-state model we attribute these two peaks to the $1S$–$1S$ and $1P$–$1P$ optical transitions[5] as indicated by S and P in the figure.

The 4 K PL spectrum of 2-61 excited by the 457.9-nm line of the argon-ion laser is depicted in Fig. 3(b). As can be seen from the spectrum, the position of the $1S$–$1S$ peak shifts to higher energy and its FWHM (58 meV) decreases by a factor of 2 in comparison with room-temperature data. The latter indicates that the broadening of the $1S$–$1S$ transition at room temperature is not entirely dominated by the size fluctuation. The inset of Fig. 3(b) shows a spectrum fit by assuming a Gaussian shape of the probability density function for the random variable d. The fit gives a mean value of 74 Å for the effective diameter and a full width at half-maximum of 15 Å which characterizes the size fluctuation of microcrystallites. The structure next to the main $1S$ peak is from the $1P$–$1P$ transition since its energy separation with the $1P$ peak is about 210 meV.

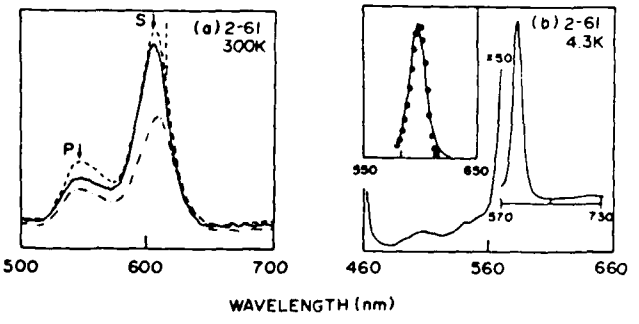

FIG. 3. (a) Photoluminescence spectra of sample 2-61 at various excitation levels taken at room temperature using the 488 nm line of an argon-ion laser. The excitation levels (intensity scale) were 2.5 (2) and 10 (10) times higher for the broken curve and the dot-dashed curve than the solid curve, respectively. The broken vertical line indicates the peak position of the first derivative of reflectance at room temperature. S and P stand for the $1S$–$1S$ and $1P$–$1P$ transitions, respectively. (b) Photoluminescence spectra of 2-61 at 4.3 K. The inset shows that the $1S$ peak broadening is dominated by the diameter fluctuation of microcrystallites. The solid dots are calculated by assuming a Gaussian shape of the probability density function for the random variable d with a variance of 25 Å^2.

We have also measured 4 and 300 K luminescence spectra of 2-59, 2-58, and 2-64 samples. The two-peak structure was observed for 2-59 at both 4 and 300 K. The peaks were broader for 2-58 and 2-64 than for the other two samples and the $1P$ structure was not clearly identified.

In summary, we have reported on the measurements of recombination lifetimes of $1S$–$1S$ and $1P$–$1P$ transitions in quasi-0D electron systems in CdS_xSe_{1-x}. The assignment to these observed transitions is supported by calculations of eigen energy levels and the corresponding squared matrix element ratio as well as the direct observation of optical transitions between quantized energy levels $1S$ and $1P$ in the conduction band and the valence band.

This work was supported by Air Force Office of Scientific Research AFOSR-86-0031.

[1] R. Rossetti, S. Nakahara, and L. E. Brus, J. Chem. Phys. 79, 1086 (1983).
[2] A. I. Ekimovand and A. A. Onushchenko, JETP Lett. 40, 1136 (1984).
[3] J. Warnock and D. D. Awschalom, Phys. Rev. B 32, 5529 (1985); Appl. Phys. Lett. 48, 425 (1986).
[4] E. Cohen and M. D. Sturge, Phys. Rev. B 25, 3828 (1982).
[5] L. E. Brus, IEEE J. Quantum Electron. QE-22, 1909 (1986).
[6] R. K. Jain and R. C. Lind, J. Opt. Soc. Am. 73, 647 (1983).
[7] S. S. Yao, C. Karaguleff, A. Gabel, R. Fortenberry, C. T. Seaton, and G. I. Stegeman, Appl. Phys. Lett. 46, 801 (1985).
[8] The samples were sent to Schwarzkopf Microanalytical Laboratory, Inc. (56-19 37th Ave., Woodside, NY 11377) for chemical wet analysis to obtain accurate x values.
[9] J. A. Kash, A. Ron, and E. Cohen, Pnys. Rev. B 28, 6147 (1983).
[10] F. L. Pedrotti and D. C. Reynolds, Phys. Rev. 127, 1584 (1962).
[11] H. C. Casey, Jr. and M. B. Panish, *Heterostructure Lasers* (Academic, New York, 1978), p. 144.

A Reprint from the

PROCEEDINGS

Of SPIE-The International Society for Optical Engineering

Volume 793

Ultrafast Lasers Probe Phenomena in Bulk and Microstructure Semiconductors

25-26 March 1987
Bay Point, Florida

Energy relaxation and diffusion of photoexcited carriers in symmetric and asymmetric GaAs quantum wells

Kai Shum, Mahesh R. Junnarkar, Hsieh Shin Chao, R. R. Alfano
Institute for Ultrafast Spectroscopy and Lasers
Departments of Physics and Electrical Engineering
The City College of New York, New York, New York 10031

H. Morkoc
Coordinated Science Laboratory
University of Illinois
Urbana, Illinois 61801

Invited Paper

Energy Relaxation and Diffusion of Photoexcited Carriers in Symmetric and Asymmetric GaAs Quantum Wells

Kai Shum, Mahesh R. Junnarkar, Hsieh Shin Chao, and R. R. Alfano
Institute for Ultrafast Spectroscopy and Lasers
Departments of Physics and Electrical Engineering
The City College of New York, New York, NY 10031
and
H. Morkoc
Coordinated Science Laboratory
University of Illinois
Urbana, Ill 61801

Abstract

Subpicosecond time-resolved photoluminescence studies of a symmetric multiple quantum well structure and an asymmetric quantum well with a similar well thickness have revealed several important experimental results on the behavior of photoexcited carriers in these microstructures: (1) The energy relaxation process is substantially suppressed due to the existence of a large population of nonequilibrium phonons after an initial rapid cooling. (2) The two different well structures do not show any difference in the energy relaxation process under the same experimental conditions. (3) The photoexcited carrier density deduced from exact and consistent fittings of the time-resolved photoluminescence profiles at various emitted photon energies decreases nonexponentially and very rapidly within the first 30 ps after the end of a 0.5 ps pulse. An effective carrier depletion time is determined to be as short as 10 ps in either well. A mechanism which leads to such short carrier depletion time is found to be associated with the nonequilibrium phonon enhanced phonon replica emission. Unlike conventional stimulated emission behavior, this mechanism is even more effective in exhausting carriers from the system at higher temperatures. (4) The difference in potential well profile corresponds to a very different behavior of carrier diffusion process in the lateral well plane. The carrier diffusion is enhanced in the well plane of the asymmetric well by restricting carrier diffusion in the growth direction. Diffusivity D of the photoexcited carriers in the asymmetric well has been directly determined to be $10^6 cm^2/s$ at 4.3K, which is about four orders of magnitude larger than the value in bulk GaAs.

Introduction

Over the last few years, there has been a growing interest to understand the fundamental interactions of confined and free electrons and holes with the phonons in bulk semiconductor and its multiple quantum well structures. This understanding is crucial for the operation of ultrahigh speed devices based on the principles of ultrafast carrier dynamics. The slowing of carrier cooling in bulk semiconductors was attributed to the screening[1] of the electron-phonon interaction or the re-heating of carriers by hot-phonons.[2,3] The first comparison[4] of the hot-electron cooling rates in undoped multiple quantum well (MQW) structures and in the bulk GaAs was achieved by time-resolved measurements of optical absorption and gain. The cooling rates were approximately the same for bulk and MQW at a carrier density of $2.5 \times 10^{17} cm^{-3}$. This is expected from a simple theory[5] where the lattice is treated as a heat bath for the quasi-equilibrium carriers. Quasi-steady state experiments have been carried out by two groups[6,7] to investigate the interaction of electrons and holes with phonons in modulation-doped MQW structures. These experiments have generated conflicting results regarding the presence of nonequilibrium phonons. The first measurements of time-resolved photoluminescence from modulation doped semiconductor MQW with greater than 20 ps time resolution were reported by Ryan et al.[8] who found that the cooling of hot carriers was anomalously slow after 40 ps. By reviewing these and other previous works we noticed three important points: First, by studying the carrier dynamics in modulation-doped MQW structures which are designed for high mobility devices, one can obtain the energy loss rates of the photo-injected majority carriers by extracting the carrier temperature as a function of time from the high energy tails of time-resolved photoluminescence spectra. Due to a large extrinsic carrier density, at least comparable to the photoexcited carrier density, one cannot obtain information on photo-injected carrier lifetimes. In these experiments the carrier lifetime is essentially close to the value in bulk which is about 1 ns.[8] It is necessary to study photo-injected carrier dynamics in undoped MQW structures in order to obtain information on both the energy loss rates and carrier lifetimes. The latter is crucial for applications in high speed optoelectronic devices. Several attempts have been made to reduce the carrier lifetime through nonradiative recombination processes.[9,10] Second, one cannot extract information on the initial carrier relaxation process from both quasi-steady state experiments and time-resolved measurements with time resolution greater than 10 ps. Study of the initial carrier relaxation process is crucial to substantiate the existence of nonequilibrium phonons and its importance to the hot-carrier relaxation since the phonon lifetime is about 5-7 ps. Third, the rapid expansion of photoexcited electron-hole plasma at high density in quantum well structures has not been experimentally investigated on a picosecond time scale. Only an indirect measurement of the expansion of electron-hole plasma in GaAs MQW structures at low carrier density has been reported where the drift velocity of the electrons was comparable to the Fermi-velocity, and therefore, the transport of the photoexcited carriers in GaAs quantum wells was thermodiffusive.[11]

In this paper, several experimental results are reported from the measurements of time-resolved photoluminescence with 2 ps time resolution as well as the studies of lattice temperature dependence, excitation dependence, and polarization of integrated luminescence spectra from an undoped GaAs symmetric

MQW structure and an **asymmetric** quantum well. We have found: (1) The energy relaxation process is substantially suppressed due to the existence of a large population of nonequilibrium phonons after an initial rapid cooling. (2) The two different well structures do not show any difference in the energy relaxation process under the same experimental conditions. (3) The photoexcited carrier density extracted from fittings of time-resolved photoluminescence profiles at various emitted phonon energies decreases non-exponentially and very rapidly within the first 30 ps after the end of a 0.5 ps laser pulse. An effective carrier depletion time is determined to be as short as 10 ps in either type of wells. A mechanism which leads to such a short carrier depletion time is associated with nonequilibrium phonon enhanced phonon-replica-emission. Unlike the conventional stimulated emission process this mechanism is even more effective in exhausting carriers from the system at higher temperatures. The bandgap renormalization in the photoexcited region is not observed from integrated luminescence spectra as a consequence of ultrashort carrier depletion time and hot carrier temperature. (4) There is no or little carrier diffusion in the lateral well planes of the symmetric wells except for the carriers at the subband edge, while in the asymmetric well, the diffusion process is enhanced in the lateral well plane by restricting carrier diffusion in the growth direction. The diffusivity, D, of photoexcited carriers in the asymmetric well has been determined to be $10^6 cm^2/s$ at 4.3K, which is about four orders of magnitude larger than corresponding value in bulk GaAs.

Samples

The undoped GaAs/$Al_xGa_{1-x}As$ symmetric MQW structure and the asymmetric quantum well investigated in this work were grown by molecular-beam epitaxy on a (001)-oriented undoped GaAs substrate. The symmetric MQW consists of 50 periods of 55Å thick GaAs and 100Å thick $Al_{0.3}Ga_{0.7}As$ layers followed by a 1.2 μm buffer GaAs layer. The asymmetric quantum well consists of layers from the front surface to substrate 150Å $Al_{0.3}Ga_{0.7}As$, 50Å GaAs well, 200Å AlAs (asymmetric barrier), followed by 1 μm $Al_{0.3}Ga_{0.7}As$, and 0.2 μm GaAs buffer layer on Si-doped GaAs substrate. The lateral sizes are 2x4mm, 2x6mm for the symmetric MQW structure and the asymmetric well, respectively. The samples were mounted on a cold finger in a helium cryostat.

Experimental

An ultrashort light pulse of 500 fs duration at 620 nm was used to excite the electron-hole pairs with a carrier density of $10^{19} cm^{-3}$. This light source was generated from a colliding-pulse passive[14] mode-locked dye laser and amplified by a four-stage dye amplifier pumped with a frequency doubled Nd:YAG laser at 20 Hz. The photoluminescence was spectrally filtered using various narrow band filters, and temporally dispersed by a 2 ps time resolution Hamamatsu streak camera system. The luminescence intensities were corrected for nonlinearity of the streak rate, the spectral response, and the transmission of each narrow band filter. The time resolution for the present work is about 2 ps. The experimental apparatus used in this research has been described in detail by Ho et al.[12]

Schematic energy band diagrams are shown in Fig. 1 for a symmetric and an asymmetric quantum well. Using a finite-depth square well model and material parameters given in Ref. 13 the subband energy positions in the wells were calculated. There are two subbands for electrons (e) and heavy-holes (hh) and only one subband for light-holes (lh). The good quality of the samples is confirmed by spectrally well resolved heavy-hole and light-hole excitonic structures at room temperature. The FWHMs for the heavy-hole excitons are about 15 meV and 12.7 meV for the symmetric and asymmetric quantum wells, respectively.

The electron-hole pairs were generated by photo-excitation. These photogenerated carriers thermalize within themselves via carrier-carrier interaction to reach a quasi-equilibrium state in less than 1 ps. Simultaneously, three other processes take place. The first one is the loss of energy of the electron-hole system through the electron-phonon interaction. The second process is the carrier diffusion process due to the gradient of carrier density between photoexcited and non-excited areas. The third process is recombination of electron-hole pair through either nonradiative or radiative mechanisms. The work reported here on the photoluminescence experiments uses the last process to probe the first two processes.

Energy Relaxation

a) Steady State Luminescence

Time-integrated luminescence spectra of the symmetric MQW structure excited by the subpicosecond laser pulse at various lattice temperatures (T_L) are shown in Fig. 2. These spectra were taken in the $z(y,y)\bar{z}$ configuration. The conventional Raman notation (x,y,z are the crystal axes, and z is the growth direction) is used. In order to eliminate radiation from the edges of the sample the luminescence spot was imaged on an aperture with the aid of a streak camera and then focused onto a vertical slit of a grating spectrometer. Several features are displayed in the data.

(1) The emission peak (A) on the high energy side of the spectra is from the recombination of photogenerated n=1 electrons and n=1 heavy-holes. This peak shifts towards the low energy side as T_L increases. A high energy tail on the main peak (A) develops with the increase of T_L. For T_L>150K, a shoulder on the high energy side of the peak A arising from the recombination of n=1 electrons and n=1 light-holes can be identified.

(2) A broad emission band (C) at the low energy side of the spectra arises from the 1.2 μm GaAs buffer layer. The total emission intensity decreases as T_L increases.

(3) The most interesting feature of the data is the appearance of an emission band (B) below the n=1 electron to n=1 heavy-hole transition which is attributed to the emission from the nonequilibrium phonon enhanced phonon replica.

The following reasons support this assignment:

(i) The B emission band does not appear in the steady-state photoluminescence spectra taken at low power excitation of about $1W/cm^2$ at 4.3K using a 488 nm line of an argon-ion laser. However, the photoluminescence spectra using a weak train of laser pulses (~ 200 fs) directly from the colliding-pulse passively mode-locked (CPM) dye laser oscillator as the excitation source, with an excitation power density in the range of 10^{-5}-$10^{-3}W/cm^2$, show a weak electron-acceptor emission band separated by 17 meV from the n=1 electron-heavy-hole transition accompanied by its phonon-replica[14] at low temperatures. This extrinsic emission band disappeared completely when the sample temperature was raised to ~ 80K, whereas the B band in Fig. 2 exists up to room temperature. Moreover, the relative time-integrated intensity ratio between B and A bands in Fig. 2 detected under amplified 0.5 ps light pulse excitation decreases as the excitation power density decreases and the B band is not visible when the excitation power density is lower than $10^{-3}P_m$, where P_m ~ $10^{12}W/cm^2$ is the maximum value of the excitation power density. This contradicts what is generally expected for an impurity emission. Since the concentration of acceptors is low in our sample as confirmed by the luminescence studies using the weak train of 200 fs light pulses, the impurity emission should be readily apparent and more pronounced at lower excitation. Therefore, the B emission band shown in Fig. 2 cannot be attributed to electron to acceptor luminescence.

(ii) The ratio of emission intensities of B and A emission bands increases as T_L increases. The values of the ratio as a function of T_L are shown in Fig. 3 as triangles. This behavior is remarkably different from the conventional stimulated emission process in which phonons do not participate. As in semiconductor lasers, the stimulated emission is less effective when the sample is at room temperature. To convince us that the emission band B is due to a phonon-assisted process, we calculated the sum of occupation numbers for both equilibrium phonons (lattice temperature T_L) and nonequilibrium phonons (carrier temperature T_c) by assuming the carrier temperature is the same as the effective temperature for the nonequilibrium phonons after 30 ps (see later discussion on the carrier temperature). The calculated result is shown by the solid line in Fig. 3. The fitting of the total phonon occupation number to the obtained intensity ratio from the spectra is impressively good. This implies that the intensity of peak B is well correlated with the LO-phonon population. Because of participation of nonequilibrium phonons the intensity of the B band (see also time-resolved luminescence at 780 nm in Fig. 4) is strongly enhanced especially at low temperatures. This further supports our assignment of the B band to the nonequilibrium phonon enhanced phonon replica.

(iii) It is not possible to attribute the emission band B to the emission from the renormalized band-band transition because the peak positions of the A band (766.7nm) and B band as well as the energy separation between them at 4.3K do not change with variation of the excitation intensity by a factor of $9x10^{-4}$ (2ND3). Further support to the above statement is the fact that the spectral position of peak-A exactly coincides with each other for two different luminescence studies using different light excitation sources; the one is the weak 200 fs-pulse train with a repetition rate of 114 MHz, while the other is the amplified 0.5 ps-pulse with a 20Hz repetition rate. As the observed band edge transition energy does not change over a range of photogenerated carrier densities (10^{19}-$10^{15}/cm^3$) the bandgap renormalization in this study must be excluded.

(iv) We have also measured the polarization of the emission bands A, B, and C by adopting a "right-angle"[15,16] geometry for obtaining integrated luminescence spectra. It was found that the emission of band B detected along the y-direction (emitted at the sample edge) was strongly polarized in the x-direction, while the A and C emission bands are depolarized independent of excitation power density and lattice temperature. The intensity ratio between the x- and z-polarization for the B band was about 20 and independent of lattice temperatures from 4.3 to 300K at full excitation power density P_m. But it is strongly dependent on the excitation power density at a given lattice temperature. For example at T_L=100K, the B band cannot be clearly identified from the A band and shows no difference between the two polarizations at the excitation power density 0.017 P_m (2ND13), while the ratio at full excitation P_m is 20. The polarization behavior of the B band is consistent with the Raman scattering measurements reported by Zucker et al.[11] where the initial photons are provided by the external laser source. In our case, the initial photons are provided by the luminescence from the recombination of n=1 electrons and n=1 heavy-holes at the subband edges. This process is strongly enhanced by the presence of a large number of nonequilibrium phonons emitted by the hot-electrons at high excitation. The polarization behavior of emission band C is expected since the emission is from the 1.2μm GaAs buffer layer. This, in fact, provides a good check of our system. However, the polarization behavior of the emission band A is not understood in terms of the selection rules of dipole recombination described by Iwamnra et al.[17], where the emission intensity for x-polarization (TE polarization) should be at least four times larger than that for z-polarization (TM polarization) due to different density of states for heavy-holes and light-holes.

There has been much debate[17-19] on the interpretation of the spectral feature below the n=1 electron heavy-hole transition energy. This is because the energy levels for impurity states, longitudinal optical phonon (LO)-phonon replica, and intrinsic bandgap-reduction due to many-body interactions roughly coincide

with each other. Holonyak and co-workers[18] have demonstrated the LO-phonon participation in GaAs-AlGaAs based QW laser emission by the observation of more than one LO-phonon sideband of laser operation below the n=1 confined-particle transition. Also, the phonon replica of n=1 electron to heavy-hole emission has been observed in the InGaAs based systems. The observation of the coupling at both the GaAs- and InAs-like bulk LO-phonon energies of InGaAs QW by Skolnick et al.[20] has confirmed that the peak below the n=1 electron-heavy-hole transition is a phonon replica. Furthermore, it should be pointed out that our assignment for the B emission band is consistent with the time-resolved photoluminescence data described in the next section.

b) Time-Resolved Luminescence

Time-resolved photoluminescence emitted from the symmetric MQW structure at 4.3K are shown in Fig. 4 for various emitted photon energies. The emission centered at 770 nm arises from the recombination of electrons and heavy-holes near the respective first subband-edges. The emission with wavelengths less than 770 nm is from the recombinations of hot carriers. The time-resolved luminescence intensity assigned to the phonon replica at 780 nm is shown in Fig. 4. Each luminescence profile was the average of 10 individual shots using a prepulse[21] for averaging. The left peak of the dotted curve is the prepulse which reflects the 2 ps temporal resolution. The right peak on the same curve is the Rayleigh scattering light from the sample surface which defines the "zero" time for our analysis. Several features appear in the data displayed in Fig. 4. (i) Although the risetime for all the luminescence profiles is instrumental, the 2 ps upper-limit reflects the rapid thermalization and initial cooling. (ii) The shape of the rise-time of the luminescence profile at 780 nm is similar to that at 770 nm, but delayed by 3 ps. This implies that the emission at 780 nm does not originate from the same band as the emission at 770 nm; otherwise, the rise-time of the luminescence at 780 should start at the same zero point as that at 770 nm. The 3 ps delay is consistent with our assignment of the emission band center at 780 nm to the phonon band. This time is just the effective time required to establish a large nonequilibrium hot phonon population. (iii) The luminescence decay time of 30 ps (broken curve) for the phonon replica emission at 780 nm cannot be due to impurity emission at high excitation.

The decay times were obtained by fitting the data in Fig. 4 to the expression given by:

$$I(E,t)=I_o[1-e^{-t/\tau_r}]e^{-t/\tau_d}, \tag{1}$$

where the parameters (I_o, τ_r, τ_d) are the proportional constant, the risetime, and the decay time, respectively.

To study the energy relaxation process quantitatively, the carrier temperature as a function of time must be determined. There are many ways to obtain the time evolution of carrier temperature. One way is to analyze the high energy tail of time-resolved spectra using a Maxwell-Boltzmann distribution.[6-8] Another way is to measure the ratio of luminescence intensity profiles as a function of time at two energy positions within the exponential energy tail by also assuming a Maxwell-Boltzmann distribution. The above two methods cannot extract information on the photogenerated carrier density. An expression in the time domain is introduced to fit the experimental luminescence temporal profiles by using two adjustable parameters, namely, the carrier densities (n_e, n_{hh}, n_{lh}) and the electron temperature (T_c).

Assuming the direct optical transition, the luminescence intensity is given by:

$$I(E_i,t)=C_i(1-e^{-t/\tau_r})[|M_{e\text{-}hh}|^2\rho_e f_e \rho_{hh} f_h + |M_{e\text{-}lh}|^2\rho_e f_e \rho_{lh} f_h], \tag{2}$$

where $\rho_{e\,hh\,lh} \sim m_{e\,hh\,lh}$ is the density of state for electrons, heavy-holes, and light-holes; $M_{e\text{-}hh(lh)}$ is the matrix element for electron to hh(lh) transitions; C_i absorbs all the constant factors including the corrections for detector response and the transmission of each narrow band filter used; τ_r is the risetime of luminescence and is set to be 1 ps (approximately the response time of the system) which is an upper-limit of thermalization time of the electron-hole system;

$$f_{e,h} = 1/(e^{(\epsilon_i-u_{e,h})/KT_c} + 1) \tag{3}$$

is the Fermi-Dirac distribution for electrons in the conduction band (with subscript e) and for holes in the valence band (with subscript h). The quasi-Fermi energy of holes (u_h) is related to the quasi-Fermi energy of electrons (u_e) and the carrier temperature by the relation,

$$n_e=n_{hh} + n_{lh} \tag{4}$$

This value is given by:

$$u_h = KT_c\ln[e^{a\ln(1+e^{u_e/KT_c})-1}] \tag{5}$$

with

$$a = \frac{m_e}{m_{hh} + m_{lh}} \tag{6}$$

An unique set of parameters of $T_c(t)$ and $u_e(t)$ was used to consistently fit all the luminescence profiles

detected at different photon energies E_i. Three typical calculated luminescence profiles are shown in Fig. 4 by the thick solid curves.

In Fig. 5 the time-resolved photoluminescence profiles from the asymmetric quantum well are shown at three typical energies. The emission centered at 760 nm arises from the recombinations of electrons and heavy-holes near the respective first subband-edges. The theoretical solid curves in Fig. 5 were generated using Eq.(2). The same set of values for T_c and u_e used to fit the data for the symmetric quantum well were used to fit the luminescence profiles of the asymmetric quantum well. The energy relaxation process is similar for both wells despite the different shape of the well. This is as expected!

The experimentally determined values of T_c as a function of time are plotted as the solid curve in Fig. 6. The shaded area reflects the extent of uncertainty in deducing the carrier temperature within the first 4 ps due to our limited time resolution. The plot of T_c vs t is interpreted as follows: carrier-carrier collisions quickly lead to a thermalized distribution at very high T_c within 1 ps due to a large number of excited carriers.[22] **The thermalization process of carriers can only be probed by femtosecond spectroscopy. The initial cooling of the thermalized distribution is studied with our present time resolution of 2 ps, providing information about both the electron-phonon interaction and the carrier lifetime.** The initial cooling within the first 5 ps is very fast (250K/ps) assuming a Fermi-Dirac distribution for electrons. After the initial cooling, a large number of longitudinal optical phonons in finite wavevector space are accumulated due to the finite phonon lifetime.[23] The phonons emitted by the hot electrons may be reabsorbed by the electrons as the reverse process of emission giving rise to a slower cooling for the hot-carriers. It should be emphasized here that the rapid initial cooling rules out the importance of significant screening of the electron-phonon interaction in the present study. If the initial screening was important, the initial rapid cooling would be slow and a nonequilibrium phonon population would not be built up. Another important observation displayed in Fig. 6 is that the time constant ~ 30 ps for the slow component of the carrier temperature cooling curve is the same as the decay time of the nonequilibrium phonon enhanced phonon replica emission at 760 nm. This suggests that the time required for the electron and the nonequilibrium phonon systems to equilibrate with each other is 4-5 ps. The system then decays with a single decay constant of 30 ps as a coupled hot electron-phonon system.

The experimentally determined quasi-Fermi-energies for electrons and holes are plotted in Fig. 7. The changes of u_e and u_h are very rapid within the first 10 ps and the behavior of the degeneracy for electrons and holes as a function of time are reversed.

Using the experimentally determined distributions for electrons and holes in terms of $T_c(t)$ and $u_{e,h}(t)$ the energy loss rates for electrons and holes as function of T_c or n_e can be obtained. The energy loss rate ($P_{e,hh}$) is defined as follows:

$$P_{e,hh} = \frac{d\langle E\rangle_{e,hh}}{dt} = \frac{d}{dt}\frac{\left[\int_0^\infty \varepsilon\, f\,(T_c,u_{e,hh},\varepsilon)d\varepsilon\right]}{\int_0^\infty f\,(T_c,u_{e,hh},\varepsilon)d\varepsilon} \tag{7}$$

However, if the electron-hole system is treated as a Maxwell-Boltzmann gas, i.e., the electrons and holes have the same distribution function which is a Maxwell-Boltzmann distribution, the energy loss rate for the carriers (c=e,hh) is given by:

$$P_c = K\,\frac{dT_c(t)}{dt} \tag{8}$$

It should be pointed out that the energy loss rates for electrons and heavy-holes obtained by Eq. (7) are the net loss rates. It includes the energy loss due to electron(hole)-phonon interactions and the energy exchange between electrons and holes by carrier-carrier scattering. The hole-phonon scattering rates were calculated[24] and measured[6] to be 2.5 to 3 times larger than the rate for electrons due to the additional coupling through the deformation-potential. Therefore, an energy transfer process from electrons to holes should be expected in our photogenerated carrier system. The experimentally determined energy loss rates using Eq. (7) or Eq. (8) are shown in Fig. 8. The solid and dotted curves were obtained from Eq. (7) for electrons and heavy-holes, respectively. The dot-dashed curve was obtained from Eq. (8). It should be pointed out that the curves obtained from either Eq. (7) or Eq. (8) are the experimental data because the distribution $f(T_c,u_{e,h})$ was experimentally determined. The broken line is calculated based on the simple theory[18] where lattice can be treated as a heat bath for quasi-equilibrium carriers. This theoretical curve does not agree with experimentally determined curves. The smaller P_{hh} and P_e is because of the presence of light-hole population and the different masses for electron and hh which lead to different behaviors of quasi-Fermi energies for electrons and heavy holes as a function of time.

The salient features of the experimental data displayed in Fig. 8 are:

(i) The experimentally obtained energy loss rate for electrons is more than two orders smaller than predicted by the simple theory[5] (broken line). The reasons for the differences arise from the reabsorption of nonequilibrium phonons by electrons. As stated above, the energy loss rate determined for electrons by scattering alone with LO-phonons via the wave-vector dependent Frohlich interaction may be even smaller than our determination because the net energy loss rate determined from Eq. (7) is the sum of rates caused by electron-phonon and electron-hole interactions.

(ii) The net energy loss rates for electrons and heavy-holes almost follow the rate obtained from Eq. (8). The reasons for this are the rapid decrease of u_e as shown in Fig. (8) and the slow cooling of the carrier temperature which results in $u_e/KT_c < 0.5$. This makes the electron-hole system behave more like a Boltzmann gas.

(iii) The energy loss rates increase as T_c increase. The dot-dashed curve even bends over and approaches the maximum value of 5.3×10^{-8}W for bulk GaAs. This "bending" behavior reflects the initial rapid cooling of hot carriers and was also observed by Shah et al.[2] This may be the indication for the presence of nonequilibrium phonons in the system.

In Fig. 9, we have plotted the average phonon emission time for hot carriers defined by:[8]

$$\tau_{avg} = \frac{E_{LO}}{P_e} e^{-E_{LO}/KT_c} \tag{9}$$

as a function of the carrier temperature. This is just another way to describe the energy relaxation process. As can be seen the τ_{avg} is carrier temperature dependent and therefore time dependent. For $T_c>1200K$ or $t<5$ ps the τ_{avg} remains at a value of about 1 ps. As time $t>5$ ps (or $T_c<1200K$) the τ_{avg} increases quickly with decrease of the carrier temperature. At T_c = 480K, τ_{avg} is 10 ps. Ryan et al.[8] obtained a constant value of 7 ps for τ_{avg} by studies of time-resolved photoluminescence of modulation doped-MQW. The reason for the difference is simply because their time resolution did not allow them to monitor the entire carrier cooling process. Our upper limit of 0.9 ps for the initial carrier cooling agrees with the theoretically predicted[7] value of 0.16 ps within our resolution. As soon as a large nonequilibrium phonon population is built up the carrier cooling is suppressed.

We have extensively discussed the energy relaxation process based on the experimentally determined distribution function $f_{e,h}(T_c,u_{e,hh},\varepsilon)$. In the same manner information about the carrier lifetime can be also obtained using determined $f_{e,h}$.[7] In Fig. 10 the carrier densities for electrons, heavy-holes, and light-holes as a function of time are determined from the experimental data. The densities are obtained by the following expressions:

$$n_e(t) = \int_0^\infty \rho_e f_e \, d\varepsilon \tag{10}$$

$$n_{hh}(t) = \int_0^\infty \rho_{hh} f_h \, d\varepsilon \tag{11}$$

$$n_{lh}(t) = \int_{\Delta E}^\infty \rho_{lh} f_h \, d\varepsilon \tag{12}$$

where ΔE is the energy separation between the hh- and lh-subbands at the zone center. The relation $n_e = n_{hh} + n_{lh}$ must be satisfied. The quantity of $\ln[n_e(t)]$ is also plotted in Fig. 10 as a broken curve.

The salient feature of the data in Fig. 10 is that the carrier density decreases nonexponentially and very rapidly within the first 30 ps after the end of a 0.5 ps pulse excitation. One cannot define a single carrier lifetime due to the nonexponential nature of the density decay curves. However, an effective carrier depletion time (time for the density to decrease by a factor of e^{-1} from $n_e(t=0)$) can be deduced to be as short as 10 ps. This decrease of carrier density occurring in such a short time cannot be accounted for by the usual bimolecular recombination, which is a much slower process, on the nanosecond time scale in the bulk GaAs and about 350 ps in quantum well structure with well thickness of ~ 5 nm.[23] This short carrier depletion time is not caused by the rapid carrier diffusion which will be discussed in the diffusion section.

Such a short carrier depletion time can be explained consistently by the participation of nonequilibrium phonons. The nonequilibrium LO phonons in the quantum well system can play two essential roles. First, they substantially suppress the energy relaxation process of carriers due to reabsorption of these phonons by carriers. Second, since these phonons are localized in both wavevector space and the real physical space (in the well plane) they will behave like coherent Bosons. The existence of the coherent Bosons will tend to

increase the number of the bosons in the system with a rate proportional to the present number of Bosons causing a rapid carrier relaxation. This is a stimulated phonon emission process and can only be accomplished by the phonon replica emission, i.e., when an electron in the conduction subband recombines with a hole in the valence subband not only a photon but also a phonon or more phonons will be emitted to join the Boson system. Since this is a stimulated process, it is very effective in exhausting carriers from the system. Unlike the conventional stimulated emission in a semiconductor laser, this process is expected to be even more effective at room temperature since equilibrium phonon occupation will also increase as lattice temperature increases. We have confirmed the nonequilibrium phonon induced stimulated-phonon-emission by the detailed polarization studies of integrated luminescence spectra discussed in the last section. By employing the nonequilibrium-phonon model we are able to explain not only the slow carrier cooling, but also the ultrashort carrier depletion time in highly photoexcited undoped quantum well structures.

Carrier Diffusion

Electron-hole plasma expansion at high photoexcitation power density in semiconductor bulk and quantum well structures is a subject of great interest from both the points of view of theory and device application. Various methods have been employed to study the dynamic process of carrier diffusion such as spatially and spectrally time-resolved luminescence spectroscopy[26,27] and Raman scattering.[11,28] Different mechanisms have been suggested to explain the rapid carrier diffusion in bulk semiconductors. Rapid electron-hole diffusion has been observed[27] in CdSe at 4K but not at room temperature. The absence of a larger number of thermal phonons at low temperature made it possible to observe the rapid carrier diffusion process. Using a streak camera, Junnarkar and Alfano[29] were able to measure the difference of spatial profiles of the pump laser and the photoluminescence at various excitation levels by which the diffusion velocity was estimated. Junnarkar and Alfano[29] obtained a diffusion velocity on the order of 10^8cm/s at high photoexcitation even at room temperature. Such a large diffusion velocity was attributed to screening of polar electron-phonon interactions and partially screened nonpolar electron-phonon interactions. High internal pressure of a very dense electron-hole plasma has been proposed[30] to account for the rapid expansion of plasma. The pioneering work of Tsen and Morkoc[11] using the time-resolved Raman scattering technique has shown no influence on photogenerated carrier diffusion by carrier confinement, zone folding of phonon modes, and phonon confinement in symmetric GaAs/AlGaAs MQW structure at low carrier density. In view of their works we should point out that the well thickness of their MQW structure was so thick that any confinement effects would be smeared out; and the carrier density deduced from Raman data was the total carrier density within whole energy distribution. Therefore, they could not obtain the information about dynamic diffusion of carriers with different kinetic energies. In the following subsection the results on dynamics of carrier diffusion processes in the x-y plane (lateral) will be presented.

A schematic diagram of the photoluminescence image on the screen of the streak camera is depicted in Fig. 11 to show how we study dynamics of carrier diffusion. The area inside the filled-line circle is the laser excited area. If there is no carrier diffusion photoluminescence should be restricted to inside this circle. Suppose sufficient electrons and holes can diffuse far enough to the unexcited area where they can recombine one should be able to detect the luminescence from the unexcited area (outside the filled-line circle). Using the streak camera we were able to measure the laser spatial profile and luminescence profile at the sample surface. Those spatial intensity profiles were integrated over a time duration of 1 ns. The width (FWHM) of spatial profile should give information on the carrier diffusion length within 1 ns. However, this information is not adequate to deduce accurate values of diffusion constant and diffusion velocity. To study the dynamic diffusion process quantitatively we make use of two electronic windows to obtain time-resolved photoluminescence from the excited (I_{sc}) and unexcited (I_{se}) areas at the same time (and thus laser intensity fluctuation was completely avoided).

The time-integrated laser and luminescence profiles at the surface of the 55Å symmetric MQW structure are plotted in Fig. 12. The dotted-curve is the laser profile. The inside and outside solid curves are the luminescence profiles at 740 nm and 770 nm, respectively. The broken-curve is the luminescence profile at 830 nm, which comes from the 1.2 μm buffer layer. The gain of the detecting system was adjusted such that the maximum intensity recorded was roughly the same. The widths of luminescence profiles above the subband edge (760-700 nm) are exactly the same as the width of the laser profile (dotted-line) reflecting no or little diffusion for high energy carriers within our spatial resolution. The width of the luminescence profile at the subband edge (770 nm) is about 2 times wider than the width of the laser profile. This energy dependence of the carrier diffusion process is not usually expected because a larger kinetic energy is associated with larger carrier velocities. However, the nonequilibrium phonons in the system during the first 30 ps after the laser excitation may inhibit carrier diffusion, especially for the carriers with high energy. The extent of carrier diffusion at the subband edge seems to be consistent with the results given by Tsen and Morkoc.[11] The diffusion velocity determined by them[11] is 8.6×10^6cm/s. According to this value the carriers will travel about 100 μm within 1 ns which will broaden the width of luminescence profile from 200 μm to about 400 μm. This agrees with the measured lateral width of the luminescence profile at 770 nm in Fig. 12. It should be pointed out that the initial carrier density in our experiment was about 100 times larger than in their experiment. Due to the short carrier depletion time (10 ps) in our case, the average carrier density within 1 ns would be similar in both cases.

The time-integrated laser and luminescence profiles at the surface of the asymmetric quantum well are plotted in Fig. 13. The innermost solid curve and dotted curve are the laser profile and the Gaussian-line-fit of the laser profile, respectively. The center wavelengths of the luminescence are indicated on the

curves. The key differences of the spatial luminescence intensity profiles of the asymmetric well from that of the symmetric wells are: the widths of luminescence profiles are much wider than the width of the laser profile; and the width of the luminescence profiles do not depend much on the wavelength of luminescence. The possible mechanisms are given below.

In Fig. 14, we have plotted the time-resolved photoluminescence from I_{se} and I_{sc} measured at 4K with 2 ps time resolution for asymmetric well. Based on the fact that the width of the spatial luminescence profile does not depend on the photon energy detected within our spatial resolution, we placed a wide-band filter centered at 700 nm in the luminescence path to increase the strength of the luminescence intensity. The broken curve is the Rayleigh scattering light from the sample surface. As can be seen, the risetime of the I_{sc} is time-resolution limited, while the rise of I_{se} is much slower than that of I_{sc} and also well resolved. The fast decay of I_{sc} has been discussed in the energy relaxation section. It should be emphasized here that using the same set of experimentally determined $T_c(t)$ and $u_e(t)$ we have determined the carrier depletion time is 10 ps. The only choice for theoretical fittings to I_{se} is the use of standard classical diffusion equation to calculate the carrier density as a function of time t and distance r. The exact values of separation between the two windows and the widths of the windows are given in Fig. 11. This method should be adequate as long as electrons act more like particles rather than waves.

The diffusion equation is given by:

$$\frac{\delta n(r,t)}{\delta t} = -\frac{n(r,t)}{\tau} + D\frac{\delta^2 n(r,t)}{\delta r^2} \tag{13}$$

where τ is the carrier lifetime, and D is the diffusion constant of carriers. The initial condition for carrier density is assumed[27] to be the same as the laser profile which is:

$$n(r,t=0) = n_0 e^{-4\log 2\frac{r^2}{a^2}} \tag{14}$$

where n_0 is the carrier density at the center of the laser spot at t=0, and a is 100 μm obtained by fitting the laser profile to Eq. (14). The solution of the second order differential Eq. (13) with the given initial condition Eq. (14) is given by:[27]

$$n(r,t) = n_0 e^{-t/\tau}\left[1 + \frac{16\log 2\, Dt}{a^2}\right]^{-1/2} e^{-r^2/(a^2/4\log 2 + 4Dt)} \tag{15}$$

Assuming ambipolar diffusion, i.e. electrons and holes have the same diffusion velocities,

$$I_{se} \sim \int_{r_1}^{r_2} n^2(r,t)\,dr \tag{16}$$

Using Eq. (16) the parameters of D and τ have been determined to be $10^6 cm^2/s$ and 10 ps, respectively.

The results are very surprising in two respects. First, the value for D is more than four orders of magnitude greater than the conventional diffusivity. The diffusion velocity $v = \sqrt{(D/\tau)} = 3.2\times10^8 cm/s$ is four times larger than the initial Fermi-velocity. It should be pointed out that the values for D and τ deduced from the time-resolved luminescence profile I_{se} with the theoretical expression Eq. (16) are consistent with time-integrated spatial luminescence profile. Second, the carrier lifetime at t<25 ps deduced from the diffusion Eq. (13) is the same as the carrier depletion time determined from the time-resolved luminescence data shown in Fig. 4. **This demonstrates that our analysis is self-consistent.** Using the determined n(r,t) we can show the contribution of the second term in the right-side of diffusion Eq. (13) in losing the carrier at a given position r is always smaller than the first term and thus the ultrashort carrier depletion time cannot be attributed to the carrier diffusion but to the nonequilibrium phonon enhanced phonon replica emission.

Several possible origins of the extraordinary rapid carrier diffusion in the x-y plane of the asymmetric quantum well can be given at this stage. (1) The internal pressure[30] of high electron-hole pairs may be extremely large when the density is well above the electron-hole liquid density. (2) There are a large number of the coherent nonequilibrium phonons emitted by hot electrons in the system. These phonons have momenta parallel to the x-y plane and may also drive the carriers outside the excited region by adding the phonon momenta to the carriers. (3) Due to the asymmetric potential well profile there are no transmission states (virtual states or unconfined states) above the energy barriers unlike the symmetric well case. This is the intrinsic property of asymmetric quantum wells. The photogenerated carriers may be immediately scattered by the higher energy barrier and obtain the momentum from the interface which assists carriers to expand in the x-y plane. Due to a large kinetic energy of ~300 meV, the photogenerated carriers acquire a large initial diffusion velocity. The origins (1) and (2) seem to be inconsistent with the symmetric well case. However, whether the mechanism described in (3) is responsible for the observed rapid diffusion is still an open question worthy of further study.

Conclusion

In this paper extensive data have been presented on time-resolved photoluminescence studies as well as other related investigations of a symmetric MQW structure and an asymmetric quantum well with similar well thickness. With 2 ps time resolution we were able to study the initial energy relaxation and carrier diffusion processes simultaneously under the same conditions.

The existence of a large population of nonequilibrium phonons in highly excited semiconductor quantum well structures is experimentally verified. Its effect on the energy relaxation is to slow down the cooling rate after an initial rapid cooling (0-5 ps). The symmetric and asymmetric potential well profiles do not show any difference in the energy relaxation process under the same conditions.

A new mechanism to explain the ultrashort carrier depletion time deduced from the consistent fitting of time-resolved photoluminescence profiles at various emitted photon energies, is proposed to be nonequilibrium phonon enhanced phonon replica emission rather than other nonradiative processes such as Auger recombination, carrier diffusion, and the conventional radiative stimulated emission.

The differences in carrier diffusion for two different potential well shapes are remarkable. For the first time we have observed the ultrafast carrier diffusion in the x-y plane of the asymmetric quantum well, while there is little or no carrier diffusion except for carriers at the subband edge in the x-y plane of the symmetric quantum well under similar experimental conditions.

Acknowledgements

We thank Jimmy Zheng for the technical help and Dr. K. Bajaj for helpful discussions. The research is funded by the U.S. Air Force Office of Scientific Research under Grant No. AFOSR-86-0031.

References

1. R. J. Seymour, M. R. Junnarkar, and R. R. Alfano, Solid State Commun. 41, 657 (1982).
2. J. Shah, Solid-State Electronics 21,43 (1978).
3. H. M. Van Driel, Phys. Rev. B 19, 5928 (1979).
4. C. V. Shank, R. L. Fork, R. Yen, J. Shah, B. I. Greene, A. C. Gossard and C. Weisbuch, Solid State Commun. 47, 981 (1983).
5. E. M. Conwell, "High Field Transport in Semiconductor" (Academic, New York, 1967).
6. J. Shah, A. Pinczuk, A. C. Gossard, and W. Wiegmann, Phys. Rev. Lett. 54, 2045 (1985).
7. C. H. Yang, Jean M. Carlson-Swindle, A. Lyon, and J. M. Worlock, Phys. Rev. Lett. 55, 2359 (1985).
8. J. F. Ryan, R. A. Taylor, A. J. Turberfield, A. Maciel, J. M. Worlock, A. C. Gossard, and W. Wiegmann, Phys. Rev. Lett. 53, 1841 (1984).
9. Y. Silberberg, P. W. Smith, D. A. B. Miller, B. Tell, A. C. Gossard, and W. Wiegmann, Appl. Phys. Lett. 46, 701 (1985).
10. Y. H. Lee, M. Warren, G. R. Olbiright, H. M. Gibbs, N. Peyghambarian, T. Venkatesen, J. S. Smith, and A. Yariv, Appl. Phys. Lett. 48, 754 (1986).
11. K. T. Tsen, and H. Morkoc, Phys. Rev. B 34, 6018 (1986).
12. P. P. Ho, A. Katz, R. R. Alfano, and N. H. Schiller, Optics Commun. 54, 57 (1985).
13. Kai Shum, P. P. Ho and R. R. Alfano, Phys. Rev. B 33, 7259 (1986).
14. Kai Shum, Mahesh R. Junnarkar, H. S. Chao, R. R. Alfano (unpublished).
15. R. Sooryakumar, D. S. Chemla, A. Pinczuk, A. C. Gossard, W. Wiegmann, and L. J. Sham, Solid State Comm. 54, 859 (1985).
16. J. E. Zucker, A. Pinczuk, D. S. Chemla, A. C. Gossard, and W. Wiegmann, Phys. Rev. Lett. 53, 1280 (1984).
17. H. Iwamnra, T. Saku, H. Kobayashi, and Y. Horikoshi, J. Appl. Phys. 54, 2692 (1983).
18. N. Holonyak, Jr., R. M. Kolbas, W. D. Laidig, B. A. Vojak, H. Hess, R. D. Dupuis, and P. D. Dapkus, J. Appl. Phys. 51, 1328 (1980).
19. P. Blood, E. D. Fletcher, P. J. Hulyer, and P. M. Smowton, Appl. Phys. Lett. 17, 1111 (1986).
20. M. S. Skolnick, K. J. Nash, P. R. Tapster, D. J. Mowbray, S. J. Bass, and A. D. Pitt, Phys. Rev. B 35, 5925 (1987).
21. The absolute intensity at different transition energies was obtained under identical excitation conditions. To do this, we fixed the channel plate gain, temporal analyzer gain, prepulse intensity as well as time scale for the weakest signal (at high energy tail) to be detected. The intensity of prepulse was then treated as the standard of excitation level. As intensity increases at lower energies, neutral-density (ND) filter(s) can be placed in the luminescence path if necessary. For the curves in Fig. 4 and Fig. 5 ND filters were not used to attenuate the luminescence intensity.
22. For a recent review, see J. Shah and R. F. Leheny in "Semiconductors Probed by Ultrafast Laser Spectroscopy" edited by R. R. Alfano, Academic Press, New York, 1984; pg. 45.
23. R. K. Chang, J. M. Ralston, and D. E. Keating, in "proceeding of the International Conference of Light Scattering Spectra of Solid", edited by G. B. Wright (Springer-Verlag, New York, 1969), pg. 369.
24. M. Costato. and L. Reggiani, Phys. Status Solidi (b) 58, 47 (1973).
25. E. O. Gobel, H. Jung, J. Kuhl, and K. Ploog, Phys. Rev. Lett. 51, 1588 (1983).
26. K. M. Romanek, H. Nather, J. Fisher, and E. O. Gobel, J. Lumi. 24/25, 585 (1981).
27. A. Cornet, M. Pugnet, J. Collet, T. Amand, and M. Rousseau, J. DE Physique 42, 471 (1981).
28. C. L. Collins, and P. Y. Yu, Solid State Commun. 51, 123 (1984).

29. Mahesh R. Junnarkar, and R. R. Alfano, Phys. Rev. B 34, 7045 (1986).
30. R. Zimmermann, and M. Rosler, Phys. Stat. Sol. (b) 75, 633 (1979).

Figures

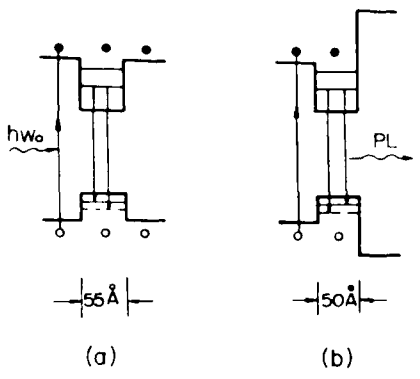

Fig. 1 The schematic potential profiles of a symmetric and an asymmetric quantum wells. The excitation photons are absorbed in both of the barriers and the wells for symmetric wells, while for the asymmetric well the absorbtion occurs in one of the barriers and the well . The photoluminescence originates from the recombination of n=1 electrons and n=1 heavy-hole as well as light-hole.

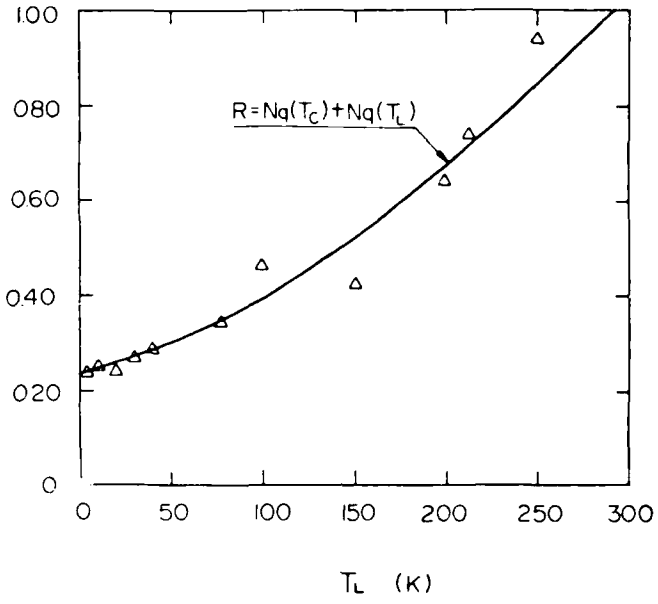

Fig. 3 The triangles are the ratios of the peak intensity of B and A indicated in Fig. 2. The solid curve is explained in the text.

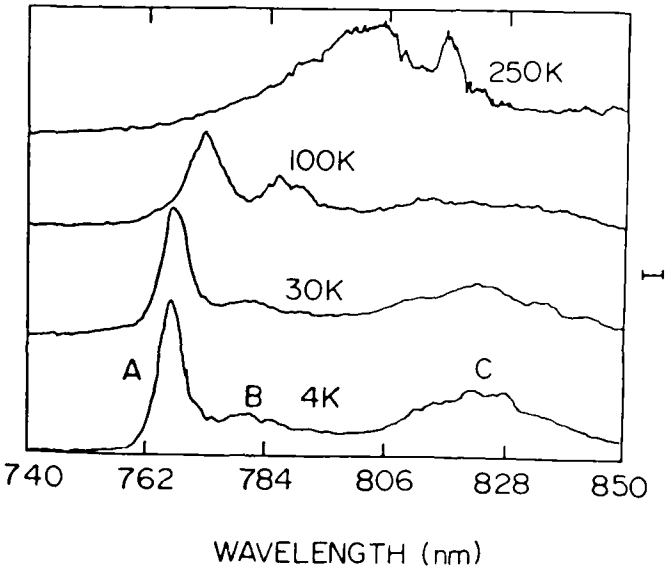

Fig. 2 The time-integrated luminescence spectra at various lattice temperatures. The peaks A, B, and C are explained in the text.

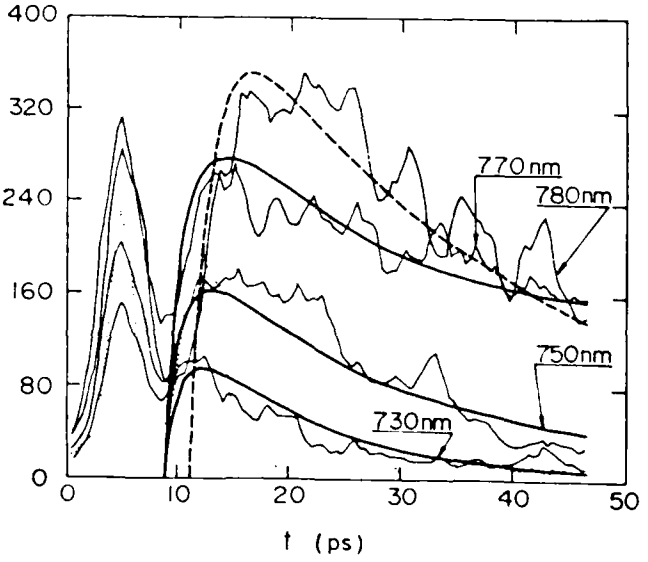

Fig. 4. Time-resolved photoluminescence profiles (solid curves) from the symmetric MQW at 4K at various wavelengths. The narrow peaks within 0-10 ps are the prepulses used for average. The next peak of the dotted curve is the Rayleigh scattering light from the sample surface

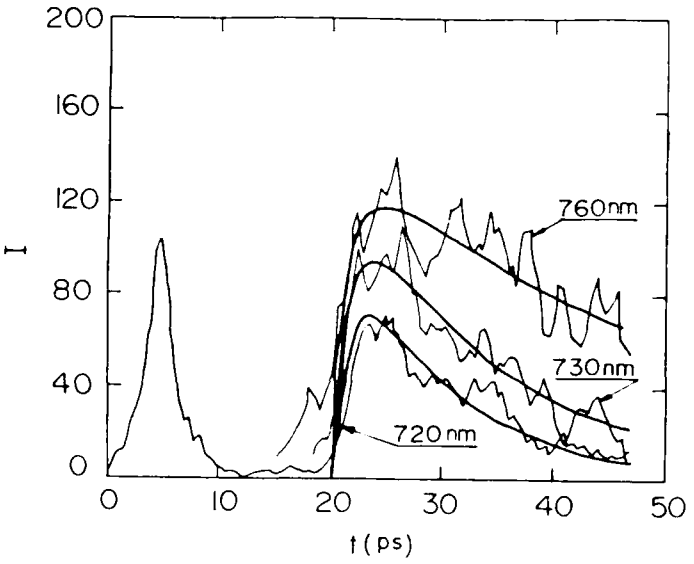

Fig. 5 Time-resolved photoluminescence from the asymmetric quantum well at 4K at various wavelengths.

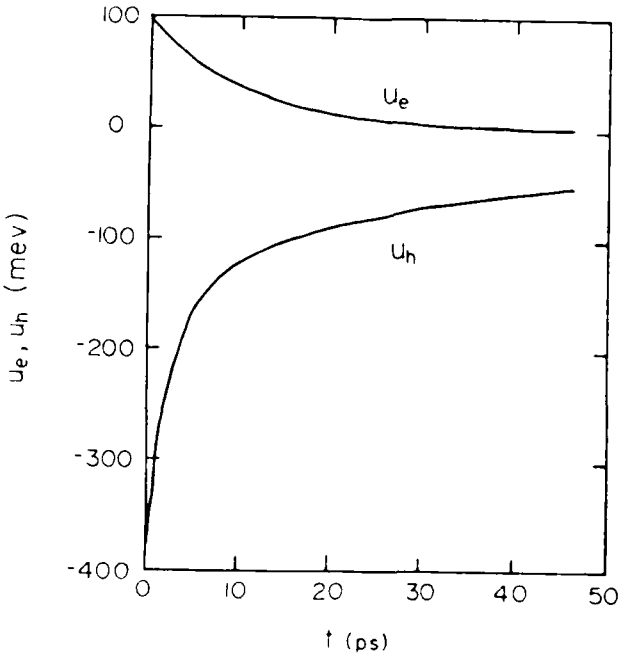

Fig. 7 Experimentally determined quasi-Fermi energies for electrons (up solid curve) and for holes (down solid curve).

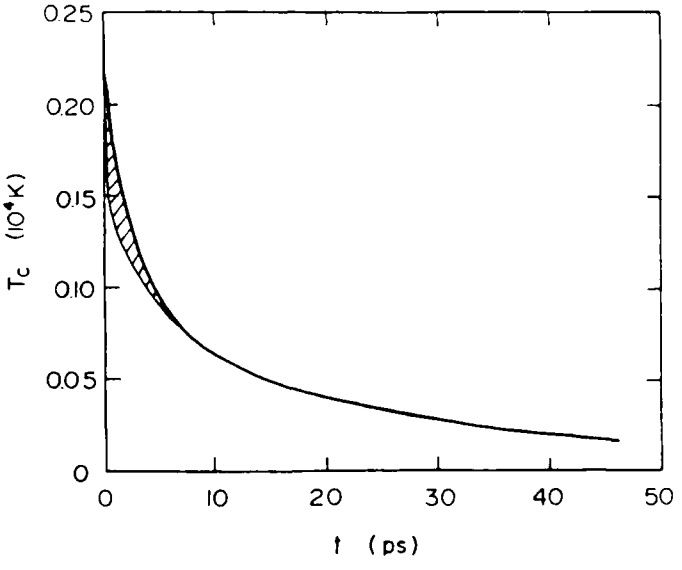

Fig. 6 Experimentally determined carrier temperature as a function of time. The shaded area indicates the extent of uncertainty in deducing carrier temperature within the first 4 ps.

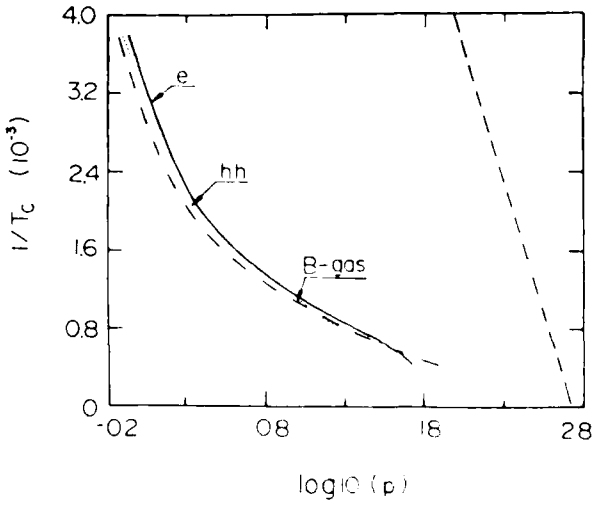

Fig. 8 Experimentally determined net energy loss rates for electrons (e) and heavy-holes (hh) obtained from Eq. (7). The dot-dashed curve is obtained from Eq. (8). The broken line is the theoretical result for bulk GaAs.

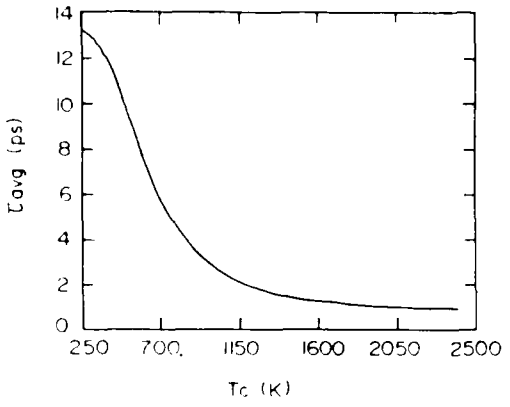

Fig. 9 Experimentally determined average phonon emission time as a function of carrier temperature obtained from Eq. (9).

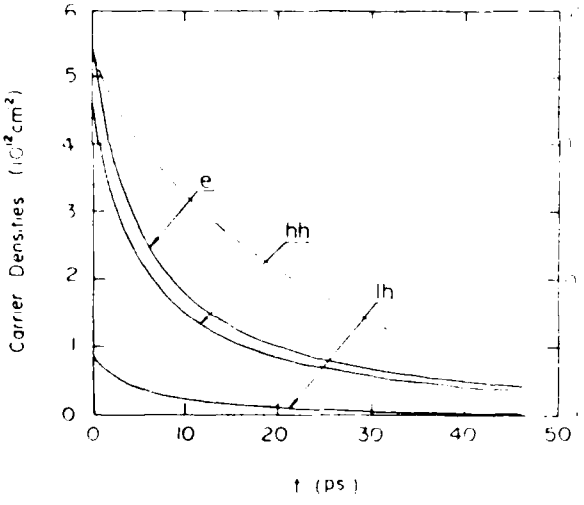

Fig. 10 Experimentally determined carrier densities as a function of time. e for electron, hh for heavy-hole, and lh for light-hole. The broken curve is the natural logarithm plot of the carrier density for electrons.

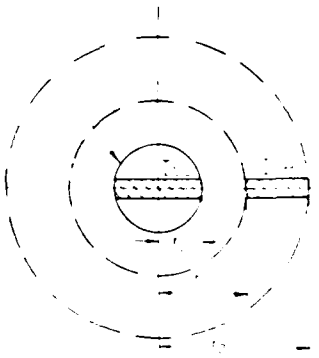

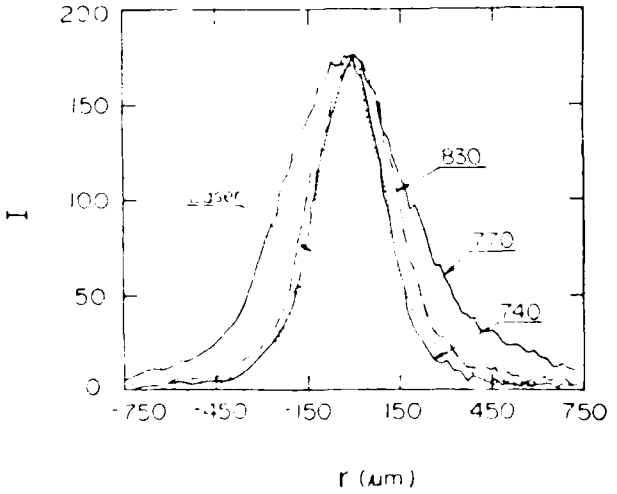

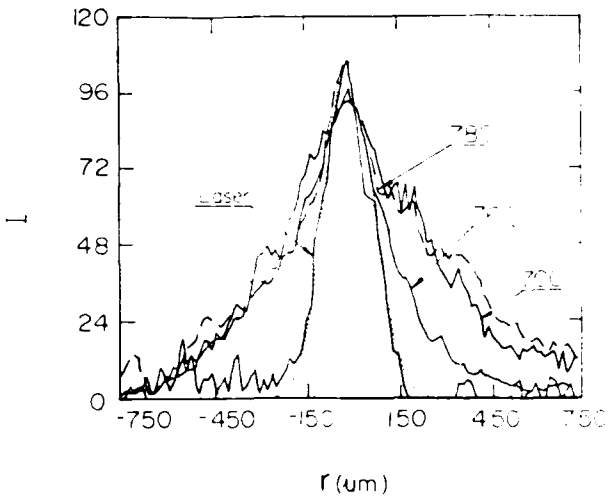

Fig. 13 Time-integrated spatial profiles of laser and the luminescence from the asymmetric well at various wavelengths at 4K.

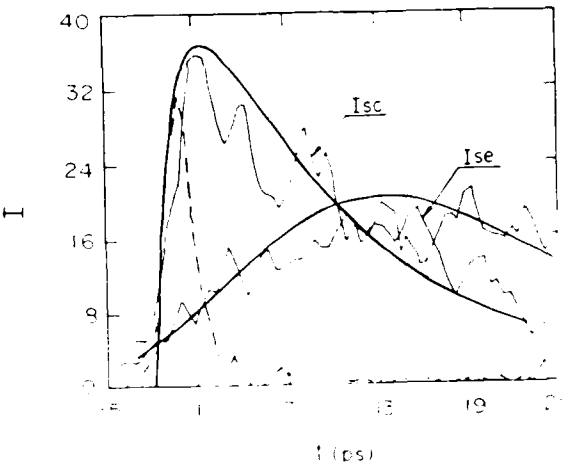

Fig. 14 Time-resolved photoluminescence of the asymmetric well at 4K from different spatial regions as distinguished by I_{sc} and I_{se}. The solid curves are the theoretical fit by using Eq. (2) and Eq. (16) for I_{sc} and I_{se}, respectively.

A Reprint from the

PROCEEDINGS

Of SPIE-The International Society for Optical Engineering

Volume 793

Ultrafast Lasers Probe Phenomena in Bulk and Microstructure Semiconductors

25-26 March 1987
Bay Point, Florida

Confinement effects on the scattering of electrons by polar optical phonons in semiconductor quantum wells

Kai Shum, R. R. Alfano
Department of Electrical Engineering, IUSL
The City College of New York, New York, New York 10031

Confinement Effects on the Scattering of Electrons by Polar Optical Phonons in Semiconductor Quantum Wells

Kai Shum and R. R. Alfano

Department of Electrical Engineering, IUSL, The City College of New York
New York, New York 10031

Abstract

The non-commutation relationship between the Hamiltonian of the system and the electron momentum operator in the confinement z-direction was taken into account using random variables in the calculation of electron scattering by polar optical phonons in quantum wells. The rate at the onset of phonon emission is found to be 3 times smaller than previously reported. Furthermore, this rate becomes an increasing function of initial electron energy instead of a decreasing function.

It is important to take into account the effect of electron confinement on the scattering of electrons by polar optical phonons (POP) in quasi-two-dimensional (Q2D) quantum wells.[1-4] The Hamiltonian H of the electron system and the operator k_z for the electron momentum in z-direction do not commute with each other because of the potential profile experienced by electrons in the confinement z-direction. That is,

$$[H,k_z]=i\frac{d}{dz}V(z), \tag{1}$$

where $\hat{V}(z)$ is the potential operator in z-direction. The usual conservation law of momentum in z-direction:

$$q_z=k_z-k'_z \tag{2}$$

must be modified in the sense that q_z, k'_z and k_z are no longer deterministic observable variables but are random variables (r.v.). Here, q_z is the z-component of the phonon wave vector, k_z and k'_z are the electron wave vectors before and after scattering, respectively. The statistics of each r.v. is characterized by its probability density function. The pioneering work of Hess[1], Price[2] and Leburton[3] essentially adopted a "non-momentum-selection rule" in z-direction for calculation of phonon emission and phonon absorption rates. They treat q_z as a regular deterministic variable. Although Ridley[4] realized "fuzzy momentum conservation" in z-direction, he used instead a "momentum conservation approximation". Furthermore, the value of k_z in wave function in the coordinate representation was considered as the electron momentum in z-direction in his analysis. This approach is not valid since k_z is equal to a precise value of π/L_z in an "infinite well" approximation and for a "finite well" k_z is just a parameter that related to the eigen-value of the Hamiltonian of the electron system.

The thesis of this paper is to present a theoretical analysis of electron scattering by POP in Q2D structures placing emphasis on confinement effects by taking into account the non-commutation relationship between the Hamiltonian operator H and the electron momentum operator k_z. We show how "fuzzy momentum conservation" in z-direction is exactly treated using neither the "non-momentum-selection rule" nor the "momentum conservation approximation" but by considering q_z as a random variable. A key result that distinguishes this work from the previous works[1-4] is that the rate at the onset of phonon emission is reduced by a factor of 3.

There are two important aspects of the non-commutation relationship given by Eq. (1). First, the corresponding observables cannot be measured simultaneously with arbitrary accuracy. The product of their quantum root-mean-square deviation must not be less than the half of the quantum expectation value of the operator $i\frac{dV(z)}{dz}$ in a given state. Second, the electron energy due to the motion in z-direction has no correlation with the corresponding electron momentum in this direction. The eigen-value of momentum operator k_z cannot precisely be determined due to the electron confinement by the potential well and must be considered as a random variable (r.v.). When an electron is restricted in the first bound state the quantum expectation value of $[H,k_z]$ is zero resulting in a precise determination of the lowest eigenvalue of operator H and root-mean-square deviation for k_z can be determined. These two points play the key role in calculating the electron-POP scattering rate.

In our analysis, the unscreened electron-POP interaction, equilibrium bulk phonon spectrum and an infinite depth square well with the lowest subband occupied are assumed.

Within the framework of the effective-mass-approach, the wave function for electron in coordinate representation is then given by

$$|k>=\frac{e^{ikr}}{\sqrt{A}}\phi(z), \tag{3}$$

where

$$\phi(z)=\sqrt{\frac{2}{L_z}}\ \sin\ \frac{\pi z}{L_z} \tag{4}$$

is the wave function in z-direction describing the bound state. The vectors $r=(x,y)$ and $k=(k_x,k_y)$ denote the two dimensional electron position and the wavevector parallel to the interfaces, respectively. The corresponding electron energy can be expressed as

$$E=\frac{h^2k^2}{2m}\ +\ E_z, \tag{5}$$

where

$$E_z=\frac{h^2\pi^2}{2mL_z{}^2}. \tag{6}$$

Here m is the isotropic electron effective mass, L_z is the well width and A is the layer area.

The probability density function for the r.v. k_z can be obtained from the wave function given by Eq. (4) by a representation change to the wavevector space using

$$\phi(k_z)=\frac{1}{\sqrt{2\pi}}\int_{-\infty}^{\infty}\phi(z)e^{-ik_zz}\,dz. \tag{7}$$

This yields

$$\rho(k_z)\ =\ \left|\phi(k_z)\right|^2\ =\ \frac{4L_z\ \cos^2(k_zL_z\quad 2)}{\pi^3(1-k_z{}^2L_z{}^2\quad \pi^2)^2}. \tag{8}$$

Since there exists a "fuzzy momentum conservation law"[3] in z-direction given by Eq. (2), the probability density function for the r.v. q_z, $\rho(q_z)$, can be obtained from the convolution expression:

$$\rho(q_z)\ =\ \rho(\pm k_z)\ *\ \rho(\overline{+}k'_z). \tag{9}$$

The electron scattering rate ($w_{k'k}$) per unit area in k-space in Q2D structures can be expressed in Born approximation by Fermi's golden rule by:

$$w_{k'k}\ =\ \frac{4\pi A}{h(2\pi)^2}\ \left|M_{k'k}\ \right|^2\delta(E_k\ -\ E_k\ -\ h\ \omega_o), \tag{10}$$

where

$$M_{k'k}\ =\ \frac{-c(n_Q+1)^{1/2}}{Q}\ \delta_{k-k+q}F(q_z,L_z) \tag{11}$$

with

$$c\ =\ i\left(\left[\frac{e^2h\omega_o}{\varepsilon V_s}\right]\right)^{1/2} \tag{12}$$

is the matrix element for the Frohlich electron-POP interaction. For simplicity we have only considered phonon emission process. Q and V_s denote the three dimensional phonon wavevector (q,q_z) and the sample volume, respectively. The δ is a modified Kronecker function defined as

$$\delta_{a-b}\ =\ \begin{cases}1 & \text{if } a=b\\ 0 & \text{if } a\neq b\end{cases} \tag{13}$$

The function F in Eq. (11) is the form factor in z-direction which is defined as:

$$F(q_z,L_z)\ =\ \frac{2}{L_z}\int_0^{L^z}e^{-iq_zz}\ \sin^2\ \frac{\pi z}{L_z}\,dz. \tag{14}$$

The point here is to realize that the matrix element $M_{k'k}$ is the function of a r.v. q_z.

Therefore, the $w_{k'k}$ also becomes a r.v.. The most likely value of the $w_{k'k}$ that can be experimentally measured is given by its expected value using the statistics associated with the r.v. q_z. This is,

$$\bar{w}_{k'k} = \int_{-\infty}^{\infty} \rho(q_z) w_{k'k}(q_z) dq_z. \tag{15}$$

The total emission rate is then given by

$$w_{k'k} = \int \bar{w}_{k'k}\, d\,q = \int\int I^{Q2D}(q,L_z)\delta(E_k - E_{k'} - \hbar\omega_o)\delta_{k'-k+q}\, q\, dq\, d\theta \tag{16}$$

where

$$I^{Q2D}(q,L_z) = I_o \int_{-\infty}^{\infty}\int_{-\infty}^{\infty} g(x,y)\,dy\,dx, \tag{17}$$

and θ denotes the angle between the k and q. The factor I_o is defined as:

$$I_o = \frac{(n_Q + 1)e^2 q_o \omega_o}{2\pi\varepsilon}. \tag{18}$$

The function g(x,y) is given by:

$$g(x,y) = 0.1\,\frac{z}{q^2+x^2}\left(\frac{\sin^2(\frac{xz}{2})}{\left[1-(xz/2\pi)^2\right]^2 (xz/2)^2} \cdot \frac{\cos^2\left[(x+y)z/2\right]\cos^2(yz/2)}{\left[1-(x+y)^2z^2/\pi^2\right]^2\left[1-y^2z^2/\pi^2\right]^2}\right) \tag{19}$$

with $z = q_o L_z$, which includes $1/Q^2$ from Frohlich electron-POP interaction Hamiltonian, the form factor in z-direction and the probability density function $\rho(q_z)$ for r.v. q_z. All the wave vector are normalized by $q_o = \frac{\sqrt{2m\,\omega_o}}{\hbar^2} = L_o^{-1}$ which is about $1/40\text{Å}$ for GaAs.[5]

The integral I^{Q2D} given by Eq. (17) for Q2D structures represents the electron-POP interaction strength as function of q. It contains all the information about confinement effects as well as size effects on the scattering rates. In order to further understand how electron confinement makes the difference in the electron scattering rate between Q2D structures and its bulk counterpart, a plot of the electron-POP interaction strength I^{3D} versus q for 3D electron system is needed in such a form that can be compared with I^{2D}. It can be shown that

$$I^{3D}(q) = \frac{I_o}{q^2 + \Delta k_z^{(-)^2}} + \frac{I_o}{q^2 + \Delta k_z^{(+)^2}}, \tag{20}$$

where $\Delta k_z^{(\bar{+})} = (k_z \bar{+} k'_z)$. The first and second terms on the right side of Eq. (20) represent the scattering processes without and with change of initial direction of electron momentum, respectively. Since $\Delta k_z^{(+)}$ in Eq. (20) depends on both the magnitudes as well as the scattering angle θ, one cannot find an explicit expression for for $\Delta k_z^{(+)}$ in terms of q and θ unless a variational parameter for the electron kinetic energy ratio ($r = K^2 / k_z^2$) between the total kinetic energy and the energy due to the z-direction motion is introduced.

Using the momentum and the energy conservation laws for the 3D scattering process, the $\Delta k_z^{(\bar{+})}$ can be expressed as

$$\Delta k_z^{(\bar{+})} = \frac{(q^2+\xi)\bar{+}\sqrt{(q^2+\xi)^2 - \xi 4q^2\cos^2\theta}}{2q\cos\theta\sqrt{r-1}} \tag{21}$$

where $0 \le \theta \le \arccos\sqrt{\frac{\hbar\omega_o}{E_k}}$ and $\xi = r - \frac{1}{r}$ with $1 < r < \infty$. The value of r=3 implies that the kinetic electron

energy is equally distributed in all directions, while r<3 more electron kinetic energy is in the z-direction. The 2D electron motion in x-y plane corresponds to the case when r approaches infinite.

We now present the numerical results in the following sections.

The two solid curves in Fig. 1 show the probability density profiles for the r.v. q_z obtained from Eq. (9) for well width $L_z = 2L_o$ and $5L_o$. The larger well width L_z, the smaller is the variance of the density curve resulting in the less fuzzy momentum conservation in z-direction. The magnitudes of $F(q_z,L_z)$ versus q_z for $L_z = 2L_o$ and $5L_o$ are also displayed in Fig. 1 as two dotted curves. The two features from the plots should be noticed. First, in the limit $q_z \to 0$, $|F(q_z,L_z)|$ approaches unity independent of L_z reflecting a scattering event with an exact momentum conservation in z-direction. This is also the most favorable process according to the density curve for q_z. Second, for very thick well the $|F(q_z,L_z)|$ can be written as $\delta_{k_z-k'_z-q_z}$ which implies the momentum conservation law for any scattering event and $\rho(q_z)$ approaches a δ-function for the bulk situation. The fact that not every scattering event follows the exact momentum conservation law in z-direction is due to the electron confinement. This produces the weakening of electron-POP interaction in Q2D structures.

The solid curves in Fig. 2 show the integral I^{Q2D} as function of the parallel component of phonon wave vector q with L_z as a parameter. Curves 1, 2, 3, and 4 are plotted in Fig. 2 for the value of L_z of $0.5L_o$, L_o, $3L_o$ and $5L_o$, respectively. Our calculation procedure using the probability density function $\rho(q_z)$ for r.v. q_z yields a significant reduction by a factor 2 on the value of the integral I^{Q2D} obtained by Leburton[5] in the range from 0.1 to 4 for q. In spite of this key difference other features of our integral I^{Q2D} are very similar to what Leburton has shown.[5] Namely, the integral I^{Q2D} is a monotonic decreasing function of q for Q2D electron system and weakly dependent on L_z. This similarity occurs just because the profile of probability density function for q_z happens to have similar shape as $|F(q_z,L_z)|$.

The interaction strengths I^{3D} for 3D system with various values of θ and r are also displayed in Fig. 2 by the dotted curves 5 to 8. The values of r for curves 5, 6, and 8 are 10, 3, and 1.2, respectively. The value of θ for those three curves is set to be zero. The curve 7 with r=1.2 and $\theta=\pi/6$ is used to see the variation of $I^{3D}(q)$ by the change of the scattering angle θ. A comparison of the dotted curves 5 to 8 for 3D with the solid curves for Q2D provides the physical insight into electron confinement in quantum wells. The following three points are discussed: first, the value of I^{3D} increases with increase of the value of r. It indicates that the electron-POP interaction strength for given value of q in the system with r>3 is stronger than the system with r≤3. The reason for this is the weakness of electron motion in z-direction resulting in small amount of change of the electron momentum $\Delta k_z^{(+)}$. It should be emphasized that the value of I^{Q2D} at q as $L_z \to 0$ do not approach the value of I^{3D} with $r \to \infty$ which corresponds to the 2D case. In other words, as far as the electron scattering process is concerned the Q2D quantum well structure with $L_z \to 0$ is not equivalent to a 2D system due to the potential barriers which confine electrons inside the well. The values of I^{3D} and I^{Q2D} are close to each other for the value of the ratio r between 1.2 to 1.5. This implies the origin of the difference in electron scattering between Q2D and 3D systems comes from the fact that the electron kinetic energy is not equally distributed in all directions arising from electrons in the well obtain extra kinetic energy in z-direction from the potential barriers. These are important findings which were overlooked in previous works.[1-4]

Second, the larger scattering angle θ yields a larger value of I^{3D}. For q>1, i.e., for the scattering processes in which electrons change their initial momentum direction, the value of I^{3D} is almost independent of θ and can be distinguished from various values of r by the second term of the right hand side of Eq. (20). The value of I^{Q2D} is independent of θ and insensitive to the L_z for q≤1 giving rise to a weak L_z dependence of total electron scattering rates. It also appears that the value of I^{Q2D} for q>1 is more sensitive to L_z than for q<1.

Third, a dent occurs in each dotted curve which becomes smaller when r increases. The position of the dent moves towards the smaller q when r decreases. It should be noticed that the dent does not appear in solid curves for Q2D structures. This is because the non-commutation relationship given by Eq. (1) employed for Q2D systems which gives rise to the momentum change in the z-direction does not correlate to the momentum change in the direction parallel to the quantum well interfaces.

The total normalized phonon emission rate $(W_{k'k}/W_o)$ in Q2D quantum wells versus normalized energy $E_k/\hbar\omega_o$ is displayed in Fig. 3 by two solid curves. The normalization factor W_o is given by $W_o = 2\pi I_o/\hbar^2 q_o^2$. For GaAs $W_o = 1.24\ ps^{-1}$. For comparison, the calculated results for Q2D by Leburton[5] (dash curves) and for 3D (dotted curves) are also plotted in Fig. 3. The results of our approach clearly differ from the others[1-5] in two aspects. First, the Q2D phonon emission rates for various L_z are 3 times smaller at the onset of phonon emission $(E_k/\hbar\omega_o=1)$ than previously obtained.[1-5] Second, the phonon emission rate is a slowly increasing function of initial electron energy instead of being a decreasing function. The non-zero value of the phonon emission rate for $E_k=\hbar\omega_o$ stems from the nature of Q2D density of states. For thick quantum wells $(L_z>5L_o)$ the phonon emission rate is about a factor of 2 smaller than the 3D rate for $E_k/\hbar\omega_o>2$ resulting from the weakening of the electron-POP interaction in the z-direction for Q2D case and neglecting higher intra-subband and inter-subband contributions. The Q2D emission rate will approach the 3D result when $L_z \to \infty$ if all the contributions mentioned above are included. The phonon emission rate is comparable to the 3D rate for very thin quantum wells arising from the competition between Q2D density of states and the weakening of electron-POP interaction strength in z-direction.

For completeness, it should be pointed out that the phonon absorption scattering rate can be treated in the same way as outlined in this paper. One should expect that the emitted phonon by Q2D electrons traveling in the direction perpendicular to the quantum well interface may be easily reabsorbed. This is because those phonons are not plane-wave-like phonon mode that is extended to the whole sample. The phonons are localized inside the well the same as the localized electrons.

In conclusion, the confinement effects on the phonon emission rate of the electron in Q2D structures through the unscreened electron-POP interaction are shown by taking into account the non-commutation relationship between the Hamiltonian of the system and the electron momentum operator in the z-direction. It is explicitly demonstrated how one can exactly treat the fuzzy momentum conservation in z-direction using neither "non-momentum-selection rule" nor "momentum conservation approximation" by considering the phonon wave vector q_z as a r.v.. The phonon emission rate at the onset is found 3 times smaller than previously reported and increases with initial electron energy.

This work was supported by the Air Force Office of Scientific Research grant #86-0031. The authors would like to thank Jianping Lu and Jimmy Zheng for their help in computer analysis.

REFERENCE

(1) K.Hess, Appl. Phys. Lett., 35, 484(1979).
(2) P. J. Price, Ann. Phys.,133, 217(1981).
(3) B. K. Ridley,J.Phys. C 15, 5899(1982), and F. A. Riddoch and B.K. Ridley, J.Phys. C 16,6771(1983).
(4) J. P. Leburton, J.Appl. Phys. 56, 2850(1984).
(5) The material parameter used for GaAs are $m=0.067m_0$, $\epsilon=70$ and $\hbar\omega_0=36.8meV$.

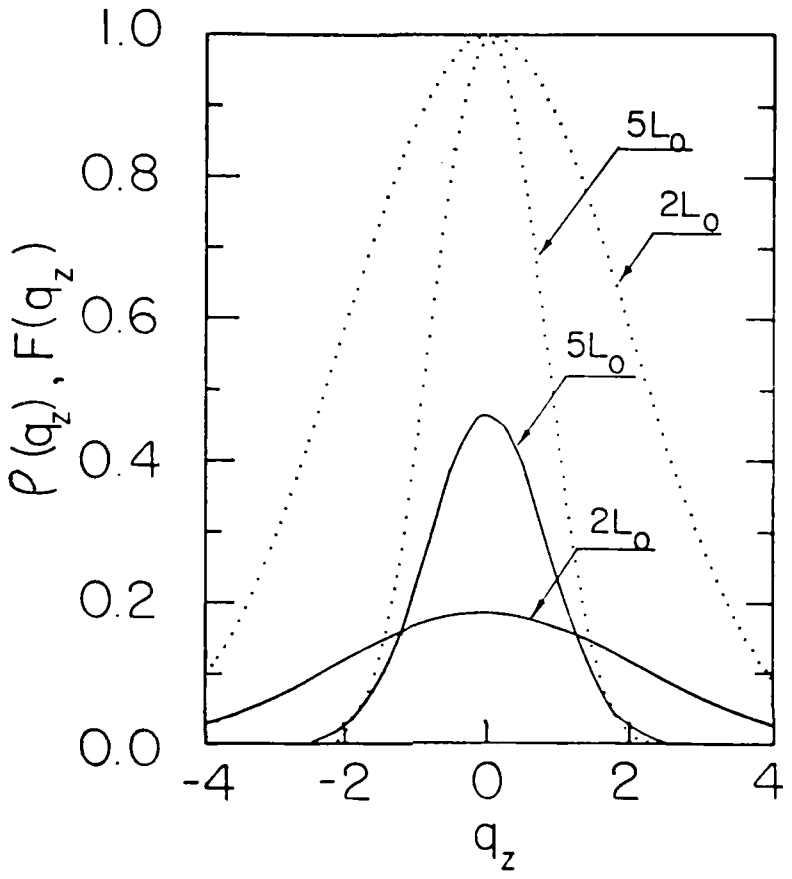

Fig. 1 The solid curves are for the probability density functions for r.v. q_z. The dotted curves are for the magnitudes of the form factor in z-direction $F(q_z, L_z)$. The well widths are indicated on the curves.

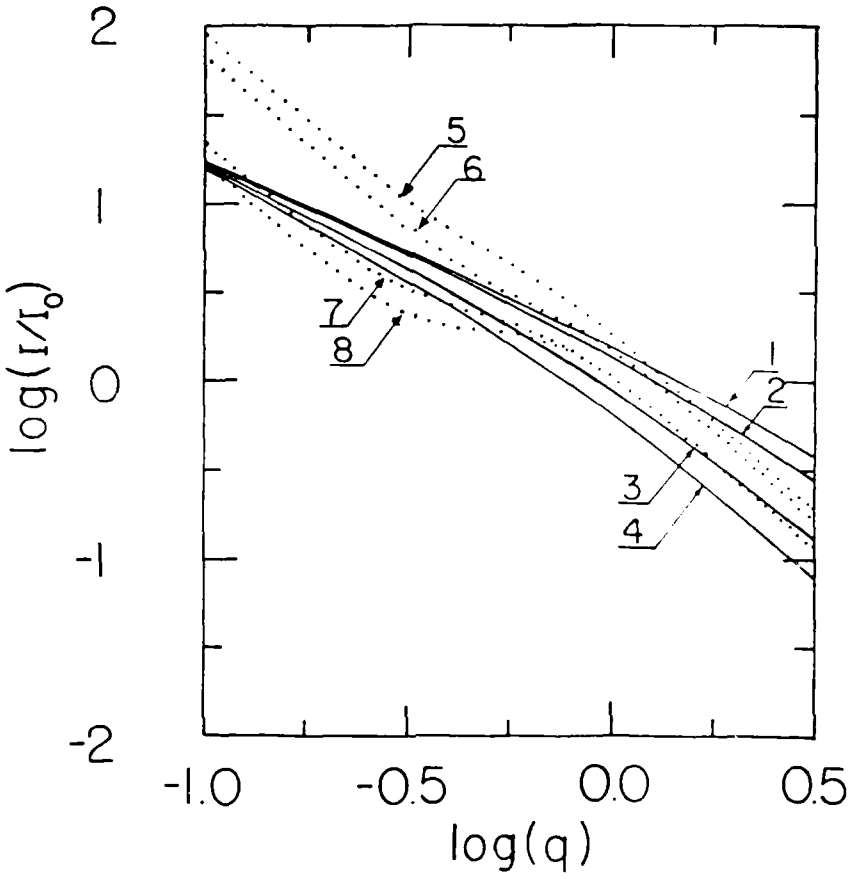

Fig. 2 The electron-POP interaction strength for Q2D and 3D systems versus the parallel component of phonon wave vector q. The solid curves from 1 to 4 are for the Q2D structures with well width 0.5 L_o, L_o, $3L_o$, and $5L_o$ accordingly. The main contribution of the integral I^{Q2D} to the total phonon emission rate occurs at q=1, where I^{Q2D} presents a weak L_z dependence. The dotted curves from 5 to 7 are for the 3D system with ratio r=10, 3, and 1.2, respectively. The scattering angle θ for those three curves are set to be all zero. The dotted curve 8 is also for 3D system with r=1.2 and $\theta=\pi/6$. The larger scattering angle θ, the larger the value of I^{3D} in the range from 0.1 to 1 for q.

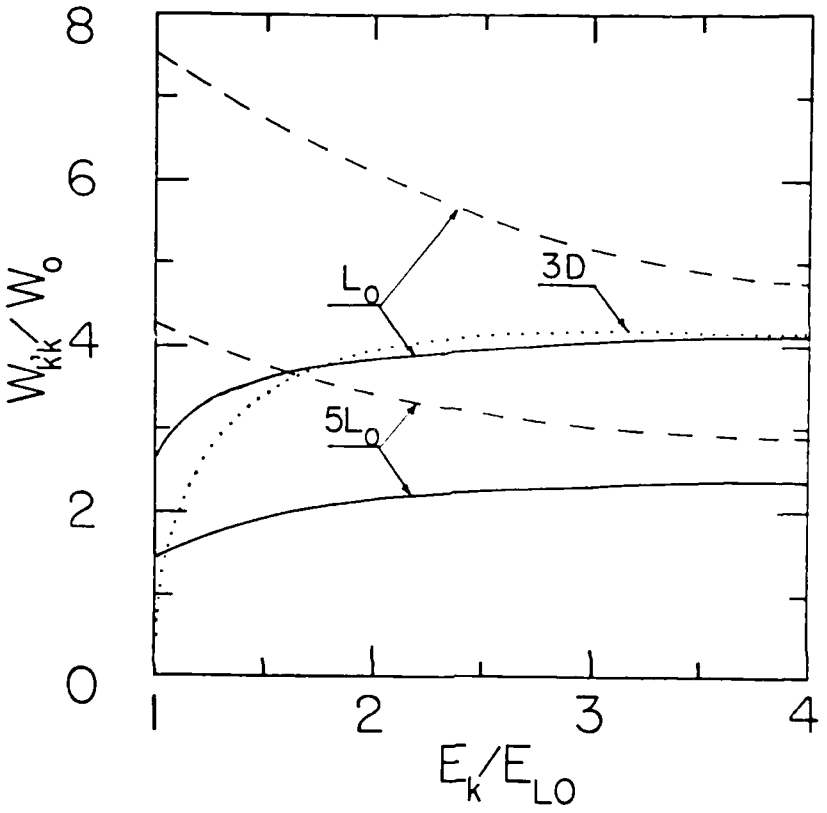

Fig. 3 The normalized phonon emission rates as function of $E_k/\hbar\omega_o$ in semiconductor structures at 0 K lattice temperature. The solid curves are from this work and the dash curves were generated from Leburton's result.[9] The well thicknesses are indicated on the curves. The dotted curve is the 3D result.

A Reprint from the

PROCEEDINGS

Of SPIE-The International Society for Optical Engineering

Volume 793

Ultrafast Lasers Probe Phenomena in Bulk and Microstructure Semiconductors

25-26 March 1987
Bay Point, Florida

Optical transitions and enhanced recombination lifetimes in quasi-zero dimensional electron system in CdS_xSe_{1-x}

Kai Shum, G. C. Tang, Mahesh R. Junnarkar, R. R. Alfano
Institute for Ultrafast Spectroscopy and Lasers
Depts. of Physics and Electrical Engineering
City College of New York, New York, New York 10031

Optical Transitions and Enhanced Recombination Lifetimes in Quasi-zero Dimensional Electron System in CdS_xSe_{1-x}

Kai Shum, G. C. Tang, Mahesh R. Junnarkar, and R. R. Alfano

Institute for Ultrafast Spectroscopy and Lasers
Depts. of Physics and Electrical Engineering, City College of New York
New York, New York 10031

Abstract

The recombination lifetimes for the radial and angular quantum number conserving 1S→1S and 1P→1P transitions from three-dimensionally confined electrons in CdS_xSe_{1-x} were measured by time-resolved photoluminescence. The assignment of the observed transitions is supported by calculations of eigen energy levels, squared matrix element ratio for those transitions, steady-state and picosecond spectroscopic studies.

Introduction

Carriers localized in semiconductor microstructures have attracted much attention both for fundamental reasons and for their potential applications. Semiconductor crystallites in a transparent insulating matrix can confine electrons in three dimensions because their diameters range from 30 Å to 800 Å.[1-3] The envelope wave functions in spherical coordinates [r, θ, φ] and eigen energies of conduction electrons and valence holes localized in an infinite-spherical-well within the effective mass approximation are given by:

$$|nLm> = C_{nL}\, j_L(\chi_{nL} r)\, Y_{Lm}(\theta,\phi), \tag{1}$$

and

$$E_{nL} = \frac{h^2 \chi_{n^2 L}}{2m_{e,h} a^2}, \tag{2}$$

respectively. The subscripts n,L, and m are effective radial, angular and magnetic quantum numbers, respectively. j and Y are the spherical Bessel and spherical Harmonic functions, respectively. a is the radius of crystallite and $m_{e,h}$ is the effective mass of electron or isotropic hole mass.[5] The value of χ_{nL} for the lowest two states of either conduction electron or valence hole 1S and 1P are π and 4.49, respectively. S stands for L=0 and P for L=1. The allowed transitions which conserve angular and radial quantum numbers are 1S→1S, 1P→1P, and higher transitions. The physical picture of the quasi-OD electron system described above has been experimentally verified by several groups.[1-3] Large and fast optical nonlinearities arising from photogenerated electron hole pairs have been also reported in quasi-OD electron systems.[6-7] Pioneering subnanosecond time-resolved photoluminescence[8] and picosecond pump-probe experiments[9] have been performed. It is important to study the dynamics of various excitations in quasi-OD electron systems in detail in order to understand the physical origins underlying these various novel optical properties.

In this paper, we report on measurements of ultrafast recombination lifetimes for the radial and angular quantum number conserving 1S→1S and 1P→1P transitions in quasi-OD electron systems in CdS_xSe_{1-x} at 4.3K using a streak camera detection system, and on the observation of optical transitions using photoluminescence spectroscopy between quantized levels (1S, 1P) in the conduction and valence bands in quasi-zero dimensional electron system in CdS_xSe_{1-x}. **The time-resolved photoluminescence detected at various emission energies allows us to unambiguously identify the 1S→1S and 1P→1P transitions.** The recombination lifetime of 1P→1P transition was measured to be 3.5 times shorter than 1S→1S transition. The ultrafast decay of 1P excitation may have practical importance for the construction of ultrafast reversible optical switches. **The assignment of the observed S and P transitions were supported by calculations of eigen energy levels and squared matrix element ratios for these transitions, as well as from steady-state photoluminescence spectra of the same samples used for the picosecond kinetic studies.**

Experimental Method

The samples investigated were four optical glass filters 2-61, 2-59, 2-58 and 2-64 manufactured by Corning years ago. The samples were mounted on a cold finger of a variable temperature helium optical cryostat (2K to 300K). The x value for each sample was accurately obtained from chemical analysis.[10] The picosecond experimental setup used in this research has been described in detail elsewhere.[11] A second harmonic (530 nm) of a Nd-glass laser pulse of 8 ps duration was used to excite the samples on the front surface. The maximum optical energy incident onto the front surface was about 40 μJ. This corresponds to 10^{16} photons per single shot. The spot size was 8×10^{-3} cm^2. The exact photoexcited carrier density in quasi-OD electron system was difficult to estimate due to the complexity of the surface of the crystallites. Assuming all the photons were absorbed with 10μm, a value on the order of 10^{18} cm^{-3} was estimated. The photoluminescence emitted from the samples was collected by a combination of lenses and imaged onto a 30-μm slit of a Hamamatsu streak camera system. Various narrow-band filters centered at different wavelengths were placed in

front of the streak camera to select different transition energies. Two color filters 3-67 were placed in front of the streak camera to block the light with wavelengths shorter than 5400Å. The photoluminescence profiles were corrected for the nonlinearity of streak rate and spectral response of the detector (S-20). For steady-state photoluminescence experiments, an Argon-ion laser, a double Spex spectrometer, S-20 photomultiplier and a lock-in amplifier were used.

Picosecond Luminescence Studies

The photoluminescence profiles in time domain were measured at different energies covering the corresponding spectral range of each sample. The expression for number of photons detected at energy E at time t is given by:

$$N(E,t) = N_0[e^{-t/\tau_d(E)} - e^{-t/\tau_r(E)}], \tag{3}$$

where E is the central energy of the narrow-band filter used; $\tau_d(E)$ and $\tau_r(E)$ are the decay and the rise times at energy E; and N_0 is the proportionality constant. The value of τ_r gives information about how fast electrons and holes scatter out from initially excited states to less energetic states where they recombine while, τ_d gives a measure of the recombination lifetime of various excited states when recombination dominates the depopulation of photo-excited carriers.

The time-resolved photoluminescence profiles obtained at various emission energies at 4.2K for sample 2-58 are shown in Fig. 1(a-e). The left curve in Fig. 1a shows the temporal profile of exciting laser pulse which reflects the time resolution of detection system (10 ps). The dotted curves in Fig. 1 are the fit to the data using Eq. (3) with a value of 12 ps for the risetime τ_r. The decay times of these time-resolved luminescence profiles show only two distinct values. For emission energies ranging from 2.213 to 2.175 eV and from 2.1 to 1.967 eV the decay times are 29 and 100 ps, respectively.

The decay time as a function of emitted photon energy E for four quasi-0D electron systems are plotted in Fig. 2. For a comparison (Fig. 2e), the exciton lifetime vs exciton energy in quasi-3D system in bulk $CdS_{0.53}Se_{0.47}$ while the other two samples do not show this feature (the reason, **the P levels have not been reached in 2-61 and 2-59 samples**). It is expected that the decay time should be nearly invariable over the energy range of emission if only the lowest confined state 1S for electrons and holes is occupied. The wide spectral range most likely reflects the crystallite size distribution and the fluctuations in the value of x from crystallite to crystallite. When the two lowest states 1S and 1P are substantially occupied and the recombination lifetimes associated with these two states are considerably different, a steplike change of decay time will be observed in two distinct energy regions. The exact lifetime ratio in the two energy regions depends on the transition matrix elements. The above argument should in principle explain what we observed in Fig. 2. However, the energy dependence of localized exciton lifetime in the bulk compound $CdS_{0.53}Se_{0.47}$ as displayed in Fig. 2e also exhibits a steplike feature. The explanation given by Kash et al.[8] was based on the model suggested by Cohen and Sturge[9] where the exciton migration from a site with higher energy into another site with lower energy. This raises a question whether the exciton migration mechanism can apply to the present case. Since exciton migration must involve a transport over a relatively large distance due to the nature of the exciton-phonon interaction,[9] such migration may occur in relatively large crystallites. This apparently may explain the results observed in the sample 2-58 and 2-64. In smaller crystallites the migration does not occur in correspondence with the samples 2-61. However, the exciton migration picture cannot explain the steplike energy dependence of lifetime as well as the ratio with the value of about 3.5 because the depth of a potential well[12] caused by compositional fluctuations are entirely random in nature. Furthermore, the exciton lifetime would be increased monotonically with a decrease of exciton energy as recently observed for CdTe-ZnTe interfaces.[13]

A two-state (1S, 1P) model is introduced here which consistently interprets all the results shown in Fig. 2 as well as other results observed by Cohen and Sturge.[9] It is possible that the excitons are confined by the potential wells in the bulk alloy compound which have two lowest states designated by 1S and 1P. The exciton in higher-lying state 1P can be scattered to the lower-lying state 1S by emission of phonons instead of migrating from site to site. The two-state model can explain not only the results of Cohen and Sturge[9] but also our time-resolved dynamic results presented here as well as the data reported by Kash et al..[8]

In order to further verify the two-states (1S, 1P) model, we have calculated the eigen energy levels of the quasi-0D electron systems and the recombination lifetime ratio for 1S→1S and 1P→1P transitions. The confinement energy for the ground states is given by

$$E_{1S} = E^{e}_{1S} + E^{h}_{1S} \tag{4}$$

for the quasi-0D electron systems, where E^{e}_{1S} and E^{h}_{1S} are the lowest confinement energies for electrons and holes, respectively. These energies were calculated from the bulk bandgaps[14] at 300K and the measured peak energies of the first derivative of room temperature reflectance ($dR/d\lambda$).[15] Using the electron effective mass and the isotropic hole effective mass given in Ref. 4, the effective diameter[16] of crystallite for each sample and eigen energies were calculated. These results are displayed in Table 1. The spin-orbit split states[14] were neglected since they were not excited in our experiments. The emitted photon energies at 4.2K for 1S→1S and 1P→1P transitions were obtained by adding corresponding confinement energies to the values of bulk gap[17] at 4.2K. The binding energies of excitons were not included. The calculated energy positions are

in good agreement with what we measured. These positions are located in Fig. 2 as arrows labeled by S and P for clarity.

In Table 1, the values of lifetime for 1S→1S transitions denoted by τ_{1S} were measured at the luminescence intensity peaks. A value of 85 ps for the 1S→1S ground state recombination time for sample 2-59 is in exact agreement with the value obtained by Warnock and Awschalom[9] using pump-probe experiment. Since the energy per pulse in our experiment is about four orders of magnitude larger than they used, the Auger mechanism of carrier depopulation is then ruled out in these quasi-OD electron systems. Furthermore, we did not observe the change in lifetimes by varying the excitation intensity over a factor of 33. One concludes that the depopulation of photoexcited carriers must be dominated by radiative recombination path in the present study. The recombination lifetimes for 1P→1P transitions denoted by τ_{1P} are also entered in Table 1. Since the present experimental condition cannot detect the 1P→1P transitions in samples 2-61 and 2-59 the numbers inside the circles are the anticipated lifetimes of 1P→1P transitions assuming the same ratio of τ_{1S}/τ_{1P} for the samples 2-58 and 2-64. Note that a value of 18 ps has been also reported by Warnock and Awschalom[9] for 2-61 although they did not identify this to be the lifetime of 1P→1P transition. It should be emphasized that strongly enhanced transition probability which leads to shortened lifetimes of various excitations in the quasi-zero dimensional electron system is not a surprising result. The recombination enhancement due to carrier confinement in quantum well structure (quasi-two dimensional electron system) was clearly demonstrated by Gobel, Jung, Kuhl, and Ploog.[18] These authors[18] attributed their measured recombination lifetime to be the spontaneous carrier lifetime in quasi-two dimensional the electron system. The measured diameter dependence of recombination lifetime supports their arguments.[18]

A further test to support the two-states picture is whether a reasonable prediction can be made to locate the energy positions of exciton localized in 1S and 1P states for the quasi-OD electron system in the bulk compound $CdS_{0.53}Se_{0.47}$ studied by Kash et al..[8] When electrons are confined in a one-dimensional semiconductor quantum well with thickness L_z, the electron-hole recombination time for ground states may be estimated to be proportional to the L_z since the wave function is "squeezed" by the boundaries.[9,18] The evidence for this has already been provided by the measurements of Gobel et al..[18] Extending the above concept, the effective diameter (d) for the spherical potential well may be estimated using a relation $\tau_{1S} = c\, d^3$. A value of about 250 Å for the diameter of the potential well in the bulk was estimated using the lifetime for energies less than 2.09 eV assigned by us to be the recombination lifetime for 1S→1S transition. Using this value the confinement eigen energies for exciton (electron and hole bound by their mutual Coulomb potential) were calculated. These results are also entered in Table 1 under bulk and displayed in Fig. 2e. The experimental results of Kash et al.[8] are in excellent agreement with our two-states model. Furthermore, when the temperature of their[8] sample was raised above 36K (3 meV) the steplike feature of lifetime in two distinct energy regions disappeared. Since exciton binding energy in this material is about 20 meV, the exciton dissociation is not responsible for this disappearance. However, the energy difference between ground state 1S and first excited state 1P for hole is just 3 meV (Table 1); therefore, the strong hole scattering between 1S and 1P states assisted by thermal energy is responsible for the absence of the two distinct regions above 36K. This temperature dependence of exciton lifetime further supports our model.

The lifetime ratio for 1S→1S and 1P→1P can be predicted following the approach given by Casey and Panish[19] and Efros and Efros.[20] The matrix element for a transition from localized state in conduction band to the localized state in valence can be expressed as:

$$M = M_b\, M_{env}, \tag{5}$$

where M_b is the average matrix element for the Bloch states for bands in absence of new eigen states due to the confinement and M_{env} is the envelope part of the matrix element which is given by:

$$M_{env} = \langle 1L \mid 1L \rangle. \tag{6}$$

Since 1P state is a threefold degeneracy state with magnetic quantum number -1, 0, and 1, a value of 5 for the ratio of $|M_{env}|_{1\hat{P}\to 1P}$ and $|M_{env}|_{1^2S\to 1S}$ can be readily calculated. This value should be compared with experimentally measured value of 3.5 for τ_{1S}/τ_{1P}. The agreement is reasonable in view of assumptions made in the theoretical approach and the uncertainty in data fitting.

Steady-state Photoluminescence Studies

Following work of Warnock and Awschalom[9] steady-state photoluminescence studies was used to confirm our findings. In Fig. 3a, photoluminescence spectra of sample 2-61 at various excitation levels taken at room temperature is plotted. The excitation wavelength was the 488 nm line of the Argon-ion laser. The excitation levels were 2.5 and 10 times higher for the broken curve and dot-dashed curve than the solid curve, respectively. The scale of luminescence intensity was 2 times and 10 times larger for the broken curve and dot-dashed curve than the solid curve, respectively. The broken vertical line indicates the peak position of $dR/d\lambda$. The most salient feature we would like to stress is the appearance of the two-peak structure at the high energy side of the peak position of the first derivative of room temperature reflectance spectrum. Based on results of picosecond studies listed in Table 1 we attribute these two peaks to the 1S→1S and 1P→1P optical transitions[5] as indicated by S and P in the figure. The energy separation between P and S is about 220 meV. This rules out the possibility of transition from 1S electron state to 1S spin-split-hole state, since the energy separation of spin-orbit splitting is about 350 meV for Se mole composition of 0.73. Two

other features should also be mentioned. The excitation dependence of luminescence intensity did not show the saturation of available electronic states up to the maximum excitation level 100W/cm^2; and the luminescence peak shifts to the lower energy when the excitation level increases reflecting the renormalization process in quasi-zero dimensional electron system.

The photoluminescence spectrum of 2-61 measured at 4.3K using the 457.9 nm line of the Argon-ion laser as excitation wavelength is shown in Fig. 1b. As can be seen from the spectrum the position of 1S→1S peak shifts to the higher energy and its FWHM (58 meV) decreases by a factor of 2 in comparison with room temperature data. The latter indicates the broadening of 1S→1S transition at room temperature is not entirely dominated by size fluctuation of the microcrystallites under the photoexcitation. The line broadening mechanisms may apply for the quasi-zero electron system. We assume the broadening of the 1S peak is dominated by the fluctuation of the diameter of the microcrystallites at 4.3 K. The inset of Fig. 1b shows a spectrum fit by assuming the Gaussian shape[21] probability density function for the random variable d.[21] The fit gives a mean value of 74 Å for the effective diameter and a variance σ^2 = 25 Å which characterizes the size fluctuation of microcrystallites. The structure beside the main 1S peak is from the 1P→1P transition since its energy separation with the 1P peak is about 210 meV. The broad peak centered at 507 nm may arise from the transition from the split orbit band.

In Fig. 4, the photoluminescence spectra of sample 2-59 measured both at room temperature (a) and 4.3K (b) are displayed. The most important feature is the appearance of both 1S→1S and 1P→1P transitions. The energy separation between 1S and 1P peaks is 214 meV. The calibrated value for the confinement energy is 213 meV. The corresponding peak positions are shifted to lower energy in comparison with 2-61 due to the larger diameter of crystallites and smaller mole percent of the composition of sulfur.

The broad peak centered at 500 nm in Fig. 4b at the 4.3K spectrum appears in the 4.3K spectrum of the 2-61 sample. The origin of this emission peak at 500 nm is unlikely from the 1D→1D transition. This emission may arise from the optical transition from the 1S electron state to the 1S spin-orbit split hole state. The energy separations between the weak peak and the main 1S peak are about 370 meV and 450 meV for 2-61 and 2-59, respectively. These energies are consistent with the measured selenium-composition-percentage dependence of spin-orbit splitting.[14]

We have also measured the room temperature spectra of 2-58 and 2-64 samples. The peaks for 2-58 and 2-64 are at 1.9537 eV and 1.9114 eV, respectively. These peaks were broad so that the 1P structures were not clearly resolved.

Summary

In summary, we have reported on the measurements of recombination lifetimes of *1S→1S and 1P→1P transitions* in quasi-0D electron systems by time resolved photoluminescence measurements. The assignment of these observed transitions are supported by calculations of eigen energy levels and the corresponding matrix element ratio as well as the direct observation of optical transitions between quantized energy levels (1S, 1P) in the conduction and valence bands by steady-state photoluminescence measurements.

Acknowledgements

This work was supported by Air Force Office of Scientific Research under Grant AFOSR-86-0031.

References

1. R. Rossetti, S. Nakahara, and L. E. Brus, J. Chem. Phys. 79, 1086 (1983).
2. A. I. Ekimovand and A. A. Onushchenko, JETP Lett. 40, 1136 (1984).
3. J. Warnock and D. D. Awschalom, Phys. Rev. B32, 5529 (1985).
4. E. Cohen and M. D. Sturge, Phys. Rev. B25, 3828 (1982).
5. L. E. Burs, J. of IEEE QE-22, 1909 (1986).
6. R. K. Jain and R. C. Lind, J. Opt. Soc. Am. 73, 647 (1983).
7. S. S. Yao, C. Karaguleff, A. Gabel, R. Fortrnberry, C. T. Seaton, and G. I. Stegeman, Appl. Phys. Lett. 46, 801 (1985).
8. J. A. Kash, A. Ron and E. Cohen, Phys. Rev. B28, 6147 (1983).
9. J. Warnock and D. D. Awschalom, Appl. Phys. Lett. 48, 425 (1986).
10. The samples were sent to Schwarzkopf Microanalytical Laboratory, Inc. (56-19 37th Ave., Woodside, NY 11377) to obtain accurate x-values. Analyses were made by technical director Dr. Edmund Petro.
11. P. Y. Lu, Z. X. Yu, R. R. Alfano, and J. I. Gersten, Phys. Rev. A26, 3610 (1982).
12. The eigenvalue problem in such a well may be best approximated by three dimensional harmonic oscillators model. For large radius well (> 100 Å), the difference in eigen energy for the two lowest states calculated using the harmonic oscillator model and a spherical well model is negligible. The degeneracy for the first excited state 1P is also the same for the two models.
13. Y. Hefetz, D. Lee, A. V. Nurmikko, S. Sivananthan, X. Chu, and J. -P. Faurie, Phys. Rev. B34, 4423 (1986).
14. F. L. Pedrotti and D. C. Reydold, Phys. Rev. 127, 1584 (1962).
15. The first derivative of room temperature reflectance was measured in a Perkin Elmer Lambda 9 spectrometer.
16. Our calculated values of effective diameter are consistently smaller than the values reported by Warnock and Awschalom.[9] This discrepancy may be caused by the complexity of boundary between semiconductor

and glass. The value of the effective diameter for the sample 2-61 calculated by us is, however, in exact agreement with that calculated by Warnock and Awschalom.[9] Note that the value of x they used for this sample is the same as we measured.
17. D. W. Langer, Y. S. Park, and P. N. Euwema, Phys. Rev. 152, 788 (1966).
18. E. O. Gobel, H. Jung, J. Kule, K. Ploog, Phys. Rev. Lett. 51, 1588 (1983). The recombination lifetime of electron and hole within quantum well decreases with L_z from 1 ns for L_z=14 nm to 350 ps for L_z=5 nm.
19. H. C. Casey, Jr. and M. B. Panish, "Heterostructure Lasers" (Academic Press, New York, 1978), p. 144.
20. Al. L. Efros and A. L. Efros, Sov. Phys. Semicond. 16, 772 (1982).
21. Kai Shum, P. P. Ho, R. R. Alfano, D. F. Welch, G. W. Wicks, and L. F. Eastman, IEEE Journal of Quantum Electronics, QE-22, 1811 (1986).

Note: After the completion of our work, we recieved a preprint from Dr. Hall, Corning glass works (to be published in J. Appl. Phys.). According to them, the wet chemical method for determining x value from 0.4 to 0.8 was uncertain by 15% from the x-ray method measured corresponding values. We should state that the energy peaks we measured can not be attributed to the changes of x determined by them for a given filter number. The IBM group does not agree with Hall et al x values. Therefore, we conclude that the each filter does not have a unique x even though the designated filter number may be same. Our response to Hall's statement, "that the crystallite size in filter glasses are such that quantum confinement effects do not exist," is: even though there is a large distribution of particle sizes, quantum confinement does exist in each particle.

Table 1: The measured energy peak of first derivative of reflection at 300K, bulk energy gaps at 4.2K and 300K, the calculated confinement energies, emission energies for 1S → 1S and 1P → 1P transitions and effective diameters (d), the measured lifetimes for 1S → 1S and 1P → 1P transitions as well as their ratio are displayed. The † are anticipated values assuming a same ratio τ_{1S}/τ_{1P} for the samples 2-58 and 2-64.

Sample CdS_xSe_{1-x}			(300 K) Energy peak for dR/dλ eV	(300 K) Bulk gap[b] eV	Confined energy (meV)					4K emission energy[b] eV		Θ	4K lifetime psec		τ_{1S}/τ_{1P}
No.	x	d			$E^e_{1S}+E^h_{1S}$	E^e_{1S}	E^h_{1S}	E^e_{1P}	E^h_{1P}	1S→1S	1P→1P	ΔE_{S_P}	1S	1P	
2-61	0.27	74A	2.0120	1.7857	226	187	39	382	80	2.156	2.392	220	70	18†	3.5
2-59	0.121	80A	1.9366	1.7333	203	168	35	344	72	2.073	2.291	224	85	24†	3.5
2-58	0.081	80A	1.9245	1.7143	210	174	36	356	74	2.065	2.284	*	100	29	3.5
2-64	0.168	102A	1.8666	1.7429	124	103	21	211	43	2.004	2.134	*	210	60	3.5
Bulk	0.530	250A		1.9368	17	14	3	29	6	2.090	2.108	18	2750	790	3.5

a from ref. 14
b the value of bulk gap is from ref. 17
* peaks are broad and unresolved.
Θ measured energy seperation (meV) between S and P peaks at 300K.

AD-A193 100 ULTRAFAST PHYSICS IN SEMICONDUCTOR MICROSTRUCTURES(U) 2/2
CITY COLL NEW YORK INST FOR ULTRAFAST SPECTROSCOPY AND
LASERS R ALFANO 19 FEB 88 RF-447230 AFOSR-TR-88-0301
UNCLASSIFIED AFOSR-86-0031 F/G 9/1 NL

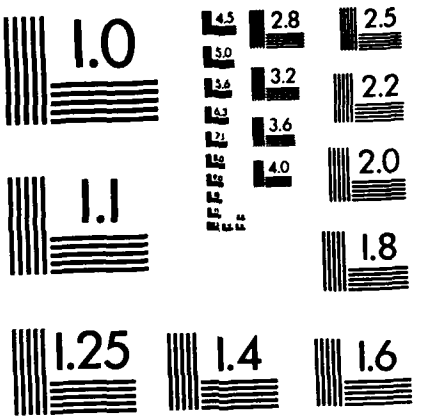
1.0
1.1
1.25
1.4
1.6
1.8
2.0
2.2
2.5
2.8
3.2
3.6
4.0
4.5
5.0

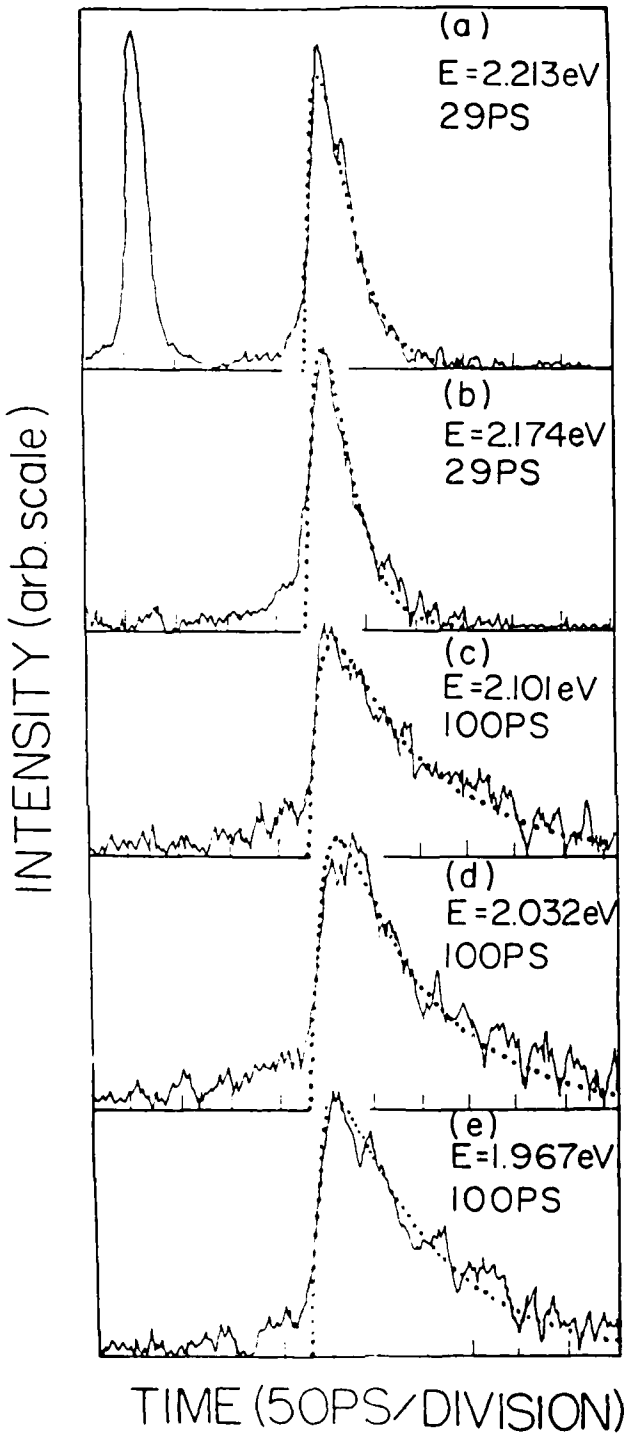

Fig. 1 Time-resolved photoluminescence profiles detected at different energies (a to e) for the sample 2-58 at 4.2K. The dotted curves are the theoretical fit with 12 ps for risetime and decay times are indicated on the corresponding profiles. The left curve of (a) is the temporal response profile to the laser pulse used to excite the samples.

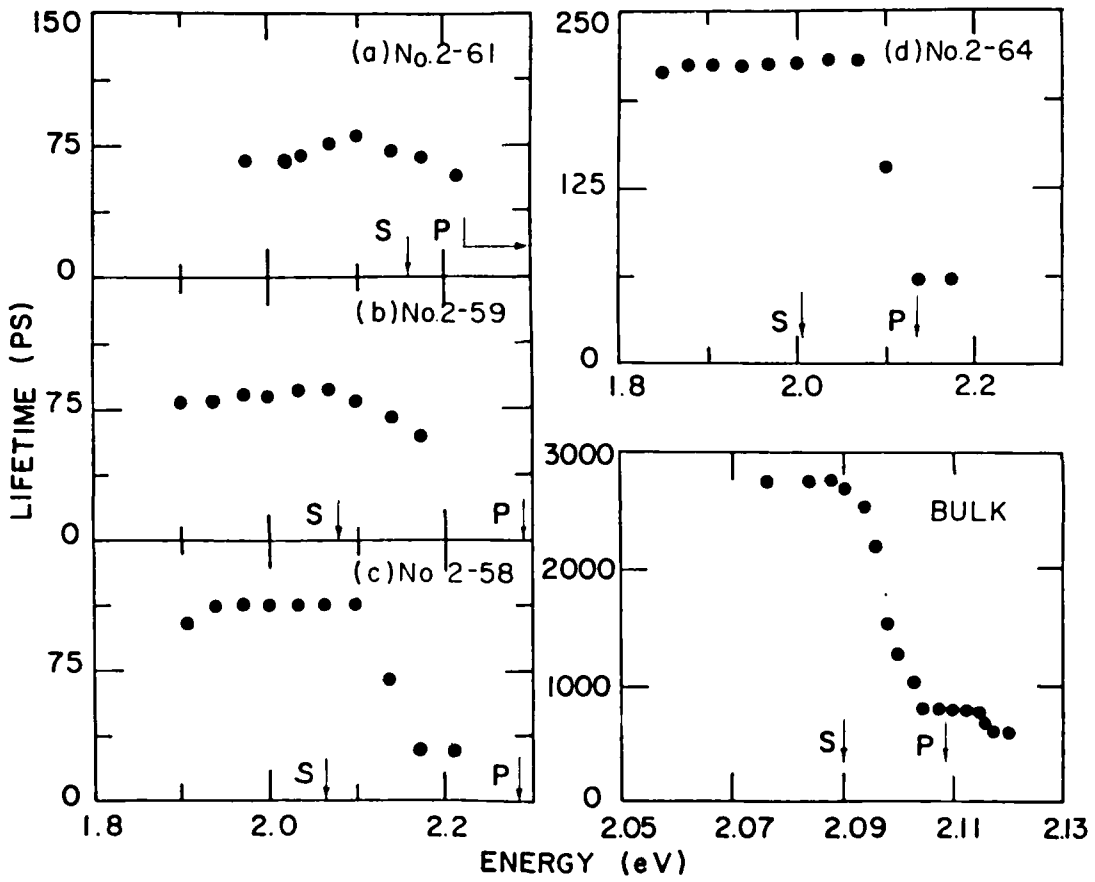

Fig. 2 The lifetimes are plotted as function of emitted photon energy. The sample temperature for (a), (b), (c), (d), is 4.3K and for (e) is 2K. The arrows indicated the energy positions for 1S→1S transition (S) and 1P→1P transition (P).

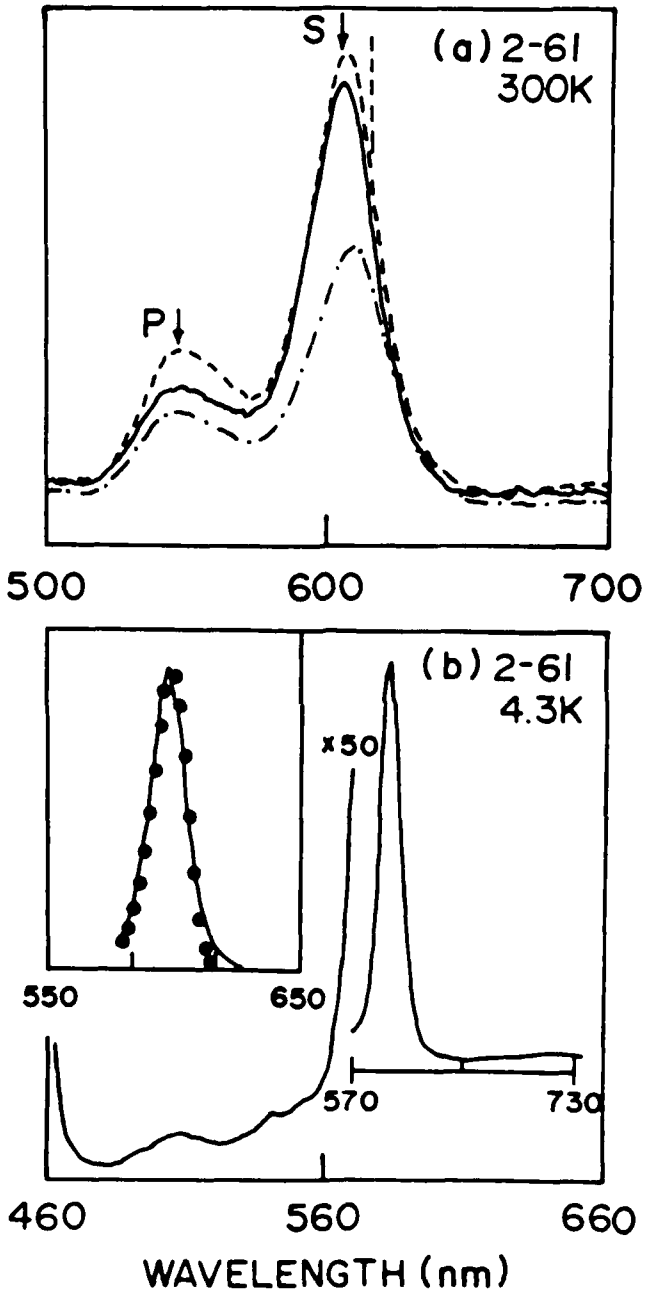

Fig. 3(a) Photoluminescence spectra of sample 2-61 at various excitation levels taken at room temperature using 488 nm line of the Argon-ion laser. The excitation levels (intensity scale) were 2.5 (2) and 10 (10) times higher for the broken curve and dot-dashed curve than the solid curve, respectively. The broken vertical line indicates the peak position of the first derivative of reflectance at room temperature. S and P stand for the 1S→1S and 1P→1P transitions, respectively. (b) Photoluminescence spectra of 2-61 at 4.3 K. The inset shows that the 1S peak broadening is dominated by the diameter fluctuation of microcrystallites. The solid dots are calculated by assuming a Gaussian shape of the probability density function for the random variable d with a variance of 25 Å.

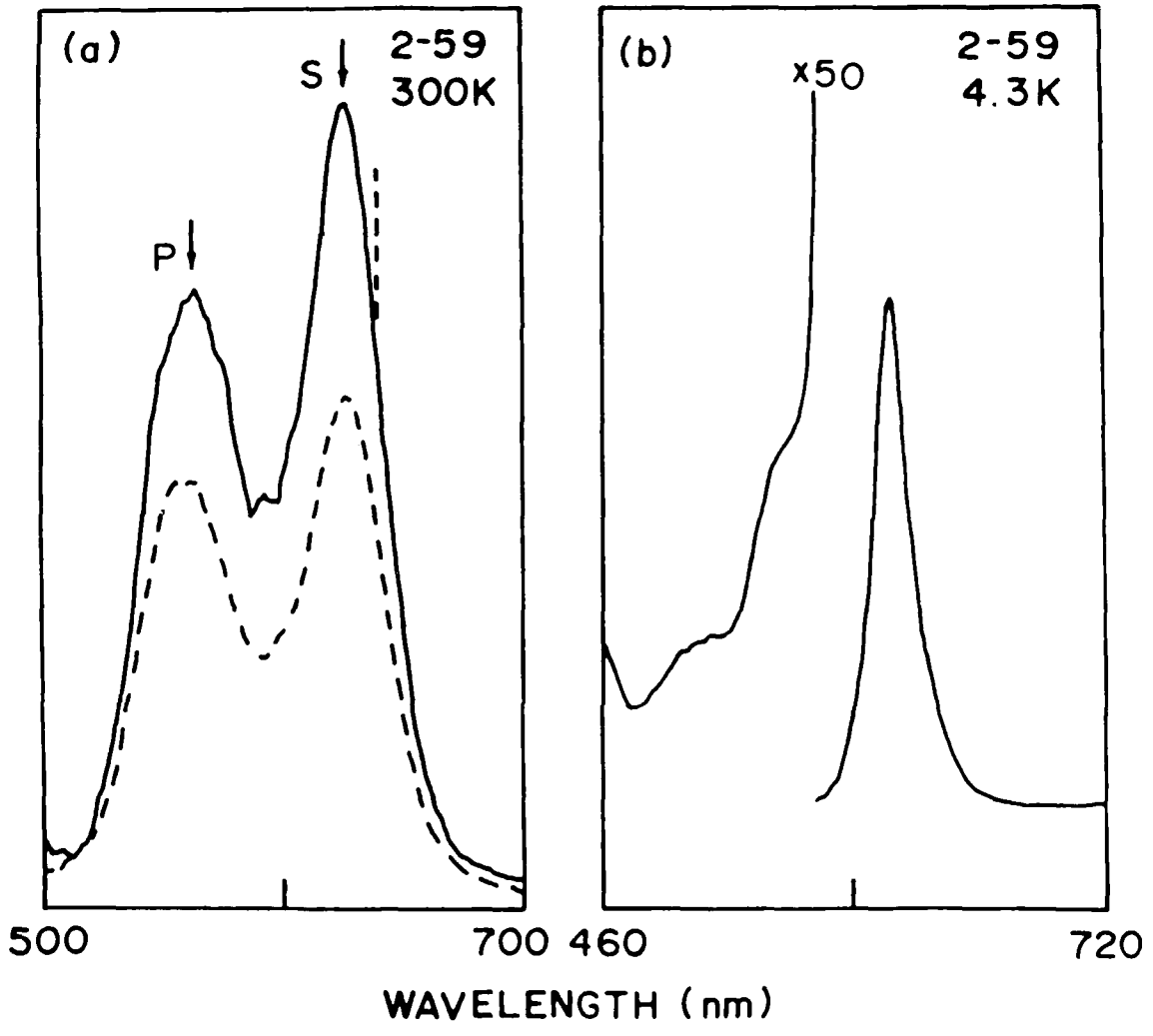

Fig. 4(a) Photoluminescence spectra of 2-59 at room temperature excited by 488 nm line of the Argon-ion laser. The excitation level for the broken curve is half of the solid curve while the intensity scale is the same for the two curves. S and P stand for 1S→1S and 1P→1P transition, respectively. The broken solid line indicates the peak position of the spectrum dR/d (at room temperature). (b) Photoluminescence spectrum of 2-59 at 4.3 K.

PHYSICAL REVIEW B VOLUME 37, NUMBER 3 15 JANUARY 1988-II

Reply to "Comment on 'Determination of valence-band discontinuity via optical transitions in ultrathin quantum wells' "

Kai Shum, C. Zhang, P. P. Ho, and R. R. Alfano
Institute for Ultrafast Spectroscopy and Lasers, Departments of Electrical Engineering and Physics, The City College of New York, New York, New York 10031
(Received 16 January 1987; revised manuscript received 20 August 1987)

The salient points of our previous paper [Phys. Rev. B 33, 7259 (1986)] are reinforced in this Reply to the preceding Comment by Miller.

The essential points of our work[1] were to demonstrate *what* experimental data from optical transitions should be used and *how sensitive* they are to the Q value of band offset. Contrary to Miller's comment,[2] Dingle *et al.*[3] did not emphasize how sensitive the Q value depended upon the value of the energy separation, $\Delta E(L_z)$, between the $n=1$ heavy- and light-hole subbands. We found[1] that the values of ΔE are most sensitive to the band offset for L_z ranging from 15 to 80 Å. Based on this key finding a currently fashionable choice of $Q_v=0.40$ proposed by Miller *et al.*[4] was ruled out using Dingle's connection rule and the then available experimental data in this range of L_z. Another key point made in our paper[1] was that systematic measurements should be performed in the sensitive zone of well width (15 Å to 80 Å) to precisely determine the Q value. These essential points are still overlooked in depth by Miller's comment[2] to our paper.[1]

It should be pointed out here that the extent of data used in our paper[1] was not the main issue of the paper and more data could not alter the essential spirit of the paper. Most recently, Miller *et al.*[5] have performed new measurements providing more data in the sensitive zone which will be discussed below in this Comment.

We have recognized that there has been a large body of data pointing to a larger $Q_v \sim 0.40$, which was the mainstream of thought in this field. However, most of the experimental probes carry their own source of uncertainties.[6] The electrical measurements are often plagued by residual doping whereas the intersubband optical transitions may prove to be too weakly dependent upon the band offset. The optical method described in our paper[1] provides a sensitive optical test of band offsets in $GaAs/Al_xGaAs_{1-x}$ structures. It should be mentioned that there are some most recent determinations of Q value for $GaAs/Al_xGa_{1-x}As$ which do not yield $Q_v=0.40$ but point to values of 0.31 from Raman scattering data[7] and 0.23 ± 0.07 from electrolyte electroreflectance study.[8]

As noticed by Miller,[2] one of the data in the original paper[1] to support lower Q_v was obtained in a circular fashion. However, the other data quoted by us do not suffer from this problem.

It is well known that the mismatch of effective mass in well and barrier is responsible for the appearance of various connection rules[3,9,10] for the envelope wave function and its derivative. In general, using a different connection rule will result in different eigen energy levels and hence differences in the spacing between the levels. Therefore, the Q value determined by ΔE versus L_z depends much on what connection rule is employed. This is where some of the problems come from.

In the spirit of our past paper, the light- and heavy-hole energy splitting is plotted in Fig. 1 as function of well thickness L_z using various connection rules.[3,9,11] The Q value is adjusted in such a way the ΔEs for $L_z > 40$ Å calculated[12] using different connection rules coincide with each other within ~ 2 meV. D, B, and N in the Fig. 1 refer to the Dingle's connection rule, Bastard's connection rule, and new connection rule.[11] The material parameters used for the calculation of the

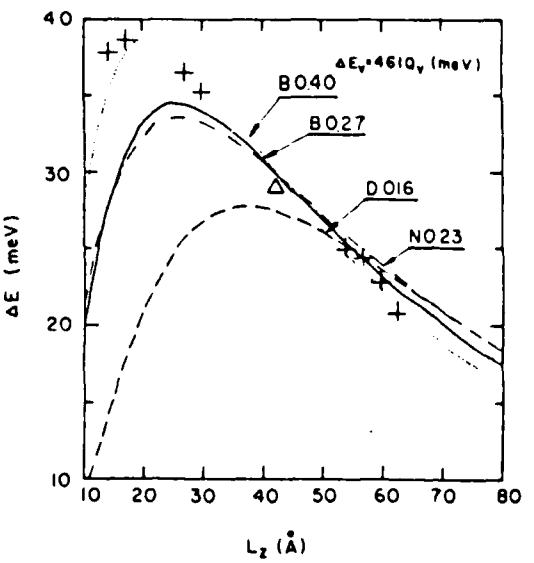

FIG. 1. Calculated light- and heavy-hole energy splitting as function of L_z. D, B, and N refer to Dingle's, Bastard's, and new connection rules. The values of Q_v are indicated on the corresponding curves. The masses used for the dotted curve is Miller's masses. The masses used for the other curves are the conventional masses given in the text. The plus and triangle data are from Refs. 5 and 15, respectively.

curves are $x=0.37$, $\Delta E_v=1247xQ_v$ (meV) (the value of Q_v is indicated next to the corresponding variable in the Fig. 1), masses[13,14] of heavy hole (light hole) for GaAs and AlAs are $0.403m_0$ ($0.087m_0$) and $0.487m_0$ ($0.208m_0$), respectively; except for the curve where the heavy-hole mass ($0.34m_0$) and light-hole mass ($0.094m_0$) proposed by Miller *et al.*[4] were used. The plus and triangle data points in Fig. 1 are from Refs. 5 and 15, respectively.

Figure 1 shows two important features. First, as expected the energy splitting ΔE is sensitive to the connection rule in the sensitive zone of L_z, especially for $L_z<40$ Å. This features makes it possible to experimentally demonstrate which connection rule is appropriate by systematically measuring ΔE in the sensitive zone. Based on the data given by Miller *et al.*,[5,15] Dingle's connection rule which was used by us to show how to determine Q value in the sensitive zone of L_z seems to be not appropriate. However, the method itself described in our paper[1] is still very useful. Second, for the given connection rule the splitting ΔE is very sensitive to the effective masses. In order to fit simultaneously the data given by Miller *et al.*[5,15] it seems to be necessary to use the Bastard's connection rule and the mass parameter set ($m_{HH}=0.34m_0$, $m_{LH}=0.094m_0$) and $Q_v=0.40$ proposed by Miller *et al.*[4] The use of new connection rule[11] with $Q_v=0.23$ seems to fit the data for $L_z>30$ Å. It should be pointed out here that in our calculation the binding-energy difference between the light hole and the heavy hole is taken to be a constant (~ 0.5 meV). This may be a good approximation for $L_z>40$ Å. In order to compare the measured ΔE with the calculated ΔE for $L_z<40$ Å an exact analysis taking the proper exciton binding energy into account must be performed.[16]

In Fig. 2, the energy separation ΔE_{12} between first and second conduction subbands is plotted as function of L_z using three different connection rules by including[17] the energy-dependent mass $m_w(E_n)$ (Ref. 18) as well as $m_b(E_n)$, $n=1,2$, for well material GaAs and barrier material $Al_{0.3}Ga_{0.7}As$, respectively, and compared ΔE_{12} with the published experimental data by West and Eglash.[19] This work is not affected by the valence-band complexity, the exciton binding energy, and can provide an independent test of Q value.

The $m_b(E_n)$ is obtained by

$$\frac{\partial^2}{\partial k^2}\left[\left|\frac{E_g^2}{4}+\frac{\hbar^2k^2E_g}{2m_{CB}}\right|^{1/2}-\frac{E_g}{2}\right]=\frac{\partial^2}{\partial k^2}\left[\frac{\hbar^2k^2}{2m_b(E_n)}\right]. \tag{1}$$

The expression inside of the large brackets on the left-hand side of Eq. (1) is the energy-momentum relationship within semiconductor band gap.[20] After differentiation the $m_b(E_n)$ reduced to

$$m_b(E_n)=m_{CB}(1+4\chi_n)^{3/2},\quad n=1,2,\ldots, \tag{2}$$

where m_{CB} is electron effective mass at conduction band edge of $Al_{0.3}Ga_{0.7}As$, $\chi_n=|\hbar^2k_{bn}^2/2m_{CB}E_g|$, and $n=1,2$ for first and second subbands. Note that k_b^2 is negative and k_b is imaginary reflecting the electron wave function within the gap of $Al_{0.3}Ga_{0.7}As$ is exponentially damped. The dispersion relations dependent upon the real and imaginary wave vectors in the well and the barrier are schematically shown in the inset of Fig. 2. The connection rule and the Q value used are indicated on the corresponding curves. The value of x is equal to 0.30 in order to make a comparison with the data ΔE_{12} of West and Eglash.[19]

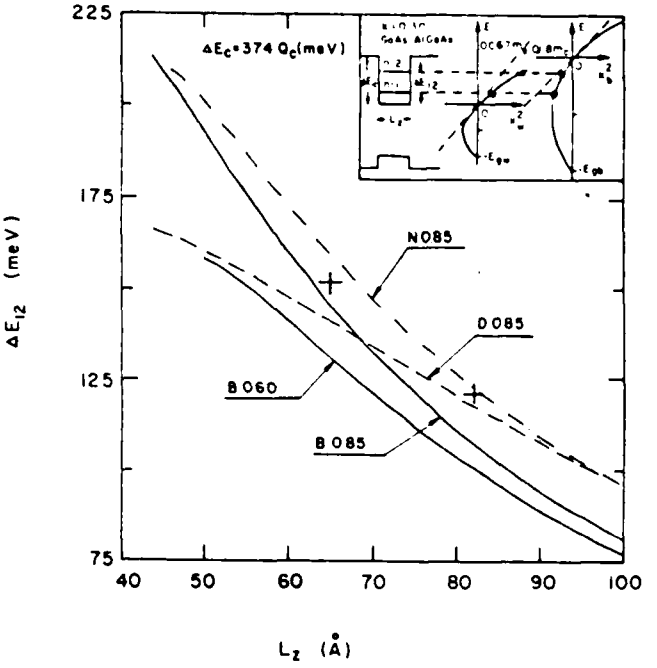

FIG. 2. Calculated energy separation ΔE_{12} between first and second conduction subbands as a function of well width L_z using Dingle's (D), Bastard's (B), and new (N) connection rules. The curves are calculated using $\Delta E_c=Q_c\Delta E_g$ ($\Delta E_c=1247x$ meV, $x=0.30$). The values of Q_c are indicated on the corresponding curves. The data of West and Eglash (Ref. 19) are indicated as two plus signs. The inset shows schematically the well and the energy-momentum dispersion curves. The electron effective masses at band edges for GaAs and $Al_{0.3}Ga_{0.7}As$ are also indicated in the inset.

Several features are very apparent in Fig. 2. First, for the given connection rule ΔE_{12} is very sensitive to the Q value in the sensitive zone of L_z giving rise to a possibility of extracting the value of ΔE_c and Q value. Second, the value of ΔE_{12} calculated using the new connection rule approaches the values of ΔE_{12} at ~ 45 Å and at $L_z>100$ Å calculated using Bastard's and Dingle's connection rules, respectively. Third, the two experimental points support neither Bastard's nor Dingle's connection rules, but seems to be more favorable to the new connection rule with $Q_c=0.77$.

In conclusion, we have shown different connection rules and hole masses yield different Q values. Furthermore, the appropriate connection rule can be discriminated by systematically measuring ΔE and ΔE_{12} in the sensitive zone of L_z. Dingle's 85-15 rule is based on his connection rule while Miller's 60-40 rule is based on Miller's effective masses and Bastard's connection rule.

The essential information described in our paper[1] is not compromised by the comments raised by Miller but reinforced here. We stress that more systematic photoluminescence, PLE, and inter-conduction-subband transition data must be taken in the sensitive zone (15 to 80 Å) to determine the proper connection rule and an accurate Q value.

This work was supported by Air Force of Scientific Research under Grant No. AFOSR-86-0031.

[1]K. Shum, P. P. Ho, and R. R. Alfano, Phys. Rev. B **33**, 7259 (1986).

[2]R. C. Miller, preceding Comment, Phys. Rev. B 1406 (1987).

[3]R. Dingle, W. Wiegmann, and C. H. Henry, Phys. Rev. Lett. **33**, 827 (1974).

[4]R. C. Miller, D. A. Kleinman, and A. C. Gossard, Phys. Rev. B **29**, 7085 (1984).

[5]R. C. Miller, C. W. Tu, S. K. Sputz, and R. F. Kopf, Appl. Phys. Lett. **49**, 1245 (1986).

[6]G. Duggan, J. Vac. Sci. Technol. B **3**(4), 1224 (1985).

[7]J. Menendez, A. Pinczuk, D. J. Werder, A. C. Gossard, and J. H. English, Phys. Rev. B **33**, 8863 (1986).

[8]P. M. Raccah, J. W. Garland, Z. Zhang, F. A. Chambers, and D. J. Vezzetti, Phys. Rev. Abstr. **18**(15), 39 (1987).

[9]G. Bastard, Phys. Rev. B **24**, 5693 (1981).

[10]Qi-Gao Zhu and H. Kroemer, Phys. Rev. B **27**, 3519 (1983).

[11]A. Ishibashi, Y. Mori, K. Kaneko, and N. Watanabe, J. Appl. Phys. **59**, 4087 (1986).

[12]The eigen energies are calculated by Eq. (1) of Ref. 1 using Dingle's connection rule. the eigen energy equation can be obtained using Bastard's connection rule by changing m_a/m_b to m_b/m_a in the Eq. (1). There are two typing errors in Eq. (1) of Ref. 1. The squares are missing in the terms of $(1-\sigma_n^2)^{1/2}$ and $\sigma_n^2 = E_n/\Delta E$.

[13]M. S. Skolnick, A. K. Jain, A. Stradling, J. Leotin, J. C. Ousset, and S. Askenasy, J. Phys. C **9**, 2809 (1976).

[14]E. Hess, I. Topol, K. R. Schulze, H. Neumann, and K. Unger, Phys. Status Solidi B **55**, 187 (1973).

[15]R. C. Miller, D. A. Kleinman, W. T. Tsang, and A. C. Gossard, Phys. Rev. B **24**, 1134 (1981).

[16]C. Zhang, Kai Shum, and R. R. Alfano (unpublished).

[17]In the case of the new connection rule, the energy dependence of effective masses m_a and m_b is self-contained.

[18]S. Chaudhuri and K. K. Bajaj, Phys. Rev. B **29**, 1803 (1984).

[19]L. C. West and S. J. Eglash, Appl. Phys. Lett. **46**, 1156 (1985).

[20]C. H. Parker and C. A. Mead, Phys. Rev. Lett. **21**, 605 (1968).

Gallium arsenide photoluminescence under picosecond-laser-driven shock compression

X. Z. Lu, R. Garuthara, S. Lee, and R. R. Alfano
Institute for Ultrafast Spectroscopy and Lasers, The City College of New York, New York, New York 10031

(Received 8 September 1987; accepted for publication 10 November 1987)

A pump-and-probe technique was used to investigate shock effects on the photoluminescence spectra (~833 nm) at $T = 80$ K due to the direct transition E_0 from the Γ_6 conduction band to the Γ_8 fourfold degenerate top valence band in GaAs. Under the shock loading condition, the photoluminescence peak was observed to blue shift and split into two components, corresponding to the transitions from the Γ_6 conduction band to the valence heavy- and light-hole subbands, because of symmetry breaking by the uniaxial shock compression along the [001] direction. From the blue shift of the photoluminescence peaks, we deduced our picosecond-laser-driven shock pressure of ~10 kbar.

Significant changes in the optical and transport properties of semiconductors occur with the application of a uniaxial stress due to changes in symmetry and lattice parameters.[1-4] Knowledge of stress effects on band structure is important for operation of GaAs in high-speed ultrasmall devices and switches. In this letter we report on a new observation of the photoluminescence spectra from gallium arsenide (GaAs) under picosecond-laser-driven shock wave loading. The shock waves were generated by focusing intense picosecond laser pulses onto an aluminum (Al) foil[5-8] attached to the sample.

GaAs has a zinc-blende structure[9] of the space group T_d^2. The lowest conduction band is s-like and twofold degenerate, having a Γ_6 symmetry at the Brillouin zone center. The top valence band is a sixfold degenerate p-like band that splits into a fourfold $P_{3/2}$ multiplet ($J = 3/2$, $M_J = \pm 3/2$, $\pm 1/2$) with a Γ_8 symmetry and $P_{1/2}$ doublet ($J = 1/2$, $M_J = \pm 1/2$) with a Γ_7 symmetry due to the spin-orbit interaction. The band structure is shown in Fig. 1 (the left-hand side). The lowest energy band-to-band direct transition (labeled E_0) occurs at the center of the Brillouin zone. The total Hamiltonian matrix for the valence band in the presence of a uniaxial compression P along the [001] direction can be written[9]

$$H = \begin{pmatrix} & v_2 & v_1 & v_3 \\ & -\delta E_H - \tfrac{1}{2}\delta E_S & 0 & 0 \\ & 0 & -\delta E_H + \tfrac{1}{2}\delta E_S & 2^{-1/2}\delta E_{S'} \\ & 0 & 2^{-1/2}\delta E_{S'} & -\Delta_0 - \delta E_H \end{pmatrix}, \tag{1}$$

where $\delta E_H = -a(S_{11} + 2S_{12})P$, $\delta E_{H'} = -a'(S_{11} + 2S_{12})P$, $\delta E_S = -2b(S_{11} - S_{12})P$, $\delta E_{S'} = -2b'(S_{11} - S_{12})P$, and Δ_0 is the spin-orbit splitting, S_{11} and S_{12} are components of the elastic compliance constants, a and a' are the deformation potentials of the Γ_8 and Γ_7 valence bands for hydrostatic effects, and b and b' are the deformation potentials of the Γ_8 and Γ_7 bands for shear effects. If the pressure-induced shift and splitting are much smaller than Δ_0, the eigenvalues of Eq. (1) can be written

$$\delta E_{v_2} = -\delta E_H - \tfrac{1}{2}\delta E_S, \tag{2a}$$

$$\delta E_{v_1} = -\delta E_H + \tfrac{1}{2}\delta E_S + \frac{(\delta E_{S'})^2}{2\Delta_0}, \tag{2b}$$

$$\delta E_{v_3} = -\Delta_0 - \delta E_{H'} - \frac{(\delta E_{S'})^2}{2\Delta_0}. \tag{2c}$$

Including the effect of the conduction-band shift, the pressure dependence of the energy gap changes is given by

$$\delta(E_c - E_{v_2}) = \Delta E_H + \tfrac{1}{2}\delta E_S, \tag{3a}$$

$$\delta(E_c - E_{v_1}) = \Delta E_H - \tfrac{1}{2}\delta E_S - \frac{(\delta E_{S'})^2}{2\Delta_0}, \tag{3b}$$

$$\delta(E_c - E_{v_3}) = \Delta_0 + \Delta E_{H'} + \frac{(\delta E_{S'})^2}{2\Delta_0}, \tag{3c}$$

where $\Delta E_H = -(c_1 + a)(S_{11} + 2S_{12})P$, $\Delta E_{H'} = -(c_1 + a')(S_{11} + 2S_{12})P$, and c_1 is the deformation potential of the conduction band. For light polarized perpendicularly to the stress axis c, the transitions between the s-like Γ_6 conduction band and all three valence bands, v_1,v_2, and v_3, are allowed.[9] From Eqs. (3a) and (3b), we deduce that under shock loading condition, the photoluminescence peak corresponding to the E_0 transition will be subject to a blue shift because of the hydrostatic component of the pressure [represented by the term ΔE_H in Eqs. (3a) and (3b)]. It will also split into two components corresponding to the transitions $E_0(1)$ and $E_0(2)$ (see Fig. 1, the right-hand side) because of the reduced symmetry by the uniaxial nature of the shock pressure [represented by the term δE_S in Eqs. (3a) and (3b)]. Since the heavy-hole band v_2 has a lower energy under uniaxial compression,[10] the corresponding transition

 0003-6951/88/020093-03$01.00

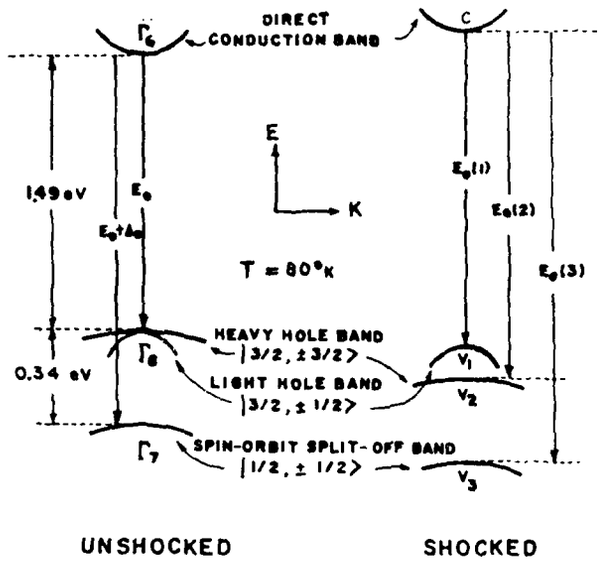

FIG. 1. Band structure of GaAs at $T = 80$ K for unshocked (left) and shocked (right) crystals.

$E_0(2)$ will have a larger blue shift. In addition, the blue shift of the emission peak of the electron-light-hole recombination [the transition $E_0(1)$] will increase sublinearly with the increasing pressure because of the pressure-induced coupling between the sets of $M_J = \pm\frac{1}{2}$ bands (v_1 and v_2).

A schematic diagram of the experimental geometry is shown in Fig. 2. The experimental setup was described in Ref. 11. A Quantel Nd:YAG laser of 30 ps pulse width and 25 mJ pulse energy at 1.064 μm was utilized as the pump beam to generate shock waves in the aluminum foil. The shock waves were launched into the GaAs sample located behind the aluminum foil. The probe beam of 27 ps at 532 nm was delayed through a white cell approximately by 46 ns relative to the arrival of the pump beam at the aluminum foil to ensure that the probe pulses reach the sample surface area right after the arrival of the shock front. This was necessary to observe the maximum effect of shock pressure.

The GaAs sample was n type with a carrier concentration of $\sim 10^{18}$ cm^{-3}. The thickness of the sample was about 50 μm with the cubic [001] axis perpendicular to the sample surface. The aluminum foil had a thickness of 20 μm. The sample and aluminum foil were loaded between two quartz plates and placed in the center of a liquid-nitrogen Dewar.

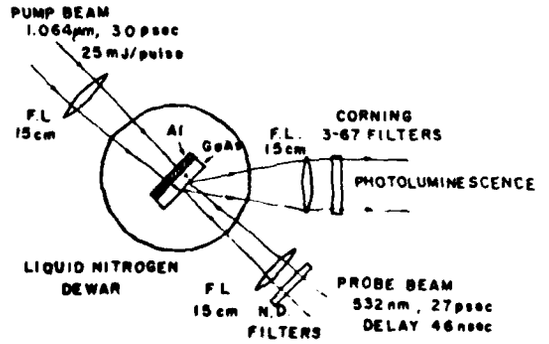

FIG. 2. Schematic diagram of the experimental geometry.

APIEZON N-grease was added to the interface of the sample and aluminum foil to ensure efficient mechanical coupling at $T = 80$ K. The pump beam was focused by a 15-cm focal length lens to a 500-μm-diam spot on the aluminum foil, which ensured planarity of the shock wave and a peak power density of $\sim 4.2\times 10^{11}$ W/cm^2. The probe pulse was focused to a 400-μm-diam spot by a 15-cm focal length lens on the sample, giving a peak power density of $\sim 1.6\times 10^7$ W/cm^2.

The emitted light was dispersed by a 1/4 m spectrometer, detected by a silicon-intensified target coupled to an optical multichannel analyzer and stored in a PDP 11/23 + host computer. The resolution of the detection system was about 2 nm. All spectra were recorded at $T = 80$ K by single shots of the laser.

The observed photoluminescence spectrum of GaAs without shock loading is dominated by a single peak due to the band-to-band recombination at the lowest energy gap E_0, as shown in Fig. 3 (left). No emission lines due to impurity transitions were observed. The effect of shock waves was most pronounced for the delay time between the pump and probe beam, $\tau = 40\sim 60$ ns. At $\tau \leq 35$ ns, no shock effect was observed. A typical spectrum showing the shock effects on the photoluminescence from GaAs is displayed in Fig. 3 for $\tau = 46$ ns and probe intensity 1.6×10^7 W/cm^2. Under shock loading, the emission peak was split into two, with blue shifts of 20 and 85 meV, respectively.

The lowest energy band gap in GaAs in the absence of the shock pressure can be written[12]

$$E_g(T) = 1.530\,\text{eV} - (5.0\times 10^{-4}\,\text{eV K}^{-1})T. \qquad (4)$$

The peak energy of the emission due to the band-to-band transition E_0 at $T = 80$ K is $E_p = E_g(80\text{ K}) = 1.490$ eV, i.e., $\lambda_p = 832$ nm, which agrees with our observed unshocked emission line at 833 nm (Fig. 3) within our experimental accuracy. Since the energy gap $E_c - E_v$ expands linearly with the increasing pressure P, the blue shift of the transition energy $E_0(2)$ was chosen to calibrate the shock

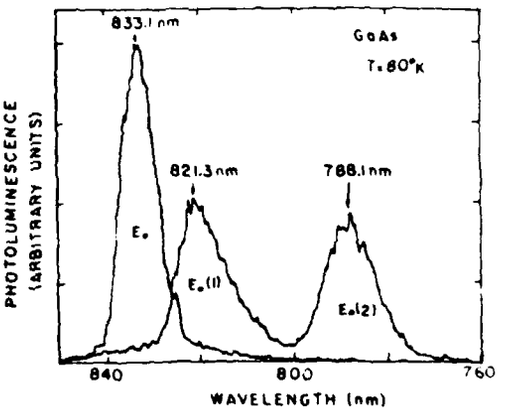

FIG. 3. Unshocked (left) and shocked (right) photoluminescence spectra at a delay time $\tau = 46$ ns and probe intensity 1.6×10^7 W/cm^2. The shocked spectrum consists of two peaks, corresponding to the transitions $E_0(1)$ and $E_0(2)$.

pressure. From Eq. (3a) the pressure coefficient of this transition energy is given by

$$\frac{dE_0(2)}{dP} = -(c_1 + a)(S_{11} + 2S_{12}) - b(S_{11} - S_{12}). \tag{5}$$

With the reported values,[13] $c_1 + a = -13.0$ eV, $b = -1.66$ eV, and[14] $S_{11} = 1.16 \times 10^{-3}$ kbar^{-1}, $S_{12} = -3.67 \times 10^{-4}$ kbar^{-1}, we obtain $dE_0(2)/dP = 8.5$ meV/kbar. Therefore, the experimentally measured blue shift of 85 meV (Fig. 3) for the electron-heavy-hole recombination emission line gives a magnitude of the laser-driven shock pressure in GaAs of ~ 10 kbar.

From Eq. (3b) and the reported values,[9] $b' = -2.47$ eV and $\Delta_0 = 0.34$ eV, we obtain $\delta(E_c - E_{v_1}) = 21.5$ meV for a pressure of 10 kbar, which consistently agrees with our observed blue shift of ~ 20 meV under the same shock compression condition. Therefore, the shocked system is in quasiequilibrium state.

In conclusion, the picosecond-laser-drive shock waves offer a new technique to investigate properties of materials at very high pressures with a table-top laser facility. Using this technique, we have observed blue shift and line splitting in the photoluminescence spectrum of GaAs due to band-gap expansion and symmetry breaking by the uniaxial shock compression along the [001] direction. The pressure range of the shock waves generated in our experiment by a 25-mJ picosecond laser pulse is ~ 10 kbar.

This work is supported by Air Force Office of Scientific Research 86-0031 and Office of Naval Research.

[1] F. H. Pollak, M. Cardona, and K. L. Shaklee, Phys. Rev. Lett. **16**, 942 (1966).
[2] F. H. Pollak and M. Cardona, Phys. Rev. **172**, 816 (1968).
[3] C. W. Higginbotham, M. Cardona, and F. H. Pollak, Phys. Rev. **184**, 821 (1969).
[4] R. N. Bhargava and M. I. Nathan, Phys. Rev. **161**, 695 (1967).
[5] P. S. Peercy, E. D. Jones, J. C. Bushnell, and G. W. Gobeli, Appl. Phys. Lett. **16**, 120 (1970).
[6] L. R. Veeser and J. C. Solem, Phys. Rev. Lett. **40**, 1391 (1978).
[7] K. P. Leung, S. S. Yao, and R. R. Alfano, in *Shock Waves in Condensed Matter, 1983*, edited by J. R. Asay, R. A. Graham, and G. K. Straub (Elsevier, Amsterdam, 1984), p. 343.
[8] K. P. Leung, S. S. Yao, A. G. Doukas, and R. R. Alfano, Phys. Rev. B **31**, 942 (1985).
[9] M. Chandrasekhar and F. H. Pollak, Phys. Rev. B **15**, 2127 (1977).
[10] G. D. Sanders and Yia-Chung Chang, Phys. Rev. B **32**, 4282 (1985).
[11] X. Z. Lu, R. Rao, B. Willman, S. Lee, A. G. Doukas, and R. R. Alfano, Phys. Rev. B **35**, 7515 (1987).
[12] O. Madelung, *Physics of III-V Compounds* (Wiley, New York, 1964), p. 44.
[13] See Table II of Ref. 9. For $c_1 + a$ (i.e., $c_1 + a_1 + a_2$), we took an intermediate value -13.0 eV between the "present work" -8.38 eV and "theoretical calculation" -15.2 eV.
[14] The elastic constants C_{11} and C_{12} of GaAs at $T = 77$ K are $C_{11} = 1221$ kbar and $C_{12} = 566$ kbar (see p. 345 of Ref. 12). In cubic crystals the elastic compliance constants are related to the elastic constants by $S_{11} = (C_{11} + C_{12})/[(C_{11} - C_{12})(C_{11} + 2C_{12})]$, $S_{12} = -C_{12}/[(C_{11} - C_{12})(C_{11} + 2C_{12})]$, and $S_{44} = 1/C_{44}$ [see O. Madelung, in *Landolt-Bornstein Numerical Data and Functional Relationships in Science and Technology*, edited by K. H. Hellwege (Springer, Berlin, 1980), New Series, group III, Vol. 17a, p. 25].

Shock-wave-induced collision broadening of the photoluminescence spectra in GaSe

X. Z. Lu, S. Lee, R. Garuthara, and R. R. Alfano
Institute for Ultrafast Spectroscopy and Lasers, Physics Department, The City College of New York, New York 10031

(Received 13 August 1987; accepted for publication 28 September 1987)

Significant spectral broadening of the photoluminescence in GaSe under the picosecond-laser-driven shock pressure has been observed for the first time. The broadening of the spontaneous emission was found to be proportional to the shock pressure and attributed to a shock-wave-induced exciton collision mechanism due to the directional motion of particles in the shocked region.

There are significant differences[1-4] between the observed physical and chemical properties of condensed matter which is shocked and hydrostatically compressed at the same pressure and temperature. Production of the picosecond-laser-driven shock waves offers a new powerful technique to study the properties of semiconductor circuits and devices at very high pressures with a table-top laser facility. Recently, we reported[5] on the spontaneous and stimulated emission from GaSe at different excitation intensities and attributed both the spontaneous and stimulated emission to the same origin—exciton-exciton scattering process. In this letter, photoluminescence spectral line broadening observed under picosecond-laser-driven shock loading in GaSe is reported for the first time which is attributed to enhanced excitonic collision processes associated with the shock wave.

A pump-and-probe technique was used to observe the shock effect on the photoluminescence emission in GaSe. The GaSe sample of 50 μm thickness with the c axis perpendicular to the layers was attached to an aluminum foil of thickness 20 μm. A Quantel Nd:YAG laser of 30 ps pulse width and 35 mJ pulse energy at 1.064 μm was focused to a 450-μm-diam spot on the Al foil surface to generate shock waves which propagated through the Al foil into the GaSe sample. A 532-nm probe beam of 27 ps pulse width was focused to a 350-μm-diam spot onto the GaSe surface. The photoluminescence from GaSe was dispersed by a 1/4-m spectrometer and detected by a silicon-intensified target coupled to an optical multichannel analyzer OMA III, and stored in a PDP11/23 + computer.

Typical spontaneous emission spectra from GaSe with and without shock loading are shown in Fig. 1. The salient features displayed in Fig. 1 are red shift of 28 nm and broadening of the shocked spectrum relative to the unshocked one.

The emission due to exciton-exciton scattering can be expressed as $(E_K^{1s}, E_K^{1s}) \rightarrow (h\nu, e-h)$. The spontaneous emission spectrum due to the exciton-exciton scattering process is given by[6]

$$I_{sp}(E) \propto \frac{E\rho(E)}{(E-E_x)^2+(\pi\alpha/\epsilon)E_x^2}\frac{1}{kT_x} \times \int_0^\infty d\xi \int_0^\infty dt \frac{\sqrt{\xi}}{[1+(\xi/E_b)]^4} \times \exp\left[-t-\frac{1}{4t}\left(\frac{E_x-E_b-E-\xi}{kT_x}\right)^2\right], \quad (1)$$

where $\rho(E)dE$ is the number of photon modes in the crystal between energies E and $E+dE$, where $\rho(E) \propto E^2$, E_x is the energy of the 1s exciton at $K=0$, E_b is the binding energy of excitons, $E_x = E_g - E_b$, T_x is exciton temperature, α and ϵ are the polarizability of excitons and dielectric constant of the material, respectively. The peak energy is located at $E_p = E_g - 2E_b$. Figure 2 shows a comparison between the observed spontaneous emission spectrum (solid dots) and the calculated one (solid line) from Eq. (1) with $E_x = 2.0$ eV, $E_b = 0.020$ eV, $T_x = 500$ K, and the coupling coefficient $\pi\alpha/\epsilon = 3.3\times10^{-3}$.

It is a well known fact that the direct energy band gap of GaSe shrinks under pressure causing the red shift of the photoconductivity, absorption, and luminescence spectra.[7-9] With the reported static values of[10] $\partial E_g/\partial P = -6.2$ meV(kbar)$^{-1}$ and $\partial E_b/\partial P = -0.6$ meV(kbar)$^{-1}$ we obtain the (hydrostatic) pressure coefficient of the peak energy $\partial E_p/\partial P = -5.0$ meV(kbar)$^{-1}$. There is evidence[11] showing that the stress anisotropy of the shock compression could be neglected in many cases. The red shift of 28 nm (84 meV) displayed in Fig. 1 deduces a shock pressure of $\sim$17 kbar. To see if this approximation is reasonable, we also performed an independent measurement of the shock pressure in the same experimental setup by an x-cut quartz transducer technique.[12] The pressure of $\sim$15 kbar was obtained which confirmed our approximation.

Significant line broadening of the spontaneous emission spectra under the shock loading was clearly and repeatedly observed. The magnitude of broadening was about 24 nm for a shock pressure of 17 kbar, as displayed in Fig. 1. It was

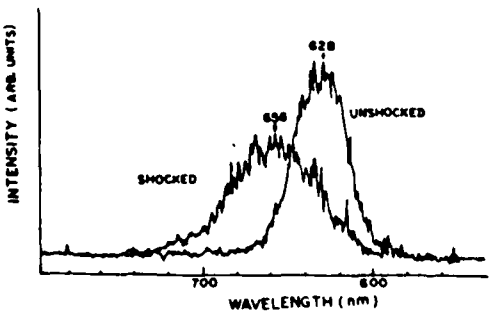

FIG. 1. Observed unshocked and shocked spontaneous emission spectra from GaSe at room temperature and excitation intensity 17 MW/cm^2.

 0003-6951/87/481789-03$01.00

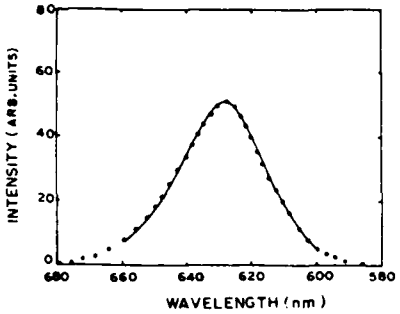

FIG. 2. Calculated spontaneous emission spectrum from the exciton-exciton scattering model of Eq. (1) with $E_x = 2.0$ eV, $E_b = 0.020$ eV, $\pi\alpha/\epsilon = 3.3\times10^{-3}$, and $T_x = 500$ K. The solid dots represent the experimental unshocked spontaneous spectrum.

found that the peak amplitude decreased under shock loading such that the integrated spontaneous emission intensity (area) approximately remains the same as that of the unshocked spectrum.

It was reported[13] that although the electronic (or excitonic) temperature in the probed region ($\sim$434 K) was considerably higher than the room temperature due to heating effect by the probe beam, no significant temperature rise due to the shock wave loading was detected. The Doppler linewidth at temperature T_x due to the thermal motion of the emitting excitons is given by[14]

$$\delta\lambda_D = \frac{2\lambda_p}{c}\left(\frac{2kT_x \ln 2}{M_x}\right)^{1/2}, \qquad (2)$$

where λ_p is the peak wavelength of the emission and M_x is the exciton mass. If this mechanism was responsible for the observed line broadening (of a factor of 2, approximately), the temperature would increase by a factor of 4 due to the shock loading, i.e., the exitonic temperature would exceed 1700 K in the shocked region which is definitely unrealistic. Also, a Doppler broadened line should have a Gaussian profile[14] which disagrees with our observed Lorentzian line shape. Therefore, the possibility of temperature effect causing the linewidth increase due to the shock loading can be safely excluded.

The probed region in our experiment formed a disk of 350 μm in diameter and 5 μm in thickness (the penetration depth of the 532-nm probe beam in GaSe). Since the shock pressure is proportional to the pump beam fluence,[12] transverse inhomogeneity of the shock pressure over the disk area (350 μm in diameter) originated from the Gaussian profile of the pump beam (450 μm in diameter) intensity should be less than 20%. There was also a longitudinal inhomogeneity of the shock pressure in the direction of shock wave propagation due to pressure decay in space. In our picosecond laser-driven shock wave case, the shock decay time was measured[13] to be $\sim$70 ns, corresponding to a decay length of $\sim$140 μm. Thus, the longitudinal variation of pressure in the shocked region was less than 0.5 kbar. However, the observed line broadening corresponded to a pressure variation from zero to twice the mean value of the shock pressure as deduced from the observed red shift. Therefore, neither transverse nor longitudinal inhomogeneity of the shock pressure can explain the observed large line broadening.

The observed line broadening of the spontaneous emission is attributed to the shock-wave-induced exciton collisions. When a shock front propagated through the sample, all molecules behind it would gain a particle velocity u_p via the intermolecular bonding, but excitons would not, since there was no such tight bonding between excitons or between exciton and molecules. Therefore, the emitting excitons in the shocked region all suffer from additional collisions with the entire array with a directional particle velocity u_p. The collision frequency for each exciton is $f_c \simeq a^2 u_p N_{\rm mol}$, where a is the Bohr radius of the exciton in GaSe which is[15] $\sim$32 Å, $N_{\rm mol}$ is the molecular density in GaSe which is $\sim 2\times10^{22}$ cm^{-3}. The particle velocity at 17 kbar is about 2×10^4 cm s^{-1}. Therefore, the collision broadening at 17 kbar is $\Delta\nu = 2f_c/\pi \sim 2.5\times10^{13}$ Hz or $\Delta\lambda \sim 33$ nm which agrees well with the observed value. It should be noted that collisional broadening is homogeneous and should have a Lorentzian line shape.[14] This is also clearly shown in Fig. 1. Since the collision frequency is proportional to u_p which is related to the shock pressure P by the jump condition[11]: $P - P_0 = \rho_0 U_s u_p$, where U_s is the shock velocity, ρ_0 and P_0 are density and pressure in unshocked region. The shock-wave-induced collision broadening is expected to be proportional to the shock pressure. This is confirmed by our experimental data as shown in Fig. 3. The observed line broadening from different pairs of unshocked-shocked data plotted against the applied shock pressure displays a linear dependence. A pressure coefficient of line broadening for the spontaneous emission of GaSe $\sim$1.3 nm/kbar is obtained.

The observation that the shocked spontaneous emission has the same integrated intensity as the unshocked one suggests that the elastic collision (phase-perturbing collision) plays a major role in our line broadening mechanism because inelastic collision (quenching collision) will decrease the number of emitting excitons and reduce the integrated intensity significantly. Note that the usual pressure broadening which is crucial for gaseous systems essentially comes from an increase in particle density and a decrease in mean free path due to high pressure. This latter effect cannot be significant in condensed matter because of its extremely small

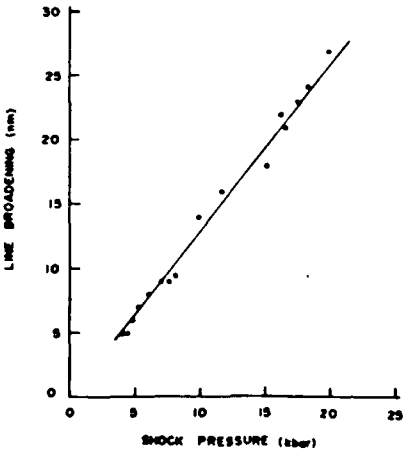

FIG. 3. Observed wavelength broadening of the spontaneous emission spectrum from GaSe vs shock pressure.

compressibility (typically $\rho/\rho_0 \sim 1.2$ at $P = 200$ kbar). The shocked-wave-induced exciton collision broadening is a new mechanism different from the usual pressure broadening and directly related to the unique nature of the shock waves and excitons in condensed matter.

This work was supported by Office of Naval Research and Air Force Office of Scientific Research No. 86-0031.

[1]L. Davidson and R. A. Graham, Phys. Rev. **55**, 255 (1979).
[2]R. A. Graham, J. Phys. Chem. **83**, 3048 (1979).
[3]R. A. Graham, in *Shock Waves and High-Strain-Rate Phenomena in Metals*, edited by M. A. Meyers and L. E. Murr (Plenum, New York, 1981), p. 375.
[4]G. E. Duvall, K. M. Ogilvie, R. Wilson, P. M. Bellamy, and P. S. P. Wei, Nature **296**, 846 (1982).
[5]X. Z. Lu, R. Rao, B. Willman, S. Lee, A. G. Doukas, and R. R. Alfano, Phys. Rev. B **36**, 1140 (1987).
[6]T. Moriya and T. Kushida, J. Phys. Soc. Jpn. **40**, 1668 (1976).
[7]A. J. Niilisk and J. J. Kirs, Phys. Status Solidi **31**, K91 (1969).
[8]J. M. Besson, K. P. Jain, and A. Kuhn, Phys. Rev. Lett. **32**, 936 (1974).
[9]G. L. Belen'kii, E. Yu. Salaev, R. A. Suleimanov, and E. I. Mirzoev, Sov. Phys. Solid State **22**, 1842 (1980).
[10]V. V. Panfilov, S. I. Subbotin, L. F. Vereshchagin, I. I. Ivanov, and R. T. Molchanova, Phys. Status Solidi B **72**, 823 (1975).
[11]G. E. Duvall and G. R. Fowles, in *High Pressure Physics and Chemistry*, edited by R. S. Bradley (Academic, London, New York, 1963), Vol. 2, p. 260.
[12]K. P. Leung, S. Yao, and R. R. Alfano, in *Shock Waves in Condensed Matter*, edited by J. R. Asay, R. A. Graham, and G. K. Straub (Elsevier, Amsterdam, 1984), p. 343.
[13]K. P. Leung, S. S. Yao, A. G. Doukas, and R. R. Alfano, Phys. Rev. B **31**, 942 (1985).
[14]W. Demtroder, *Laser Spectroscopy* (Springer, Berlin, Heidelberg, New York, 1982), p. 90.
[15]T. Ugumori, K. Masuda, and S. Namba, J. Phys. Soc. Jpn. **41**, 1991 (1976).

END

DATE

FILMED

DTIC

JULY 88